The circadian clock network of *Drosophila melanogaster*

Das Uhrneuronennetzwerk von *Drosophila melanogaster*

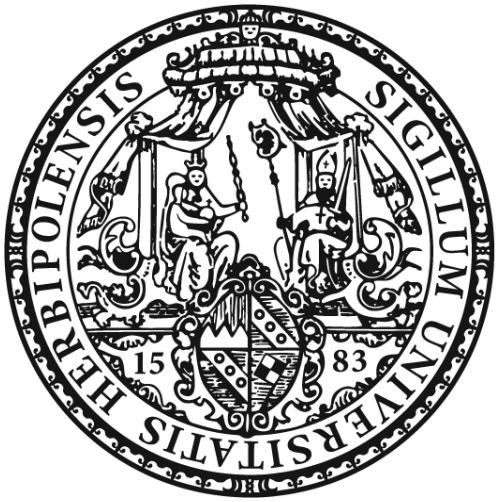

Doctoral thesis for a doctoral degree at the Graduate School of Life Sciences,

Julius–Maximilians–Universität Würzburg,

Section Integrative Biology

submitted by

Frank Klaus Schubert

from

Schweinfurt

Würzburg, 2017

Submitted on: .....

Office stamp

Members of the *Promotionskomitee*:

Chairperson: .....

Primary Supervisor:	**Dr. Dirk Rieger**
Supervisor (Second):	**Prof. Dr. Charlotte Helfrich-Förster**
Supervisor (Third):	**Prof. Dr. Ralf Stanewsky**
Supervisor (Fourth):	**Prof. Dr. Georg Nagel**

Date of Public Defence:

Date of Receipt of Certificates:

Abstract

All living organisms need timekeeping mechanisms to track and anticipate cyclic changes in their environment. The ability to prepare for and respond to daily and seasonal changes is endowed by circadian clocks. The systemic features and molecular mechanisms that drive circadian rhythmicity are highly conserved across kingdoms. Therefore, *Drosophila melanogaster* with its relatively small brain (ca. 135.000 neurons) and the outstanding genetic tools that are available, is a perfect model to investigate the properties and relevance of the circadian system in a complex, but yet comprehensible organism.

The last 50 years of chronobiological research in the fruit fly resulted in a deep understanding of the molecular machinery that drives circadian rhythmicity, and various histological studies revealed the neural substrate of the circadian system. However, a detailed neuroanatomical and physiological description on the single-cell level has still to be acquired. Thus, I employed a multicolor labeling approach to characterize the clock network of *Drosophila melanogaster* with single-cell resolution and additionally investigated the putative in- and output sites of selected neurons.

To further study the functional hierarchy within the clock network and to monitor the "ticking clock" over the course of several circadian cycles, I established a method, which allows us to follow the accumulation and degradation of the core clock genes in living brain explants by the means of bioluminescence imaging of single-cells.

Zusammenfassung

Alle lebenden Organismen benötigen Mechanismen zur Zeitmessung, um sich auf periodisch wiederkehrende Umweltveränderungen einstellen zu können. Zirkadiane Uhren verleihen die Fähigkeit, tages- und jahreszeitliche Veränderungen vorauszuahnen und sich an diese anzupassen. Die Eigenschaften des zirkadianen Systems, als auch dessen molekularer Mechanismus scheinen über sämtliche Taxa konserviert zu sein. Daher bietet es sich an, die leicht handhabbare Taufliege *Drosophila melanogaster* als Modellorganismus zu benutzen. Das relativ kleine Gehirn (ca. 135.000 Neurone) und die herausragende genetische Zugänglichkeit der Fliege prädestinieren sie dazu, das zirkadiane System in einem komplexen, aber dennoch überschaubaren Kontext zu untersuchen.

Die vergangenen 50 Jahre chronobiologischer Forschung an *Drosophila* führten zu einem tiefgreifenden Verständnis der molekularen Mechanismen, die für tageszeitliche Rhythmizität verantwortlich sind. Anhand zahlreicher histologischer Untersuchungen wurde die neuronale Grundlage, das Uhrneuronennetzwerk im zentralen Nervensystem, beschrieben. Nichtsdestotrotz, gibt es noch immer keine detaillierte neuroanatomische und physiologische Charakterisierung der Uhrneurone auf Einzelzellebene. Daher war das Ziel der vorliegenden Arbeit die umfangreiche Beschreibung der Einzelzellanatomie ausgewählter Uhrneurone sowie die Identifikation mutmaßlicher post- und präsynaptischer Verzweigungen.

Darüber hinaus war es mir möglich, eine Methode zur Messung von Biolumineszenzrhythmen in explantierten lebenden Gehirnen zu etablieren. Mit einem Lumineszenzmikroskop können die Proteinoszillationen einzelner Uhrneurone über die Dauer mehrerer zirkadianer Zyklen aufgezeichnet werden, wodurch neue funktionale Studien ermöglicht werden.

.

Contents

1 Introduction

1.1 Circadian clocks

The most prominent periodically occurring environmental change, which we and most organisms are exposed to, is the constantly recurring day and night cycle given by the earth's rotation around its own axis. The hereby-arising cyclic shift between light and dark is accompanied by the rhythmic change of several other environmental factors like temperature or humidity. Therefore, not only spatial, but also temporal adaptation to niches means an advantage that results in an increase of fitness. It is not surprising to learn that most living organisms, ranging from unicellular organisms to humans, have developed timekeeping mechanisms to track and anticipate cyclic changes in their environment. The ability to predict daily changes is endowed by circadian clocks (*lat.: circa*, *diem*, "about a day"), which control ca. 24 h rhythms in gene expression, physiology, and behavior (Fig. 1). Circadian rhythms have been known for centuries and were scientifically described for the first time by the French astronomer Jean Jacques d'Ortous De Mairan (1729), based on his observations of the periodical folding and unfolding of *Mimosa pudica* leaflets, even in constant darkness (reviewed in Roenneberg and Merrow, 2005). The continuation of the leaflet folding rhythms under constant conditions was a strong indicator for an endogenously driven phenomenon, but it took another 100 years to provide evidence for the endogenous nature of the clock in plants (De Candolle, 1832; reviewed in Roenneberg and Merrow, 2005). The paradigm, that all circadian rhythms underlie an endogenous driving force is commonly accepted (Pittendrigh, 1960; reviewed in Roenneberg and Merrow, 2005). This means that the clock is still ticking in absence of any environmental cues, but not with an exact period length of 24 h (= free-running period). Therefore, circadian clocks need to be entrainable to the exact length of the daily cycle by environmental cues, so-called *Zeitgebers* (*dt.:* "time-givers"; *e.g.* light-dark or

temperature cycles; Pittendrigh, 1960). Besides showing a period length of approximately 24 h, their self-sustaining endogenous nature and their entrainability, circadian rhythms are also temperature compensated, which means that the free-running period is largely unaffected by temperature-changes within a physiological range (Pittendrigh, 1960).

Further studies could localize the mammalian circadian pacemaker center in the suprachiasmatic nuclei (SCN) of the hypothalamus, a paired, densely packed core region of up to 50.000 cells in humans (Moore and Lenn, 1972; Stephan and Zucker, 1972; Stephan and Nunez, 1977; Hofman *et al.*, 1988). Due to this overwhelming number and the given conservation of the principal organization of circadian systems, *Drosophila* is a highly favored model to study the circadian clock on the cellular level of a complex, but yet manageable organism. Not only because of the relative small number of only ~150 clock neurons, but also due to the excellent genetic tools that are available in the fly (*e.g.* the *Gal4*/ *UAS*-system; see section 2.1 of chapter 2: Material and Methods).

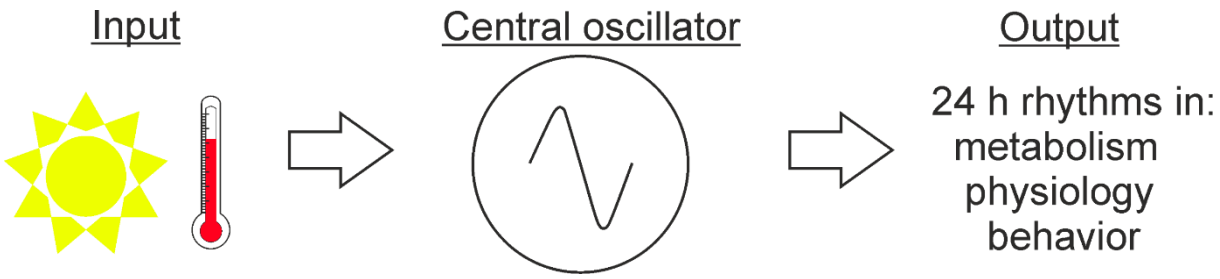

Fig. 1: Concept of the circadian system. The circadian clock is a self-sustaining oscillator that drives rhythms in metabolism, physiology and behavior. In absence of rhythmic environmental cues (*Zeitgebers*) the oscillations persist with an endogenous period length of about 24 h. *Zeitgebers* (*e.g.* light-dark or temperature cycles) can entrain the circadian clock and thereby synchronize the oscillations to the exact length of the 24 h cycle.

1.2 The circadian system of *Drosophila melanogaster*

A commonly used behavioral read-out for clock function is locomotor activity, recorded under light:dark (LD) cycles followed by a period of constant darkness (DD), as light is the most important *Zeitgeber* for flies (Foster and Helfrich-Förster, 2001). When exposed to LD cycles, *Drosophila* exhibits a characteristic bimodal activity

pattern with distinct morning (M) and evening (E) activity peaks (Fig. 2; Helfrich-Förster, 2000). This observation fits to the "Dual Oscillator Model" that was postulated for mammals by Pittendrigh and Daan (1967) to explain the occurrence of pronounced M- and E-activity peaks around dawn and dusk. However, it took over 30 years until behavioral studies and supporting immunohistochemical experiments identified those cells in the fly brain, which can be hold responsible for driving M- and E-activity (Helfrich-Förster, 1995; Renn *et al.*, 1999; Grima *et al.*, 2004; Stoleru *et al.*, 2004; Rieger *et al.*, 2006). In line with the Dual Oscillator Model, a subset of Pigment dispersing factor (PDF) expressing small ventrolateral clock neurons (s-LN_vs) have been shown to control the M-activity (Helfrich-Förster, 1995; Renn *et al.*, 1999), whereas a heterogeneous group of dorsal clock neurons (DN_1), dorsolateral clock neurons (LN_ds; Grima *et al.*, 2004; Stoleru *et al.*, 2004), and a PDF lacking s-LN_v (5^{th} s-LN_v; Rieger *et al.*, 2006) are generating the E activity (Fig. 2). This consistency with the proposed model becomes more apparent when applying it to explain the behavior of flies that were kept under varying day lengths. Rieger and his colleagues demonstrated that the two peaks are closer together under short photoperiods, whereas they move apart when the day length increases (Rieger *et al.*, 2003; Rieger *et al.,* 2012). According to the model, under long photoperiods the M-cells are tracking dawn by shortening their period upon light integration, whereas the E-cells are tracking dusk by slowing their pace down to delay the evening peak (Rieger *et al.*, 2006; Yoshii *et al.*, 2012).

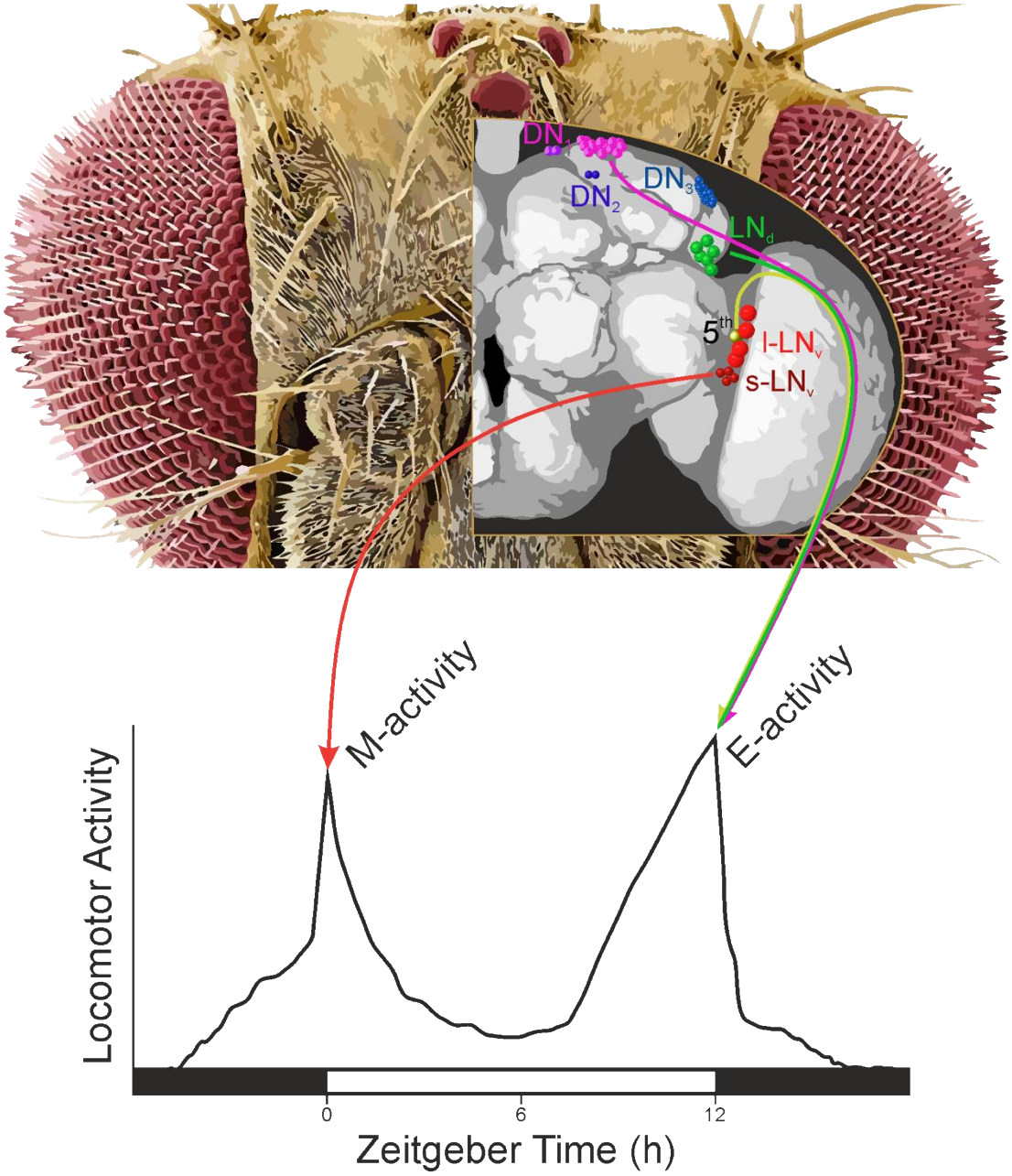

Fig. 2: The Dual Oscillator Modell for *Drosophila melanogaster*. Two functional units, the morning (M)- and the evening (E)-oscillators are responsible for the characteristic bimodal locomotor activity pattern of the fly. According to the model, the M- and E-oscillators are tracking dawn and dusk, respectively, allowing the fly to adjust its behavior to varying day lengths. Under long photoperiods, the M-oscillator speeds its pace up to phase-advance the M-activity upon light illumination, whereas the E-activity gets phase-delayed by prolonging the period of the E-oscillator. The neural substrate of these oscillators is a brain-wide network formed by the clock neurons, which are divided into several different clusters. s-LN_v, small ventrolateral neurons; 5^{th}, 5^{th} s-LN_v; l-LN_v, large ventrolateral neurons; LN_d, dorsolateral neurons; DN_1, dorsal neurons 1; DN_2, dorsal neurons 2; DN_3, dorsal neurons 3.

However, more recent studies indicate that the conception of two distinct functional units is too oversimplified, for instance, how M- and E-cells are controlling locomotor activity bouts is highly dependent on the environmental context (Rieger *et al.*, 2009; Zhang Y. *et al.*, 2010; Sheeba *et al.*, 2010; Yoshii *et al.*, 2012). By means of behavioral assays and calcium imaging in combination with sophisticated genetic manipulations, Yao and Shafer (2014) indeed established, that the fly's neuronal pacemaker network consists of multiple independent oscillators (Yao and Shafer, 2014), after several hints were already pointing in this direction (Rieger *et al.*, 2006; Shafer *et al.*, 2006).

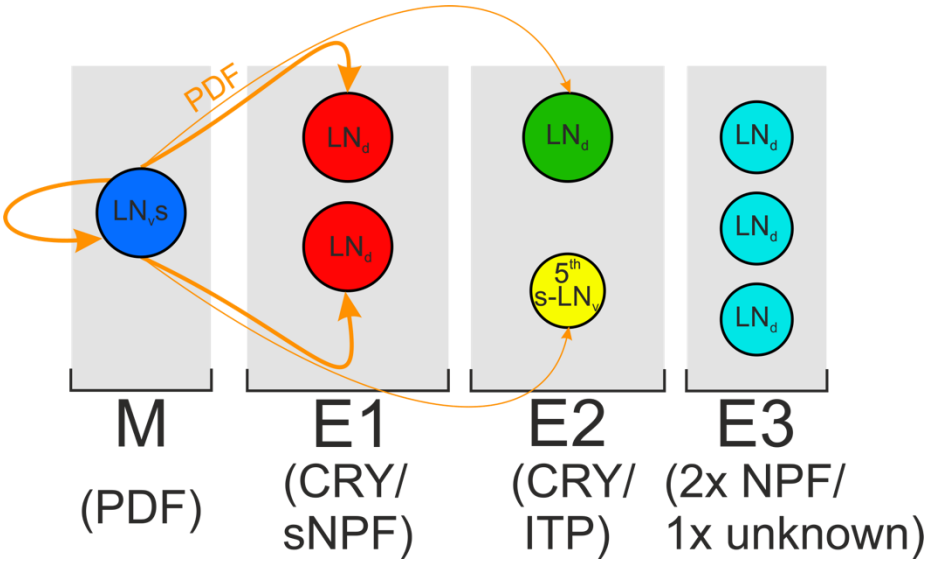

Fig. 3: Multiple peptidergic units control the fly's locomotor activity rhythm. An updated model of the functional composition of *Drosophila*'s circadian clock suggests that three E-oscillator subunits are variably coupled to the output of the PDF expressing M-cells (stronger coupling is indicated by bold arrows). The E1-subunit, consisting of the CRY and sNPF co-expressing LN_ds, is strongly coupled to the M-cells, whereas the CRY and ITP co-expressing E2-subunit appears to be only weakly coupled to the M-cells' output. The third functional subunit, E3, is comprised by three LN_ds, which do not express CRY nor the PDF receptor. Hence, they are not responsive to the PDF signaling of the M-cells and are rather more coupled to the E2-subunit. This figure was modified after Yao and Shafer *et al.* (2014).

According to their observations, the multi-oscillator network can be conceptionalized as four peptidergic units, comprised of one M- and three E-units (Fig. 3). Here, the M-cells comprise all PDF expressing ventrolateral clock neurons (LN_vs), including the l-LN_vs. The E1-oscillator consists of two LN_ds that co-express the circadian

photoreceptor Cryptochrome (CRY) and the short neuropeptide F (sNPF; Yoshii *et al*., 2008; Johard *et al*., 2009). These cells also express the PDF receptor (PDFR) and are strongly coupled to the M-cells' output (Im and Taghert, 2010; Yao and Shafer, 2014). The E2-oscillator unit consists of one CRY expressing LN_d and the 5^{th} s-LN_v. A unique feature of these cells among all clock neurons is the expression of the ion transport peptide (ITP), which can be used as a marker to identify the E2-cells. This unit is also coupled to the output of the M cells via PDFR signaling, but to a lesser extend (Im and Taghert, 2010; Yao and Shafer, 2014). Hermann-Luibl *et al.* (2014) demonstrated the rhythmic release of ITP in the dorsal brain, leading to enhanced E-activity and reduced nocturnal activity bouts. The three remaining LN_ds do not express CRY and build the E3-subunit. These cells lack PDFR expression and are more strongly coupled to the E2-oscillator than to the M-cells' output (Yao and Shafer, 2014). Together, the E-oscillator units are contributing independently to different aspects of the E-activity (Rieger *et al.*, 2006; Yao and Shafer, 2014). This functional subdivision of the E-oscillator is also the working model of the present thesis.

1.3 The molecular clock of *Drosophila melanogaster*

Even though Pittendrigh could successfully summarize the features of circadian systems early on (1960), the mechanisms underlying the observed rhythms remained elusive until Konopka and Benzer found the gene *period* (*per*) in the fruit fly *Drosophila melanogaster* (Konopka and Benzer, 1971). The identification and cloning of *per*, whose mutations altered the periodicity of locomotor activity rhythms, spawned the endeavor to identify other "clock genes" (Konopka and Benzer, 1971; Bargiello *et al*., 1984; Bargiello and Young, 1984; Reddy *et al*., 1984; Zehring *et al*., 1984), and in the following years, more genes were discovered in *Drosophila*, which had an influence on behavioral timing: *timeless* (*tim*), *clock* (*clk*), *cycle* (*cyc*), *par domain protein 1* (*pdp1*), *vrille* (*vri*), and others (Sehgal *et al.,* 1994; Allada *et al*., 1998 Rutila *et al.,* 1998; Blau and Young, 1999; Cyran *et al.*, 2003). By the time when the core clock genes *per, tim, clk* and *cyc,* the ones that are essential to maintain behavioral rhythmicity under DD conditions, had been identified, it turned out that

the molecular mechanism, which drives circadian rhythmicity is a negative transcriptional and translational feedback loop (TTFL; Glossop *et al.*, 1999) as it was postulated by Hardin *et al.* (1990). The TTFL model has since become the central paradigm in chronobiological research in animals and plants, and it turned out that circadian systems are regulated by several interlocked TTFLs (reviewed by Hardin, 2011). As already mentioned the core loop alone, comprised of the interaction of the core clock genes, is sufficient to drive behavioral rhythmicity in *Drosophila*. Since this is the only feedback loop of the circadian system that is relevant for the interpretation and comprehension of the data presented in this thesis, the description of the molecular mechanism will focus only on the core feedback loop (Fig. 4).

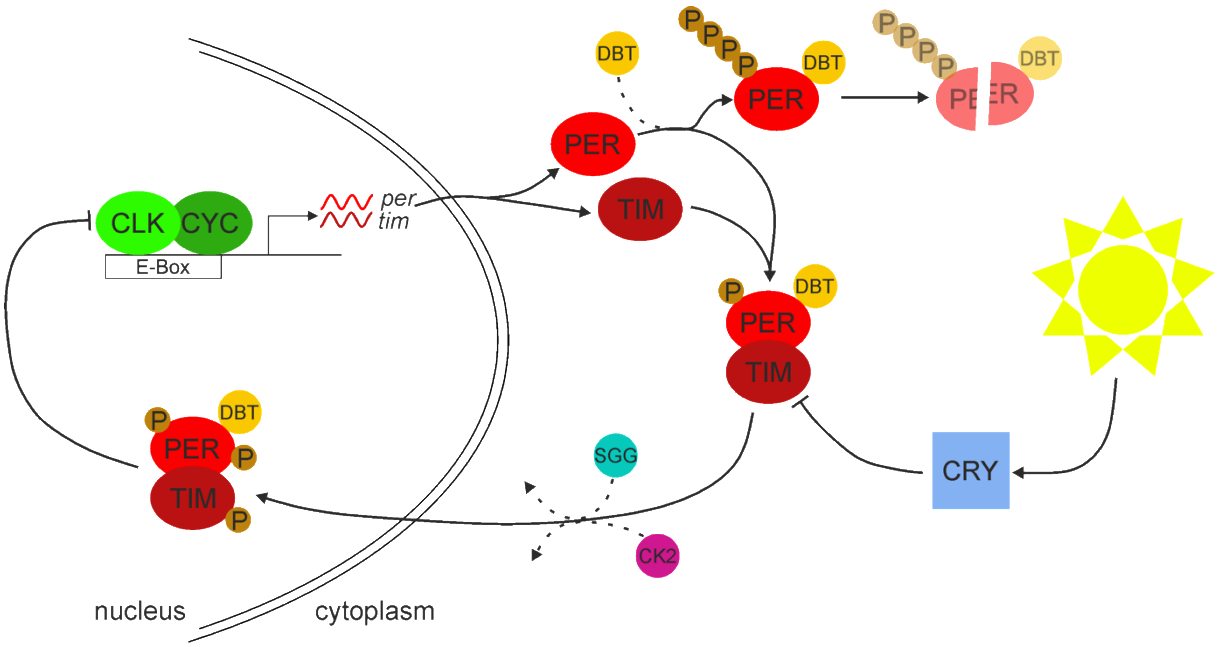

Fig. 4: The core feedback loop of the cell-autonomous molecular clock mechanism. The transcriptional activators CLK and CYC, as a heterodimer, bind to the enhancer boxes (E-Box) of *per* and *tim*, inducing their transcription. Unless the PER protein is protected and stabilized by TIM, it is phosphorylated (P) by the doubletime (DBT)-kinase, which triggers PER degradation via the proteasome. The stabilized DBT-PER-TIM complex is further phosphorylated by Shaggy (SGG) and Casein kinase 2 (CK2), leading to the nuclear localization of DBT-PER and TIM. In the nucleus, the DBT-PER-TIM complex promotes phosphorylation of CLK, resulting in the inhibition of *per* and *tim* transcription. After PER and TIM protein levels drop, the cycle begins anew. About half of the clock neurons express the intracellular blue-light photoreceptor CRY, which mediates light input directly to the molecular machinery. Upon light activation, CRY promotes the degradation of TIM via the proteasome. Hence, the now unprotected PER is phosphorylated by DBT and is designated for degradation. Double line, nuclear membrane; sinusoidal line, mRNA oscillation; blocked line, repression; dashed line, kinase activity. After Collins and Blau, 2007; Hardin, 2011.

A heterodimer of the clock proteins CLK and CYC acts as a transcriptional activator of *per* and *tim* upon binding to their respective enhancer boxes (E-boxes) (Allada *et al.*, 1998; Darlington *et al.*, 1998; Rutila *et al.*, 1998; McDonald *et al.*, 2001). In the following, the proteins PER and TIM are translated in the cytoplasm, where PER gets phosphorylated by the doubletime (DBT)-kinase, which eventually leads to PER degradation by the proteasome, unless it gets protected and stabilized by binding to TIM (Price *et al.*, 1995; Price *et al.*, 1998; Kloss *et al.*, 1998; Kloss *et al.*, 2001; Wang *et al.*, 2001). The stable DBT-PER-TIM complex accumulates in the cytoplasm over the course of six to eight hours and is then further phosphorylated by other kinases (Curtin *et al.*, 1995; Gekakis *et al.*, 1995; Zeng *et al.*, 1996; Martinek *et al.*, 2001; Lin *et al.*, 2002; Akten *et al.*, 2003). This further phosphorylation constitutes a re-nuclearization signal for DBT-PER-TIM, where the complex binds to CLK and induces its phosphorylation. Consequently, the CLK-CYC heterodimer gets released from the E-boxes of *per* and *tim*, and their transcription comes to a halt. (Lee *et al.*, 1998; Lee *et al.*, 1999; Bae *et al.*, 2000; Martinek *et al.*, 2001; Kloss *et al.*, 2001; Shafer *et al.*, 2002; Ashmoore *et al.*, 2003; Akten *et al.*, 2003; Yu *et al.*, 2006; Menet *et al.*, 2010). While in that way PER and TIM are inhibiting their own transcription, the protein concentrations are gradually decreasing until the CLK-CYC complex prevails and re-activates *per* and *tim* transcription, starting the whole cycle anew.

As mentioned before, light is the most important *Zeitgeber* for *Drosophila*'s circadian clock (Foster and Helfrich-Förster, 2001). Besides indirect light input pathways to the clock via the visual system (*i.e.* compound eyes, Hofbauer-Buchner-eyelets; reviewed by Yoshii *et al.*, 2015), there is also a direct link to the molecular mechanism in form of the intracellular blue-light photoreceptor CRY (Fig. 4). The blue-light receptor is expressed in about half of the clock neurons and mediates light-dependent TIM degradation (Hunter-Ensor *et al.*, 1996; Lee *et al.*, 1996; Myers *et al.*, 1996; Zeng *et al.*, 1996; Emery *et al.*, 1998; Stanewsky *et al.*, 1998; Yoshii *et al.*, 2008). Without TIM, the hence unprotected PER gets phosphorylated by DBT and targeted for degradation in the proteasome (Kloss *et al.*, 2001; Grima *et al.*, 2002; Ko *et al.*, 2002). After PER is degraded, CLK-CYC heterodimers bind to the E-boxes of *per* and *tim* to start a new round of transcription. Hereby the molecular cycle is reset at the beginning of every

new day, ensuring that the cell-autonomous oscillations stay in synchrony with the environment.

1.4 The clock network of *Drosophila melanogaster*

The circadian clock is a neuronal network that is built by approximately 150 so-called "clock neurons", which are by definition expressing the components of the TTFL. The clock neurons are classically named according to their location, cell-size, and neurochemical content (Fig. 5; Ewer *et al.*, 1992; Frisch *et al.*, 1994; Helfrich-Förster, 1995; Kaneko and Hall, 2000; Helfrich-Förster, 2003; Shafer *et al.*, 2006). The lateral neurons (LNs) include the small- and large ventrolateral neurons (s-LN_vs and l-LN_vs, respectively), the dorsolateral neurons (LN_ds) and the lateral posterior neurons (LPNs). The dorsal neurons (DNs) are comprised of three clusters, the DN_1, DN_2 and DN_3.

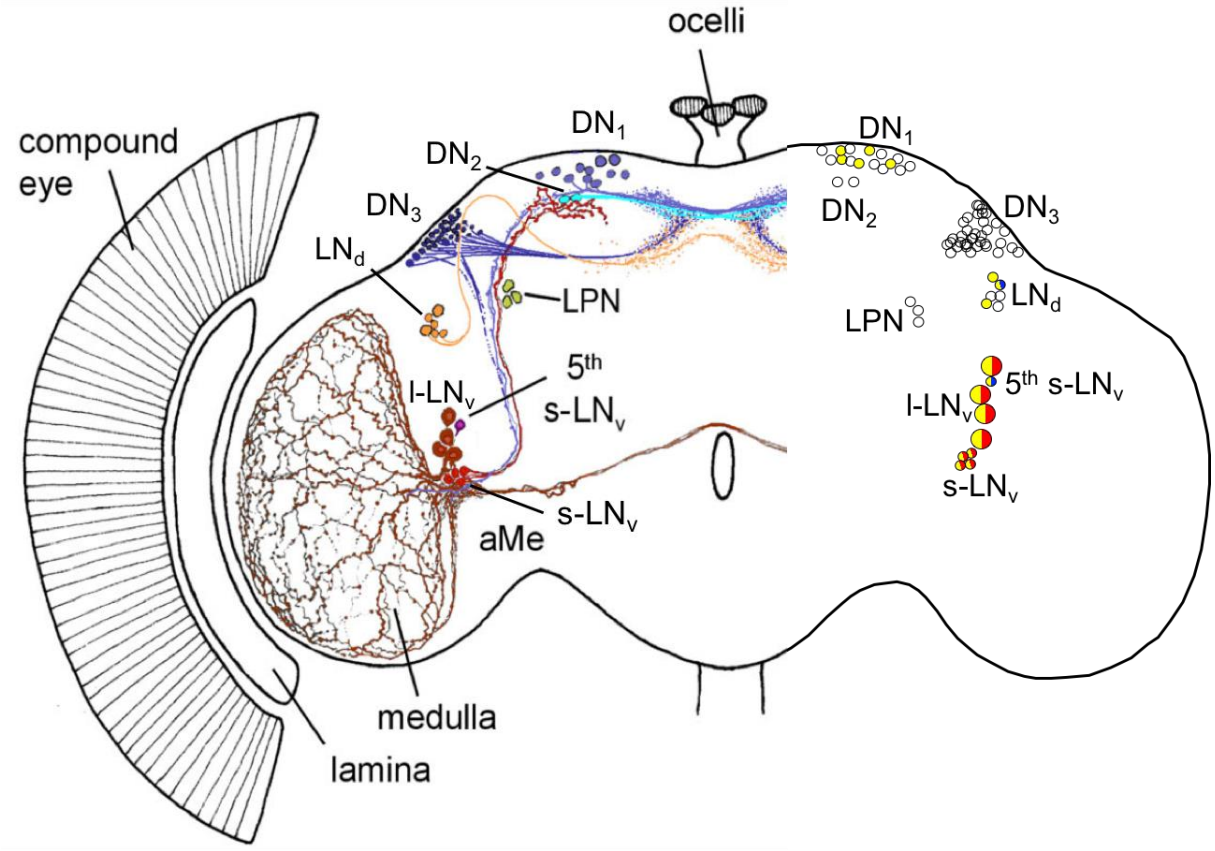

Fig. 5: The clock network of *Drosophila melanogaster*.

Schematic overview shows the projections of the cell groups (left hemisphere) and the expression (right hemisphere) of the two peptides PDF (red) and ITP (blue), as well as the circadian photoreceptor CRY (yellow). The subgroups are named after their location in the brain, small ventrolateral neurons (s-LN_vs), 5th s-LN_v, large ventrolateral neurons (l-LN_vs), dorsolateral neurons (LN_ds), lateral posterior neurons (LPN), dorsal neurons 1-3 (DN_{1-3}). The figure was taken from Helfrich-Förster *et al.* (2007), and the right hemisphere was modified after Yoshii *et al.* (2008) and Johard *et al.* (2009).

Thanks to a synthetic antibody against the crustacean Pigment dispersing Hormone (PDH), which is also reliably labeling PDF in the s-LN_vs and l-LN_vs of *Drosophila*, these neurons were the first anatomically described clock cells (Dircksen *et al.*, 1987; Helfrich-Förster and Homberg, 1993; Helfrich-Förster, 1995). The PDF expressing s-LN_vs invade the accessory medulla and further project into the dorsal brain, terminating dorsofrontally to the mushroom body calices (Fig. 5; Helfrich-Förster and Homberg, 1993; Helfrich-Förster, 1995, Helfrich-Förster *et al.*, 2007). The accessory medulla (AME) is a small neuropil adjacent to the frontomedial medulla and is demonstrably an important pacemaker center in many insects (Reischig and Stengl, 2003). The l-LN_vs' projections also run into the ipsilateral AME and proceed along its ventral elongation, but the majority of fibers run across the surface of the ipsi- and contralateral medullae (Helfrich-Förster and Homberg, 1993; Helfrich-Förster *et al.*, 2007). Thereby, the l-LN_vs are connecting the pacemaker centers of both hemispheres via projections that contribute to the posterior optic commissure (POC; formerly posterior optic tract (POT); Helfrich-Förster and Homberg, 1993; Helfrich-Förster *et al.*, 2007). Little is known about the arborization pattern of the ITP expressing 5th s-LN_v, but it is assumed to be identical to the PDF containing s-LN_vs (Helfrich-Förster *et al.*, 2007). All LN_vs express CRY, allowing those neurons to sense light cell-autonomously (Stanewsky *et al.*, 1998; Yoshii *et al.*, 2008).

While all efforts failed to clearly reveal the morphological differences within the LN_d subgroup, Yoshii and peers found an elaborate solution to overcome the lack of specific antibodies and narrow driver lines, which reliably label the initial projections of those cells. They rescued PER expression exclusively in the CRY expressing LN_ds of otherwise *per* mutant flies and kept them under constant darkness for five consecutive days (Yoshii *et al.*, 2008). In these animals, they were able to observe the initial projections of the CRY expressing cells by staining the accumulated CRY

protein. The same flies were used to visualize the primary fibers of the CRY lacking LN_ds by staining the TIM protein, which is accumulated to high concentrations in the cytoplasm, due to the lack of PER in these cells. Hence, they could show that the projections of the three CRY lacking LN_ds are restricted to the superior neuropils, whereas the three CRY positive cells additionally send projections towards the AME (Yoshii *et al.*, 2008). The CRY expressing LN_ds can be further subdivided according to their function (E1-E3, as described in section 1.2) and neurochemical content (Fig. 5), however it remains obscure whether they have identical arborization patterns. Among the three CRY producing LN_ds, there is one ITP co-expressing cell, while the other two are co-expressing sNPF instead (Johard *et al.*, 2009). Whether all LN_ds are contributing to the dorsal fusion commissure, as well as potential differences within the functional subgroups (E1-E3), still needs to be clarified. The fourth lateral cell cluster is comprised of three LPNs, whose arborization pattern has yet to be described (Kaneko and Hall, 2000).

The DN_1 are representing another heterogeneous group of clock cells, of which about half of them are expressing CRY (Fig. 5; Yoshii *et al.*, 2008). Two neurons of this cluster are located more anteriorly in the brain, hence they are referred to as DN_{1a} to distinguish them from the more posterior DN_{1p} (Klarsfeld *et al.*, 2004; Shafer *et al.*, 2006). The arborizations of the DN_{1p} are mainly to be found in the superior neuropils, whereas at least one of the DN_{1a} additionally projects towards the ipsilateral AME (Helfrich-Förster, 2003; Shafer *et al.*, 2006; Helfrich-Förster *et al.*, 2007; Zhang L. *et al.*, 2010). Two DN_2 are located ventral to the DN_{1p} and send their projections medially towards the dorsoventral midline and dorsally around the superior lateral protocerebrum to the anterior side, but not ventrally in the direction of the AME (Helfrich-Förster, 2003; Helfrich-Förster *et al.*, 2007; Kaneko *et al.*, 2012). The third and last dorsal subgroup is also the largest subcluster of clock neurons, consisting of approximately 40 smaller and larger cells. Most arborizations, stemming from the DN_3 remain ipsilaterally and do not project ventrally, but some fibers are cross the dorsoventral midline in the dorsal brain and reach towards the AME in the lateral protocerebrum (Helfrich-Förster, 2003; Helfrich-Förster *et al.*, 2007).

1.5 Aim of the thesis

The previous description of the adult fly's neuronal clock network is largely based on the findings of Helfrich-Förster and her colleagues (Helfrich-Förster, 2003; Helfrich-Förster *et al.*, 2007; Yoshii *et al.*, 2008; Johard *et al.*, 2009). Even though these studies provide the most detailed anatomical overview of the clock network to the present, the mere fact that they are almost 10 years old and that available methods drastically improved, eagerly demands for an update. Thus, the main aim of the present thesis was the detailed anatomical description of *Drosophila melanogaster*'s clock network. Since the importance of the lateral clock cells for driving behavioral rhythmicity is undisputed and the fact that anatomical studies are rather time consuming, I mainly focused on the lateral network. Three main questions were of particular interest. First, I wanted to investigate the morphological differences between the LN cell clusters and reveal the yet obscure projection pattern of the 5th s-LN$_v$s. Further, I aimed at clarifying whether all CRY expressing LN$_d$s are innervating the AME. Eventually, I endeavored to provide a complementary overview of the LNs' putative in- and output sites, hence, identifying candidate regions for possible downstream interactions.

In my second project, I sought to establish a protocol for long-term single-cell live imaging of clock protein expression in explanted brains. This approach provides the basis for functional studies of single-cells in the intact network and over the course of several circadian cycles.

2 Material and Methods

2.1 The *Gal4*/ *UAS* and other expression-systems

The binary *Gal4*/ *UAS*-system is the most important genetic tool in *Drosophila* that gets extensively used to drive targeted expression of theoretically any gene of interest (Brand and Perrimon, 1993). The method relies on crossing two transgenic lines, whose progeny shows the desired gene expression in the targeted tissue. In the driver line, which determines the expression site, the yeast (*Saccharomyces cerevisiae*) derived Galactose-responsive transcription factor (GAL4) gets expressed either under the control of a certain promotor with required spatial activity or was randomly inserted into the genome. This can be achieved via transposable P-element insertion or by a site-specific phage integrase, which leads to the tissue-specific expression of GAL4. The second fly strain, the effector line, is bearing the inserted recognition site of GAL4, the so-called *Upstream Activating Sequence* (*UAS*), followed by the transgene or gene-construct of interest. Crossing the two transgenic lines consequently generates progeny, in which the tissue-specifically expressed GAL4 binds to the *UAS* to activate the expression of the subsequent transgene. The *Gal4*/ *UAS* expression-system had a major impact on all research areas, in which *Drosophila* is used as a model organism, and enabled to study the function and spatial activity of investigated genes conveniently and efficiently. Immunohistochemistry (IHC) or the combined expression with genetically encoded reporters is a commonly applied technique to detect the transgenic product in the organism. Exposed antigenic epitopes are used for visualizing the artificially expressed proteins with fluorescence- or enzyme-tagged antibodies. The advantage of reporter genes is an easy detectable product, which is harmless to the organism, *e.g.* green or red fluorescent proteins (GFP and RFP, respectively). Modifications and target-oriented mutations of the native fluorescence proteins (FPs) yielded numerous variants with altered fluorescence spectra (*e.g.* yellow-, YFP; cyan-, CFP etc.) and improved properties (*e.g.*

enhanced GFP, EGFP or membrane directed reporters, *e.g.* myristoylated GFP, myr-GFP). The relatively easy, but efficient process of creating new driver- and effector-lines, even in the hands of inexperienced users, resulted in the generation of numerous transgenic fly lines. As a consequence, huge stock centers formed, where researchers can deposit their fly lines and request those generated by other groups (currently >24.000 *Gal4*- and *UAS*-lines at Bloomington stock center, Indiana, USA, 2017).

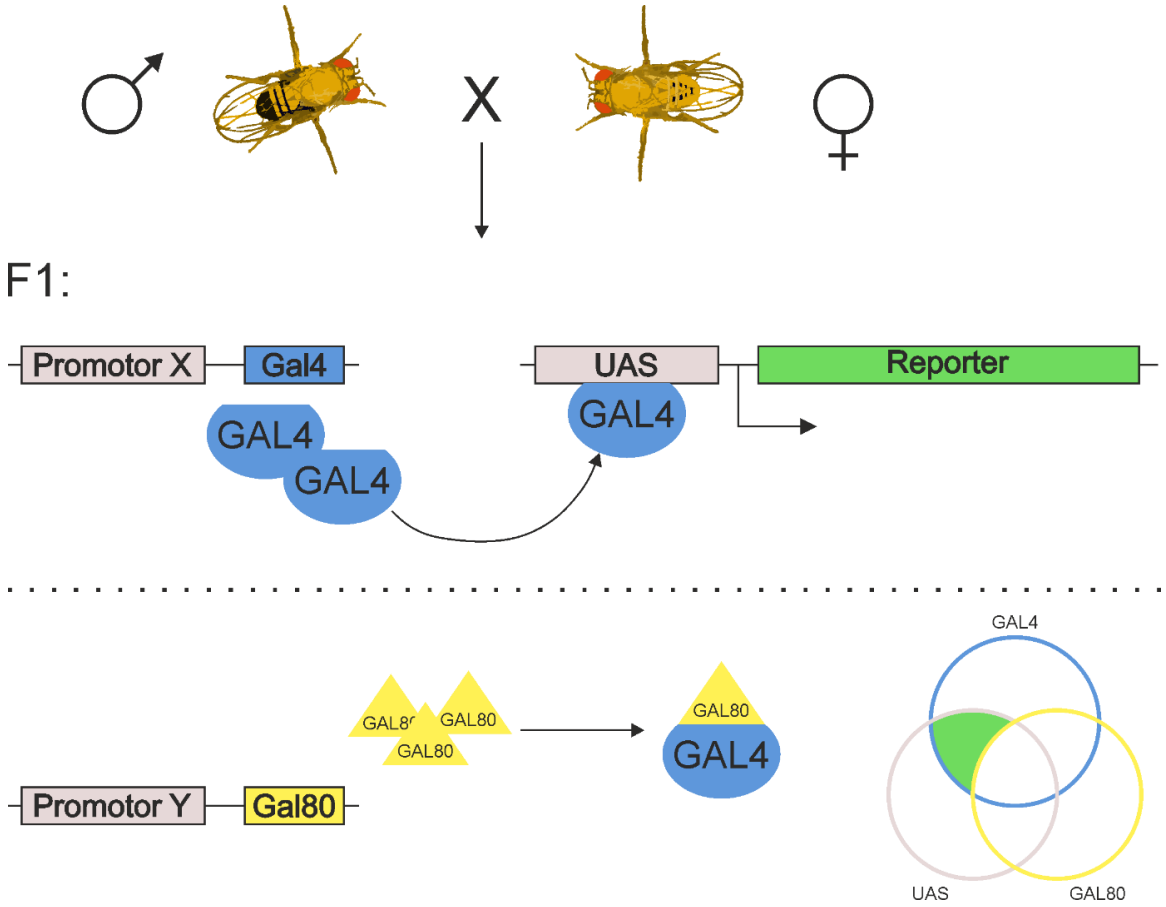

Fig. 6: The binary *Gal4*/*UAS*-system and its repressor GAL80. Two transgenic fly lines need to be crossbred in order to drive targeted gene expression with the *Gal4*/ *UAS*-system in their offspring. One of the parental lines, in this example the male, expresses the yeast transcriptional activator GAL4 under the control of a tissue specific promotor X. The female line carries the *UAS*-construct, consisting of the GAL4 binding site (UAS) and a downstream-located gene sequence (reporter). In the progeny, the tissue specifically expressed GAL4 binds to the *UAS*-site and activates the transcription of the subsequent reporter. Further spatial control can be achieved by additional expression of GAL80, a repressor of GAL4 activity. In this scenario, GAL80 is expressed independently of GAL4, under the control of a second tissue specific promotor Y. The expansion to a tertiary system also allows intersectional approaches and thus a narrower expression.

Additional benefit of the *Gal4*/ *UAS* expression-system derived by expanding it by the utilization of the GAL4 repressor GAL80 (Lee and Luo, 1999). The GAL80 protein suppresses GAL4 mediated transcription by specifically binding to the GAL4 protein and its activation domain (Lue *et al*., 1987). The repressive function is of great benefit and gives additional control over the transgene expression site. GAL80 is either directly under the control of a certain promotor (*e.g. Pdf-Gal80* or *cry-Gal80*; Stoleru *et al.*, 2004) or it is driven by a GAL4-independent expression system like *LexA*/ *lexAop* or *QF*/ *QUAS* (Lai and Lee, 2006; Potter *et al*., 2010; respectively). The *LexA*/ *lexAop*-system uses the DNA binding domain of a bacterial transcription factor, whereas the *QF*/ *QUAS* is based on a cluster of regulatory genes from *Neurospora crassa*. The use of multiple systems allows driving simultaneous and independent expression in the same animal, and is well suited for intersectional approaches.

2.2 Multicolor labeling: Flybow

The above-described method drastically improved and sped up the workflow in *Drosophila* research and the use of genetically encoded FPs enabled fast screening of newly generated drivers. However, the majority of *Gal4*-lines are not suitable for refined and precise anatomical studies, due to the broad expression in multiple cell types and tissues. On the bright side, a variety of methods has been developed over the years, empowering scientists to study the morphology of single-cells on the light-microscopic level. One essential milestone en route to present-day approaches was the transfer of a site-specific yeast recombination system into the fly genome (Golic and Lindquist, 1989; Golic, 1991). The Flippase- (Flp) recombinase, which is usually expressed under the control of a heat-shock promotor, and its recognition targets (*FRT*s) comprise the most widely used site-specific recombination system in *Drosophila*. The use of the Flp/ *FRT* system highly promoted the generation of genetic mosaics in developmental studies (Xu and Rubin, 1993, Theadosiou and Xu, 1998), but only the combination with the *Gal4*/ *UAS*-system, creating the Flp-out technique, made versatile tools like the frequently used MARCM (Mosaic Analysis with Repessible Cell Marker) and its expansions (TwinSpot-MARCM, G-TRACE) possible

(Nellen *et al*., 1996; Zecca *et al*., 1996; Ito *et al.*, 1997; Pignoni and Zipursky, 1997; Lee and Luo, 1999; Lee and Luo, 2001; Evans *et al*., 2009; Awasaki *et al*., 2014). This combination provides additional control by increasing the resolution of existing *Gal4* drivers and its success triggered the development of multicolor labeling systems such as Flybow, dBrainbow, LOLLIbow, TIE-DYE, and Raeppli, which are based on the Brainbow technique in mice (Livet *et al.*, 2007; Hadjieconomou *et al*., 2011; Hampel *et al*., 2011; Boulina *et al*., 2013; Worley *et al*., 2013; Kanca *et al.*, 2014). In respect to my study, the revised Flybow-system has following advantages over the others: it relies on the huge collection of already existing *Gal4*-lines; it employs bright, membrane targeted reporters to reveal the exact neuronal structure; and it is based on the non-toxic Flp/ *FRT* system with modified *FRT*-sites to allow the simultaneous use with classical Flp-out techniques (Hadjieconomou *et al*., 2011; Shimosako *et al*., 2014).

For the anatomical studies of the present thesis, I used the revised *Flybow2.0B*-reporter construct (Fig. 7; Shimosako *et al*., 2014). It consists of four membrane targeted FP reporters (EGFP, mCitrine, mCherry, mTurquoise), which are arranged in two modified *FRT* cassettes. The modified *FRT*-sites (*mFRT71*) are specifically targeted by a modified heat-shock recombinase (*hs-mFlp5*) and are not recognized by the canonical Flp-recombinase (*hs-Flp*). Hence, a stop-cassette, flanked by canonical *FRT*-sites could be used to facilitate sparse labeling and avoid the default GFP expression of the other Flybow-constructs. This initial cassette needs to be excised by *hs-Flp* mediated recombination to allow FP expression. The modified *hs*-mFlp5 can not only excise FP cassettes, but also drive inversions by recombining the *mFRT71*-sites with opposing orientations (Fig. 7A). Fluorescence labeling is restricted to cells, which are expressing *Gal4* and *hs-Flp*, while the expression of multiple colors is additionally dependent on *hs-mFlp5* activity (Fig. 7C).

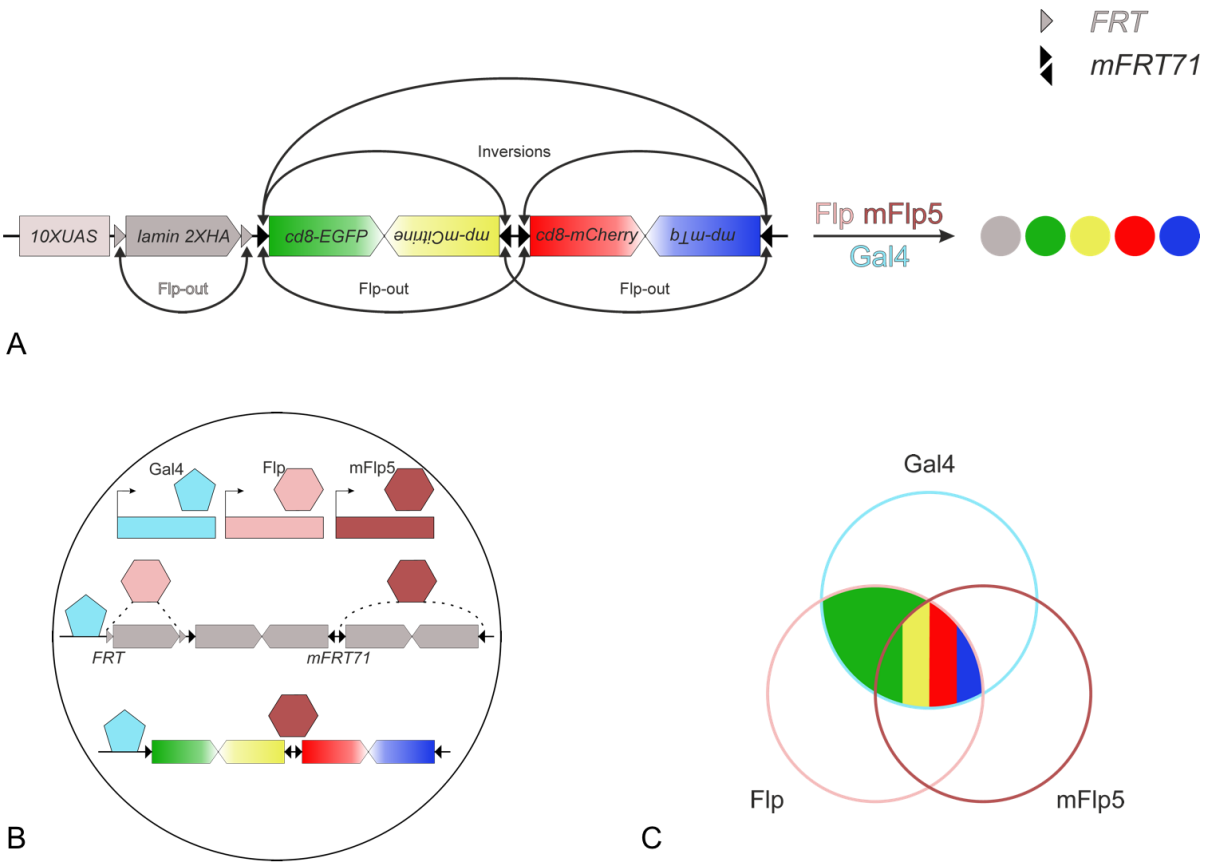

Fig. 7: The *Flybow2.0B*-reporter-system. (A) Scheme of the reporter construct. The 10-fold *UAS* is followed by a stop-cassette to restrict reporter expression. The initial stop-codon is flanked by canonical *FRT*-sites and can hence be excised by the wildtype-like *hs-Flp*. A second, modified *hs-Flp* recombinase (*hs-mFlp5*) is stochastically altering the FP expression upon heat-activation (Flp-out or inversion). (B) Components of the Flybow-labeling approach and their points of action on the reporter construct. Gal4 binds to its *UAS*, the canonical *hs-Flp* targets the wildtype-like *FRT*s, and the *hs-mFlp5* is only recognizing the *mFRT71*-sites. (C) Multicolor labeling is only possible if all regulatory components (GAL4, Flp, mFlp5) are expressed simultaneously. Modified after Hadjieconomou *et al.* (2011) and Shimosako *et al.* (2014).

2.3 Fly strains and genetic crosses

All fly strains used in this study (Tab. 1) were reared on standard cornmeal/agar medium with yeast at 25 °C ± 0.2 °C and 60% relative humidity (rH) ± 5% rH, under a 12:12 h LD cycle.

The experimental Flybow-flies (Flybow-lines crossed to *Gal4*-drivers) were held on 18 °C (18 °C ± 0.2 °C, 60% rH ± 5%, LD 12:12 h) to prevent uncontrolled Flippase recombination events. From the used *Gal4*-driver lines (Fig. 8), the *w; dvPdf-Gal4* (Bahn *et al.*, 2009), *w; +; R16C05-Gal4* and *w; +; R54D11-Gal4* (Pfeiffer *et al.*, 2008)

were crossed to a *10xUAS-myr::GFP* reporter (Pfeiffer *et al.*, 2010) and stained for the clock components TIM, PDF, ITP, and CRY to analyze the expression patterns of these drivers in more detail. To build a driver stock for usage with the Flybow-system, I balanced all *Gal4* drivers (Fig. 8) and crossed them to *y w; hs-mFlp5^{MH12}/ CyO; TM2/ TM6B* (Shimosako *et al.*, 2014) or to *y w; GlaBc/ CyO; hs-mFlp5^{MH3}/ TM6B* (Shimosako *et al.*, 2014) depending, on which chromosome the *Gal4* insertion was located. Experimental flies were obtained by crossing the balanced *Gal4/ hs-mFlp5* lines to either *hs-Flp^{1}; +; FB2.0B^{49b}* (Shimosako *et al.*, 2014) or to *hs-Flp^{1}; FB2.0B^{260b};* + (Shimosako *et al.*, 2014) virgins. I recorded the locomotor activity of animals from one of the obtained fly-lines (*hs-Flp^{1}; Pdf-Gal4/ FB2.0B^{260b}; hs-mFlp5^{MH13}* /+) after exposure to three heat-shocks during larval development (Fig. S1). The flies behaved normal under LD cycles and they were rhythmic in DD, indicating that the expression of the required transgenes does not impair the clock and its neuronal network (Fig. S1).

Tab. 1: Used fly lines

***Gal4* drivers**	**Comment**	**Reference**
y w; Pdf-Gal4	s-LN$_v$s, l-LN$_v$s	Renn *et al.*, 1999
w; dvPdf-Gal4	s-LN$_v$s, l-LN$_v$s, 5th s-LN$_v$, 4 LN$_d$s	Bahn *et al.*, 2009
w; + ; R16C05-Gal4	2 LN$_d$s, 2 DN$_{1a}$	Pfeiffer *et al.*, 2008
w; + ; R54D11-Gal4	1 LN$_d$, 5th s-LN$_v$	Pfeiffer *et al.*, 2008
w; clk206-Gal4	s-LN$_v$s, l-LN$_v$s, 4 LN$_d$s, DN$_{1a}$, DN$_2$	Gummadova *et al.*, 2009
w; clk4.1M-Gal4	DN$_{1p}$	Zhang L. *et al.*, 2010
w; clk856-Gal4	All clock neurons	Gummadova *et al.*, 2009
w; + ; repo-Gal4	Pan-glial except midline glia	Sepp *et al.*, 2001

Reporter lines		
w; + ; UAS-myr::GFP	Membrane targeted 10-fold reporter	Pfeiffer *et al.*, 2010
hs-Flp^{1}; + ; UAS-FB2.0B^{49b}	Wildtype hs-Flippase and Flybow2.0B-reporter	Shimosako *et al.*, 2014
hs-Flp^{1}; UAS-FB2.0B^{260b}	Wildtype hs-Flippase and Flybow2.0B-reporter	Shimosako *et al.*, 2014
w; UAS-DenMark::mCherry	Dendritic marker (Telencephalin)	Nicolaï *et al.*, 2010
w; UAS-nSyb::EGFP	Presynaptic vesicle marker (neuronal Synaptobrevin)	Zhang Y.Q. *et al.*, 2002
y w; Pdf::mRFP1; BG-luc	RFP reporter for PDF cells and PER-LUC reporter for all clock neurons	Ruben *et al.*, 2012 Stanewsky *et al.*, 1997
w; UAS-GFP-S65t	Cytoplasmic EGFP	Bloomington #1522
Other lines		
y w; hs-mFlp5^{MH12}/ CyO; TM2/ TM6B	Modified hs-Flippase, balanced line	Shimosako *et al.*, 2014
y w; GlaBc/ CyO; hs-mFlp5^{MH3}/ TM6B	Modified hs-Flippase, balanced line	Shimosako *et al.*, 2014
y w; Pdf-Gal80	Suppressor of Gal4 in PDF cells	Stoleru *et al.*, 2004
y w; cry-Gal80	Suppressor of Gal4 in CRY cells	Stoleru *et al.*, 2004
w^{1118}; sco/ CyO; MKRS/ TM6B	Balancer strain	Bloomington #3703
CantonS	Wildtype	Konopka *et al.*, 1989

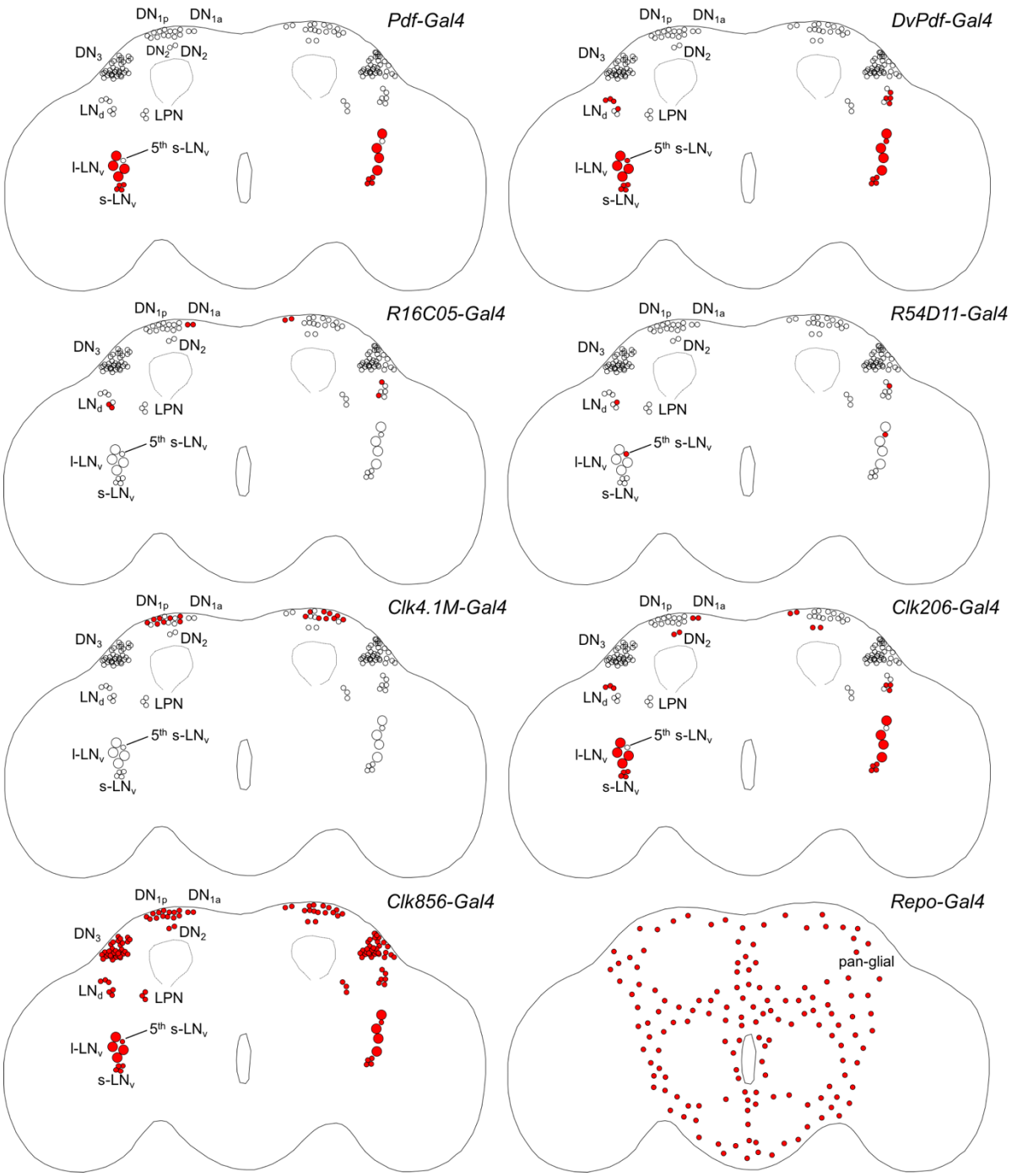

Fig. 8: Overview of the expression patterns of the used *Gal4*-drivers. The first four lines (*Pdf-Gal4*, *dvPdf-Gal4*, *R16C05-Gal4* and *R54D11-Gal4*) covered all lateral clock neurons (LNs), whereas the drivers based on the *Clk*-promotor fragments were used to investigate the dorsal neurons (DNs) and the lateral posterior neurons (LPN). A pan-glial *Gal4*-driver (*repo-Gal4*) was used for evaluation of the brain culture protocol.

I crossed the *Gal4*-drivers to *UAS-DenMark::mCherry* (Nicolai *et al.*, 2010) and *UAS-nSyb::EGFP* (Zhang Y.Q. *et al.*, 2002) to reveal the post- and presynaptic sites, respectively. For analyzing the 5th s-LN$_v$ and the ITP expressing LN$_d$, I first crossed

pdf-Gal80 (Stoleru *et al.*, 2004) into the *R54D11-Gal4* line to restrict the reporter expression to the PDF lacking cells only. Furthermore, I was able to specifically look at the synaptic sites of the CRY absent LN_ds by combining the *dvPdf-Gal4* driver with *cry-Gal80* (Stoleru *et al.*, 2004) before crossing them to the reporter lines.

2.4 Heat-shock procedure for Flybow-labeling

The parental flies of the final crossing (Flybow-lines crossed to *Gal4*-drivers) were transferred into new vials every 24 hours for seven consecutive days. Three heat-shocks (37°C) were applied in a waterbath for 30-45 minutes each at different developmental stages to each vial in order to induce Flp-recombinase activity (Fig. 9). After hatching, the flies were processed as described below (section 2.5).

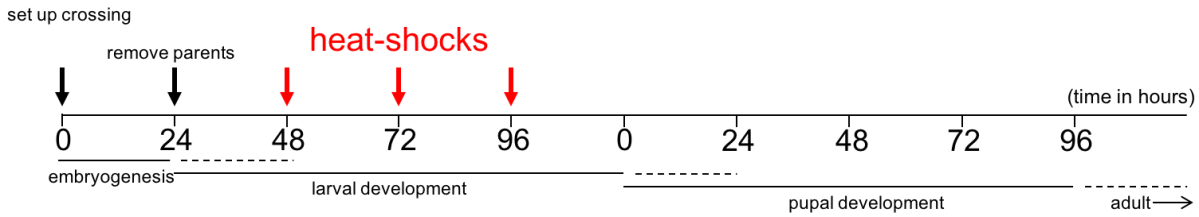

Fig. 9: Exemplary heat-shock protocol. Each vial was heat-shocked three times during larval or pupal development after the parents were removed. The heat-shocks lasted between 30 and 45 minutes and were applied in a 37°C water bath. Modified after Shimosako *et al.* (2014).

2.5 Immunohistochemical staining

After eclosion, the experimental flies were entrained to a LD cycle of 12:12 h for 4-5 days. Subsequently, the flies were collected one hour before lights on at *Zeitgebertime* 23 (ZT23) and the entire animals were fixed in darkness for 2.5 hours in a 4% paraformaldehyde (PFA) solution in phosphate buffered saline (PBS), containing 0.3% Triton-X100 (4% PFA in PBST 0.3%). After rinsing the flies with PBS (5 x 10 min), the brains were dissected in PBST 0.1%, before they were incubated in the blocking solution (5% normal goat serum, NGS, in PBST 0.5%) at 4°C overnight. At noon of the following day, I transferred the brains into the primary antibody-solution

containing 5% NGS and 0.02% sodium azide (NaN_3) in 0.5% PBT (for further information on the used antibodies, see Tab. 2) and incubated for two nights at 4°C. After washing in PBST 0.1% (5 x 10 min), they were incubated in the secondary antibody-solution (see Tab. 2 for used antibodies) at room temperature for three hours. After incubation, the brains were washed in PBST 0.1% (3 x 10 min) and rinsed two more times for 10 minutes in PBS. Subsequently, all brains were aligned on a specimen slide and embedded in Vectashield-1000 mounting medium (Vector Laboratories, Burlingame, CA, USA). The samples were stored at 4°C in darkness until scanning.

Tab. 2: Used primary and secondary antibodies

Antibody	Source	final concentration	Host species	Reference
anti-PDF-C7	DSHB	1:4000	Mouse	Deposited by J. Blau, 2005
anti-TIM	I. Edery	1:2000	Rat	Sidote *et al.*, 1998
anti-PER	R. Stanewsky	1:2000	Rabbit	Stanewsky *et al.*, 1997
anti-CRY	T. Todo	1:1000	Rabbit	Yoshii *et al.*, 2008
anti-ITP	H. Dircksen	1:10.000	Rabbit	Dircksen *et al.*, 2008
nc82/anti-Brp	MAB Hofbauerlibrary	1:100	Mouse	Hofbauer, 1991
anti-GFP	Abcam	1:2000	Chicken	
anti-mCherry	Rockland	1:2000	Rabbit	
anti-mCherry	ThermoFisher	1:2000	Rat	
anti-LUC	ThermoFisher	1:200	Mouse	

AlexaFluor488 (anti-chicken)	ThermoFisher	1:200	Goat
AlexaFluor488 (anti-mouse)	ThermoFisher	1:200	Goat
AlexaFluor555 (anti-mouse)	ThermoFisher	1:200	Goat
AlexaFluor586 (anti-rat)	ThermoFisher	1:200	Goat
AlexaFluor635 (anti-rabbit)	ThermoFisher	1:200	Goat
AlexaFluor647 (anti-rabbit)	ThermoFisher	1:200	Goat
AlexaFluor647 (anti-mouse)	ThermoFisher	1:200	Goat

2.6 Confocal microscopy and image processing

Fluorescence protein expression and antibody-staining was visualized with a Leica TCS SP8 confocal microscope (Leica Microsystems, Wetzlar, Germany), equipped with hybrid detectors (HyD); photon multiplier tube (PMT) and a white light laser for excitation, using the laser and detector settings as described in Shimosako *et al.* (2014) for all Flybow-experiments. I used a 20-fold glycerol immersion objective (HC PL APO, Leica Microsystems, Wetzlar Germany) for whole mount scans and obtained confocal stacks with 2 µm z-step size and 1024X512 pixels. For magnifications, a 63-fold glycerol objective (HC PL APO, Leica Microsystems, Wetzlar Germany) was used, and the brains were scanned with a resolution of 2048X2048 pixels and a slice-thickness of 1 µm. For the PMT all focal planes were scanned four times, and the frames were averaged to reduce background noise. The HyD were used with photon counting mode, and each focal plane was scanned and accumulated four times. The obtained confocal stacks were maximum projected and analyzed with Fiji ImageJ (Schindelin *et al.*, 2012). Besides contrast, brightness and color scheme adjustments,

no further manipulations were done to the confocal images, if not stated otherwise. For the triple (GFP, PDF, ITP) and fourfold (GFP, PDF, CRY, TIM) labelings Alexa488, 555, 635/647 and in the latter case Alexa586 were used as secondary antibodies (Tab. 2). The far-red emitting conjugates (Alexa635 and Alexa647) were visualized with the HyD, whereas the remaining dyes were scanned with PMT detectors. The Flybow-samples were counterstained with either PDF, PER or nc82-antisera which was amplified with Alexa635 dyes.

I used the Neuron2-APP2 implementation from the vaa3D software package for the 3D reconstructions of single-cells (Peng H. *et al.*, 2010, 2014a, 2014b; Xiao and Peng H., 2013). The tracing files were imported and adjusted in Fiji and visualized via the 3D viewer plug-In (Schmid *et al.*, 2010). Sample alignment to the Janelia Farm Research Campus standard brain (JFRC2) was carried out in Fiji with the computational morphometry toolkit graphical user interface plug-In (CMTK GUI, Rohlfing and Maurer, 2003; Jefferis *et al.*, 2007).

2.7 Cell-size estimation, statistical analysis and graphical editing

For the comparison of cell sizes among the different clock neurons, I measured the maximum diameter of identified cells in Fiji using the standard measurement tools. I exclusively measured cells that were labeled with cytosolic or membrane-bound markers and where I could clearly identify the orientation and therefore the maximum diameter. Using a one-way ANOVA under Bonferroni post-hoc correction (α=0.05), cell size diameters were tested for significant differences. Statistical analysis was performed using the SPSS 23 (IBM, Chicago, IL, USA) software after testing datasets for normal distribution (Shapiro-Wilkinson test). Schematic overviews, graphs and figures were edited and arranged using CorelDRAW Graphics Suite X8 (Corel Corporation Ltd., Ottawa, Canada).

2.8 Whole brain culturing protocol

To establish a bioluminescence-imaging assay over the course of several circadian cycles, I first required a protocol for the long-term cultivation of explanted brains. I adapted the whole brain culture protocol described in the dissertation of Saskia Eck (2016) and adjusted it to my requirements. The required Ca^{2+}-free Ringer solution and the culturing medium should be prepared one day prior to the start of the culturing experiment (see Tab. 3 for recipes and storage).

Tab. 3: Recipes for stock solutions

	Ca^{2+}- free Ringer solution (1 l)		
4.01 g	Sodium chloride	NaCl	Sigma aldrich
0.37 g	Potassium chloride	KCl	Sigma aldrich
1.90 g	Magnesium chloride	$MgCl_2$	Sigma aldrich
0.84 g	Sodium bicarbonate	$NaHCO_3$	Sigma aldrich
41.08 g	Sucrose	$C_{12}H_{22}O_{11}$	Sigma aldrich
1.19 g	Hepes	$C_8H_{18}N_2O_4S$	Sigma aldrich
add 1.0 l	Sterile water	ddH_2O	
	Store 50 ml aliquots at -20°C or at 4°C after thawing		
	Whole-Brain culturing medium (50 ml)		
40 ml	Schneider's Medium 20	SM20	Sigma aldrich
10 ml	Fetal bovine serum	FBS	PAA
	Sterile filtration		
add 0.5 ml	Penicillin/ Streptomycin	Penstrep	PAA
	Store at 4°C and let warm up to RT prior to usage		
	Luciferin stock (10 ml, 150 mM)		
477.63 mg	Firefly D-Luciferin, potassium salt	$C_{11}H_7KN_2O_3S_2$	Biosynth
add 10 ml	Sterile water	ddH_2O	
	Store aliquots at -20°C in darkness, vortex thoroughly prior usage		

All surfaces and the microscope were cleaned with 70% ethanol (EtOH 70%) and sprayed with a non-volatile disinfectant (Biocidal ZF, WAK Chemie Medical GmbH, Steinbach, Germany) right before dissection. Gloves were worn at all times and replaced between the working steps or whenever necessary. Precision forceps and four glass dishes were also cleaned with EtOH 70% and dried completely prior to usage. I placed the flies on ice for anesthetization and prepared the four glass dishes for the dissection procedure, one with EtOH 96% and three with ice-cold Ca^{2+}-free Ringer solution (Fig. 10). First, I quickly rinsed one anesthetized fly in EtOH 96% to wash off adherent yeast, which was added to the food, and subsequently rinsed the fly in Ringer solution, to wash off the EtOH. The dissection was carried out in a separate dish and the brains were collected in clean Ringer. I only removed the large trachea and the air sacs on the back of the brain to prevent the brain from floating, but left the remaining trachea and large parts of the lamina untouched. Thereby, I averted injuries of the brain and sought to preserve its structural integrity. Furthermore, I avoided touching the brains directly with the forceps whenever possible. After dissection, the brains were taken to the germ-free cell culture room and gently transferred into a Poly-L-Lysine coated glass-bottom petri-dish (coated with 50 µl for 1 h in a humidified chamber). Transferring the brains in a droplet of Ringer solution between the tips of a clean pair of forceps is highly recommended to avoid direct contact and to keep the amount of co-transferred liquid as small as possible. I aligned six brains closely together with the anterior part facing down for facilitated imaging with an inverted microscope setup. Excess liquid was removed with forceps, exploiting the adhesion and relatively high surface tension of the Ringer solution, until the anterior surfaces of the brains were touching the coated glass bottom. Immediately after the proper alignment, the petri dish is transferred under a sterile bench to add 3 ml of the culturing medium without rinsing the brains off the glass bottom. Finally, the luciferin gets added (final concentration in the culture: 0.75 µM), and the closed dish is subsequently transferred into a humidified tissue culturing incubator (MCO-5ACUV, Panasonic, Kadoma, Japan) with 25°C and 5% CO_2 concentration. Of the cultures maintained in the incubator, half of the volume (1.5 ml) was substituted with fresh medium on every second day. The cultures

subjected for bioluminescence imaging were stored in the incubator for 24 h after adding the luciferin, to prevent artifacts caused by an accumulated enzyme pool in the neurons (Stanewsky *et al.*, 1998). To further avoid artifacts caused by movement, the medium of these cultures was not changed during the recordings. Filter tips were used for all pipetting steps, and I worked as sterile as possible to keep the rate of contaminated cultures to a minimum.

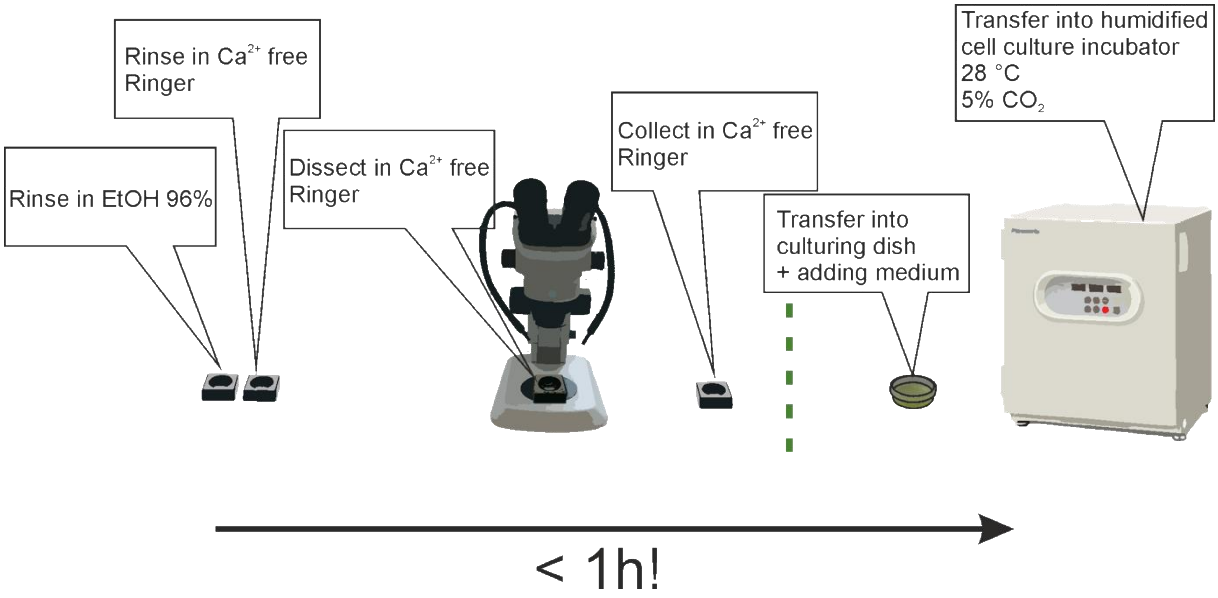

Fig. 10: Schematic workflow of the brain culturing protocol. Quick and sterile handling is essential for the successful cultivation of explanted brains, and the protocol should not exceed 1 h. Preparing a clean, organized workstation is therefore highly recommended. To avoid contaminations, the microscope workplace is set up in a separate room (indicated by the dashed green line) and flies or fly vials were never taken to the sterile culturing area, only the dish with the collected brains.

2.9 Imaging of cultured brains

2.9.1 Fluorescence imaging of living brains

To evaluate the viability of cultured brains, I used a fluorescence stereomicroscope (Leica M165 FC equipped with Leica DFC 450 C camera, Leica microsystems, Wetzlar, Germany) to assess the native fluorescence signal of genetically encoded FPs. The brains were imaged every second day right before replacing the medium. On the first day in culture, when the brains were imaged for the first time, I noted the camera

settings (exposure time, contrast etc.) and used them for the subsequent imaging events. Hence, I was able to identify decreases in signal strength and morphometrical changes, which are manifestations of incipient cell death. Prior to imaging, the whole work area was cleaned with ethanol and imaging was carried out as fast as possible to keep the time with removed lid to a minimum.

2.9.2 Bioluminescence imaging

For the bioluminescence imaging experiments, I used a Period-Luciferase (PER-LUC) reporter (Fig. 11), which encodes a functional PER fusion protein (Stanewsky *et al.*, 1998). The regulatory region and 2/3 of the protein coding sequence of *per* was cloned upstream to the firefly (*Photinus pyralis*) luciferase gene, resulting in a luciferase-reporter that sufficiently mimics PER abundance, due to the relatively short reporter half-life (Brandes *et al*., 1996; Stanewsky *et al.*, 1997; Stanewsky *et al.*, 1998). The same flies carried a *Pdf::mRFP1* reporter construct (Ruben *et al.*, 2012), allowing the immediate visualization of the PDF expressing LNs by fluorescence imaging (Tab. 1).

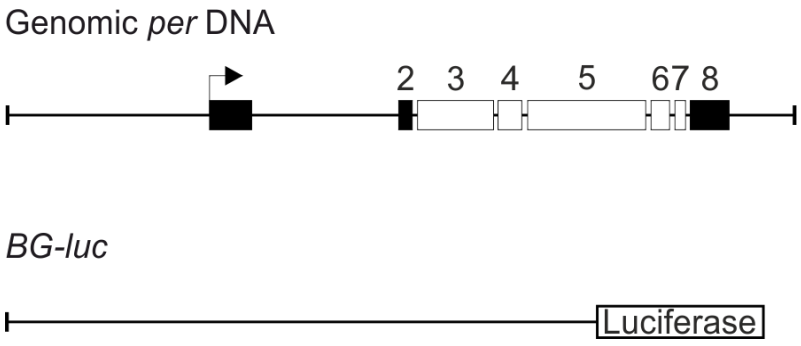

Fig. 11: PER-LUC (*BG-luc*) reporter for circadian bioluminescence imaging. *Per* genomic DNA, the black boxes indicate untranslated exons (1, 2, 8), the white boxes translated exons (3-7). The *BG-luc* construct contains the genomic *per* DNA from -4.2 to +5.6 kb fused to the *luciferase* cDNA. The translated fusion protein is a bioluminescence reporter which reflecting PER abundance. Modified from Stanewsky *et al*., (1997).

Cultures subjected for the bioluminescence imaging of PER-LUC expression were handled after a strict time schedule, allowing the estimation of the phase of PER oscillation at the time when the measurement gets started (Fig. 12). After raising the

flies under a LD cycle of 12:12 h, PER levels were peaking in the late "night", one hour before the light gets switched on (ZT23). I dissected the brains at the end of the light phase (ZT11) and put them into the incubator before ZT12, the time when the light would go off under the preceding LD cycle. Henceforth, the brains were kept in constant darkness, except for when they were brought into focus of the microscope. 24 h after the dissection, during the subjective day (Circadian time 11, CT11), the culture dish was transferred under the luminescence microscope (Luminoview, LV200, Olympus life science, Tokyo, Japan), into a humidified and temperature controlled culture chamber. Ten hours later at CT21, when PER levels and, consequently, luminescence intensity were about to peak, I adjusted the focal plane to the luminescence signal emitted by the single clock cells.

The microscope was located in a separate climate chamber (25 °C) with black interior walls and working surfaces. A red-light LED was the only illumination inside the chamber and it was switched off during the measurements. Further potential light pollution of the recording was omitted by covering all LEDs and displays of electronic devices in the microscope room.

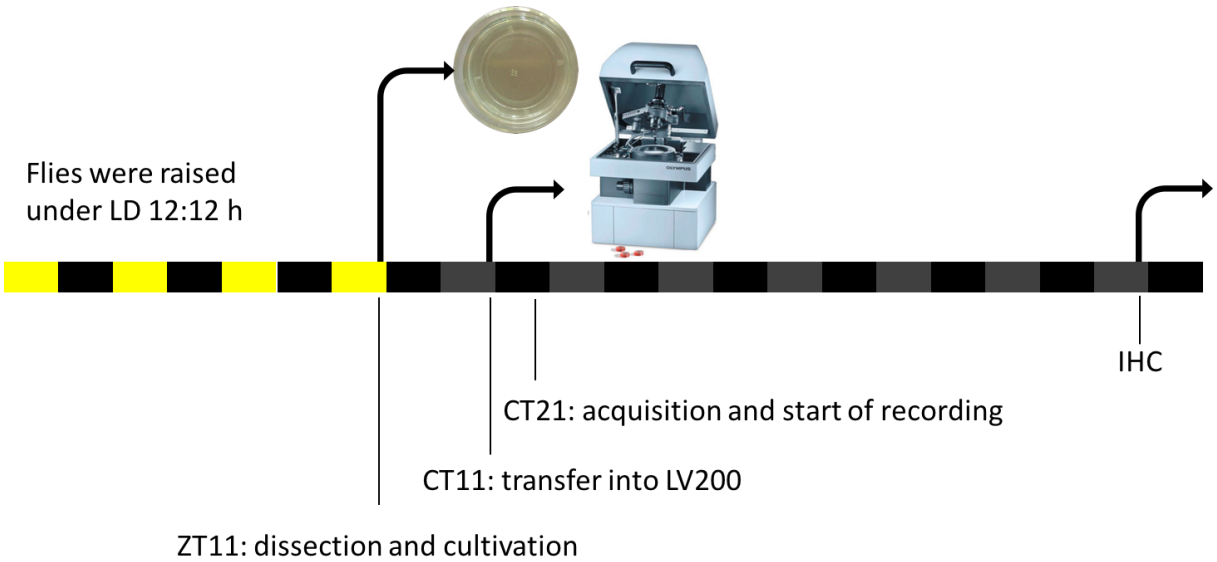

Fig. 12: Time-schedule of circadian bioluminescence imaging experiments. The flies were raised under LD cycles and dissected towards the end of the light phase (ZT11). 24 h later and under constant darkness, the cultivated brains get transferred under the luminescence microscope and brought into focus, exposing them to light for just a few seconds. At CT21, 2 h before PER levels are peaking, the focal plane is adjusted to single clock neurons using the luminescence signal.

The microscope settings were controlled with the cellSens software (Version 1.6, Olympus life science, Tokyo, Japan). Brightfield images were obtained with 512x512 pixels, using 50 ms exposure time with opened shutter. For the luminescence time-series, the images were recorded with an interval of 10 min, and exposure time was set to 300 s. I used an EM-gain of 300-600, dependent on the signal strength. The pixelclock of the equipped EMCCD camera (ImagEm X2 9100-23B, Hamamatsu Photonics, Hamamatsu, Japan) was set to 11 MHz EMCCD mode, and the pictures were taken with a resolution of 512x512 pixels with either 30-fold or 60-fold super apochromat objectives (UPLSAPO 30X, UPLSAPO 60X, Olympus life science, Tokyo, Japan).

2.9.3 Confocal imaging of cultured brain explants

After the bioluminescence imaging of the living brains, some samples were processed for confocal imaging to conclude further about the culturing conditions from the shape and quality of the staining of selected clock neurons. The staining and imaging protocol was conducted with the brains still attached to the lysine coated glass bottom of the culturing dish. Subsequently after removing the culturing medium, the brains were quickly rinsed in PBS and fixed in 4% PFA in PBST 0.3% for 20 min. The brains were then immunostained with PDF-antiserum, following the protocol as described in section 2.5 with the exception that they were directly embedded in the culturing dish to remain the spatial orientation from the previous luminescence imaging. The same microscope setup as described in 2.6 was used to visualize the PDF staining and native mRFP1 signal, but with a 10-fold air objective instead, because the higher magnification optics (20x, 63x) did not fit into the open culture dish. PDF staining was amplified and visualized with an Alexa488 secondary antibody, of which the emission spectra was detected between 495 and 540 nm, using a PMT. The native fluorescence signal of RFP1 was detected from 610 to 700 nm with another PMT.

2.10 Analysis of the bioluminescence recordings

Various methods have been tested to evaluate the bioluminescence imaging data, revealing, that calculating the period length by hand is the most reliable way. However, this does not state the significance of the analyzed rhythm. Further, since the method is a rather subjective assessment, the approach might not be the best choice for studies, in which more than one person is analyzing the data. To generalize the evaluation of the data and to ensure its comparability across experimenters, I relied on the expertise of Jade Atallah (University of Toronto, Mississauga), who kindly provided a custom written script for the analysis within the MATLAB computing environment (The Mathworks, Inc., Natick, MA, USA). By execution of the MATLAB script, the raw-data first gets low-pass filtered to reduce high-frequency noise, which results from short-term intensity fluctuations in the measurement (e.g. cosmic rays, hitting the EMCCD chip). Subsequently, the smoothed data undergoes MESA (maximum entropy spectral analysis) and autocorrelation analysis. Both methods are proven means to detect rhythmicity within a given dataset (reviewed by Dowse, 2013).

The autocorrelation function aligns the time series with itself and then sets the two series out of phase by a certain time interval (e.g. 24 h). The correspondence of the two displaced time series yields the correlation coefficient, which allows the quantification of the regularity and period of the signal. The rhythmicity index (RI, height of the third peak of the autocorrelogram) is a measure of significance of the identified rhythms and can be used for statistical analysis. A 95% confidence interval was applied as a criterion for the significance of the identified rhythmicity. A dataset is usually considered rhythmic if the peaks of the autocorrelogram repeatedly equal or exceed the confidence interval (reviewed by Dowse, 2013). However, there is room for subjective interpretation and it is always worthwhile to take a second look on the data oneself (reviewed by Dowse, 2009 and 2013).

The second method, which was used for evaluation, the MESA, is based on the Fourier transformation, but is additionally supported by stochastic modeling such as an autoregressive (AR) function. The correlation of the AR model to the data yields the

correlation coefficients, from which the spectrum is calculated. MESA provides the highest possible resolution, while eliminating most of the problems that ordinary Fourier analysis encounters (reviewed by Dowse, 2013). In the field of chronobiology, MESA became the preferred tool for the analysis of short and noisy time-series (reviewed by Dowse, 2013). For a comprehensive explanation of the algorithms that underlie MESA, have a look at Ulrych and Bishop's review (1975) of the topic's full scope.

3 Results

3.1 Characterization of the *Gal4*-lines

3.1.1 The expression pattern of *dvPdf-Gal4*

To analyze the morphology of the lateral clock neurons, I chose suitable *Gal4* lines and identified the included cells by their neurochemistry. I selected four driver lines that–cover all lateral clock neurons of *Drosophila melanogaster*. The *Pdf-Gal4* and *dvPdf-Gal4* lines were already well described and they are known to drive expression in all PDF expressing LN_vs (Fig. 8; Renn *et al.*, 1999; Bahn *et al.*, 2009). The *dvPdf-Gal4* line additionally drives expression in the 5^{th} s-LN_v and four LN_ds, of which three do not express CRY (Fig. 13 C-F; Bahn *et al.*, 2009; Guo *et al.*, 2014). The included CRY immunoreactive LN_d is also co-expressing ITP (Fig. 13 G-I).

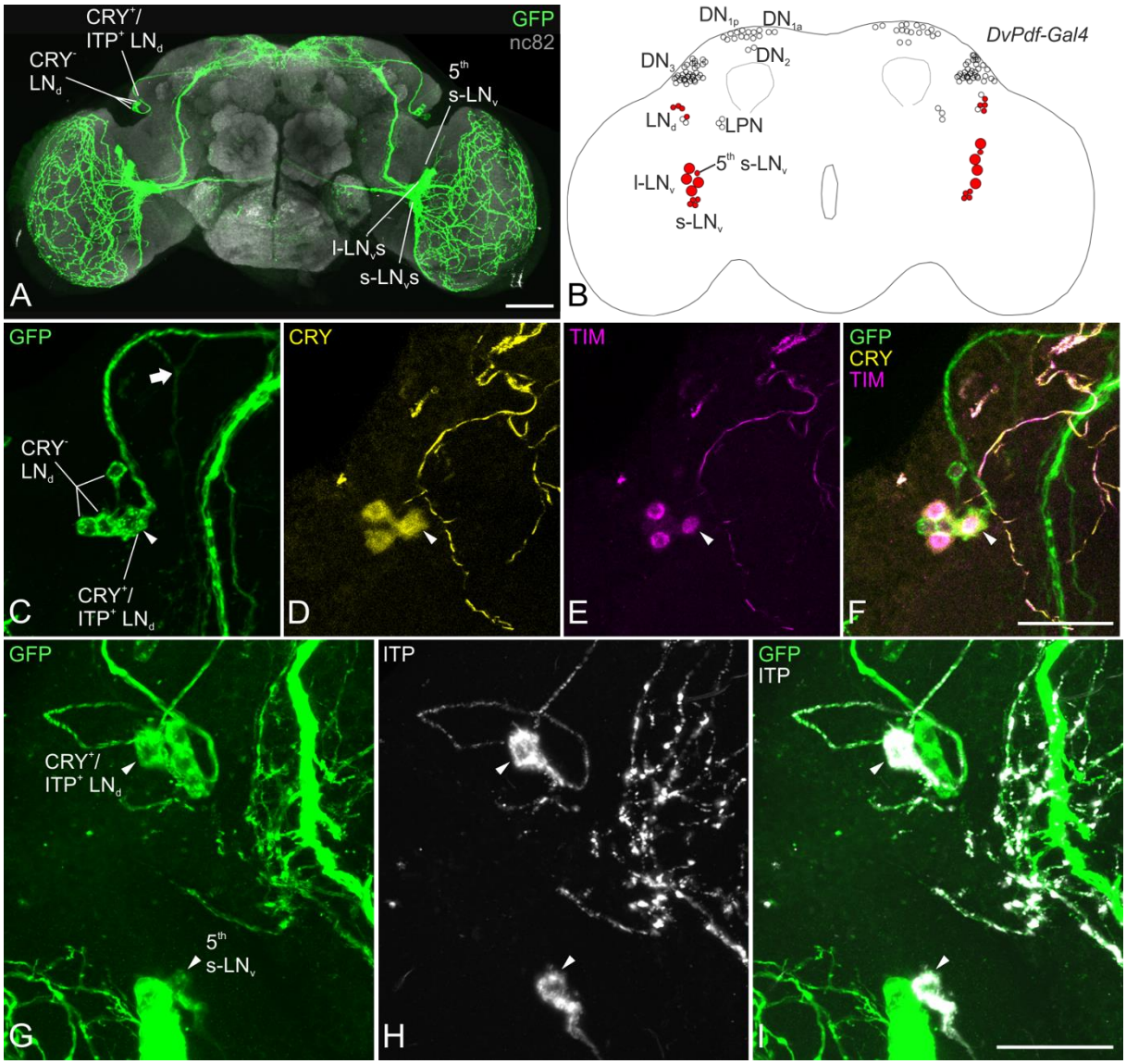

Fig. 13: Characterization of the LN$_d$s included in the *dvPdf-Gal4* driver. (A) GFP (green) and nc82 reference staining (gray) to show the overall expression pattern of the driver-line. (B) Overview of the clock neurons that are addressed by the *dvPdf-Gal4* driver. The line drives expression in all PDF$^+$ LN$_v$s, as well as in the 5th s-LN$_v$ and four LN$_d$s. (C) *DvPdf-Gal4* driven *UAS-myr-GFP* expression in four LN$_d$s. (D) Anti-CRY staining, showing that only one out of the four addressed LN$_d$s expressed the intracellular photoreceptor (arrowhead). The same neuron co-expressed ITP (shown in G-I) and sends the characteristic projections to the ipsilateral accessory medulla (arrow in C). (E) Anti-TIM staining as a marker for clock neurons showed higher intensities in the CRY expressing dorsolateral neurons compared to non-CRY LN$_d$s. (F) Merge of the previous channels. (G-I) Anti-ITP immunostaining revealed that one of the *Gal4*-targeted LN$_d$s is the CRY$^+$/ ITP$^+$ LN$_d$ (upper arrowhead), and likewise labeled the 5th s-LN$_v$. Scale bar in A = 50 µm. Scale bar in F and I = 25 µm.

3.1.2 The expression pattern of *RI6C05-Gal4*

I crossed the *RI6C05-Gal4* line to a 10X GFP reporter, and the brains were stained for the clock components TIM, PDF, CRY and ITP (Fig. 14). I found GFP signal in two dorsal neurons and in two, rarely in three, dorsolateral neurons (Fig. 14 A). Four clock neurons per brain-hemisphere could be identified by TIM immunoreactivity (Fig. 14 C, G, H). The dorsal neurons, which expressed GFP, CRY and TIM, were located in the anterior part of the brain, hence they were identified as $DN1_a$ (Fig. 14 C). Two TIM immunoreactive neurons were situated ventrally to the lateral horn (LH) in the dorsolateral brain (Fig. 14 C, G, H). These neurons belong to the LN_d cell cluster and express CRY but not ITP (Fig. 14 C-E, I, J, L). A third dorsolateral non-clock neuron appears to be weakly GFP positive in some brains (asterisk in Fig. 14 C), however, the soma of this neuron is smaller and therefore distinguishable from the dorsolateral clock cells, and the projections are barely visible due to the weak GFP expression. Additionally, there are two non-clock cells innervating the gnathal ganglion and the saddle, and sparse GFP signal in the optic lobes (Fig. 14 A).

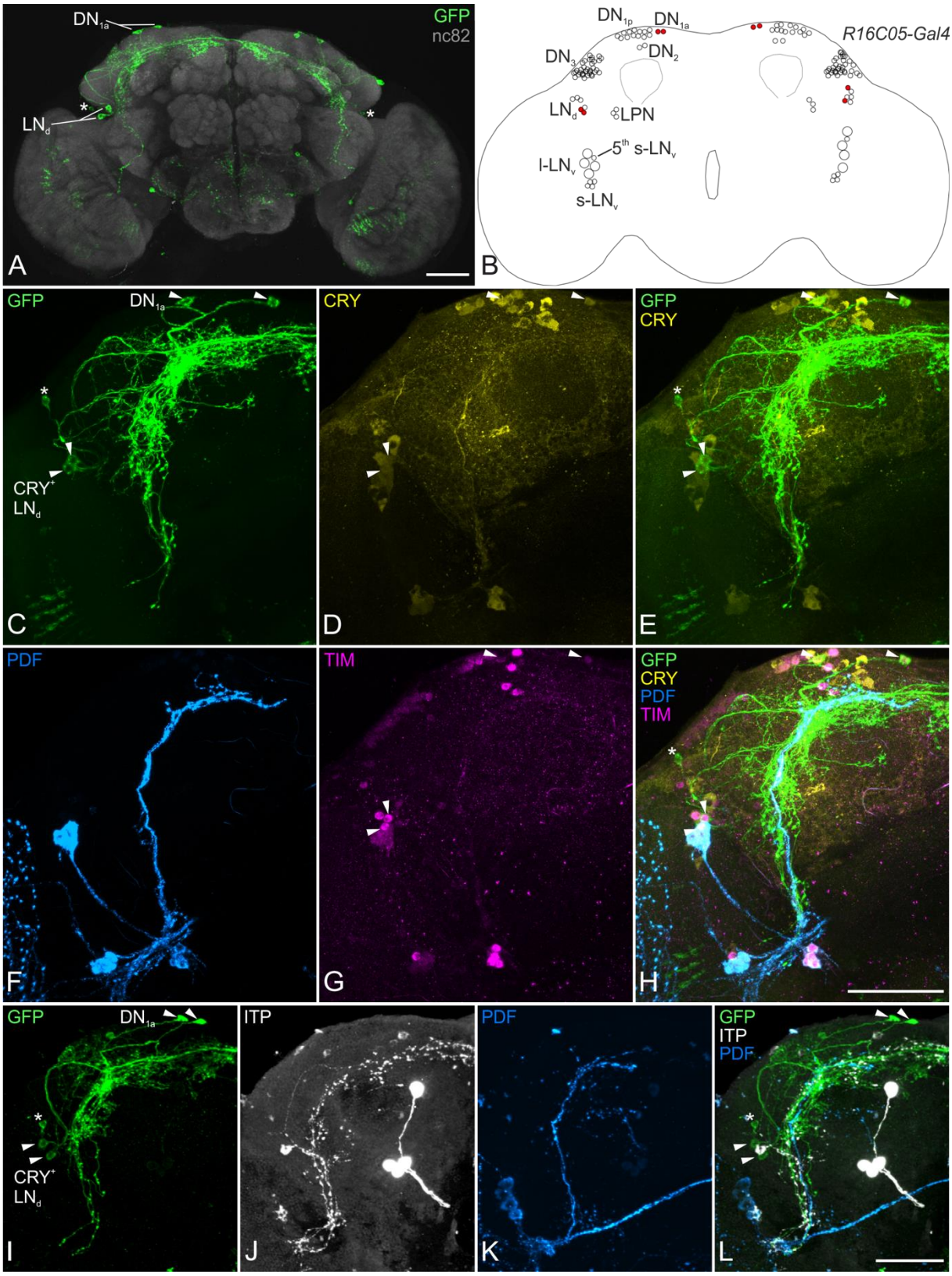

Fig. 14: Characterization of the *R16C05-Gal4* driver. (A) GFP (green) and nc82 neuropil staining (gray). (B) Overview of the clock neurons that are included in the *R16C05-Gal4* line. Alongside two dorsolateral neurons (LN_d), there are two anteriorly located dorsal neurons (DN_{1a}) addressed per hemisphere. (C-E) GFP and CRY co-staining. (F-G) PDF and TIM immunostaining. (H) Merge of channels C-G. (I-L) Staining of ITP, which is expressed in two clock neurons, the 5^{th} s-LN_v and one of

the CRY$^+$ LN_ds. Both LN_ds lack expression of ITP. A non-clock neuron in the dorsolateral brain was consistently labeled with GFP (asterisk). Scale bars = 50 µm.

3.1.3 The expression pattern of *R54D11-Gal4*

The previously described GFP reporter and antibodies were used to identify the neurons included with the *R54D11-Gal4* line (Fig. 15). GFP signal was observed in the ocelli, the gnathal ganglion, and in some small cells that were located anteriorly in the brain and innervate the bulb (Fig. 15 A). In addition, two neurons per brain-hemisphere also expressed GFP and could be identified as clock neurons by consistent labeling with TIM immunostaining (Fig. 15 C, G, H). Both lateral clock neurons express the circadian photoreceptor CRY and co-staining with PDF and TIM anti-sera revealed that the ventrally located neuron is the PDF lacking 5th s-LN_v (Fig. 15 C, F-H). I confirmed this result and further characterized the included CRY expressing LN_d by co-staining the circadian clock component ITP, which is reported to be expressed by one LN_d and the 5th s-LN_v exclusively among the clock cells (Johard *et al.*, 2009). Both lateral cells that are addressed by the *R54D11-Gal4* driver were immunoreactive to ITP anti-sera, showing that these are the 5th s-LN_v and the ITP/ CRY co-expressing LN_d (Fig. 15 I-L).

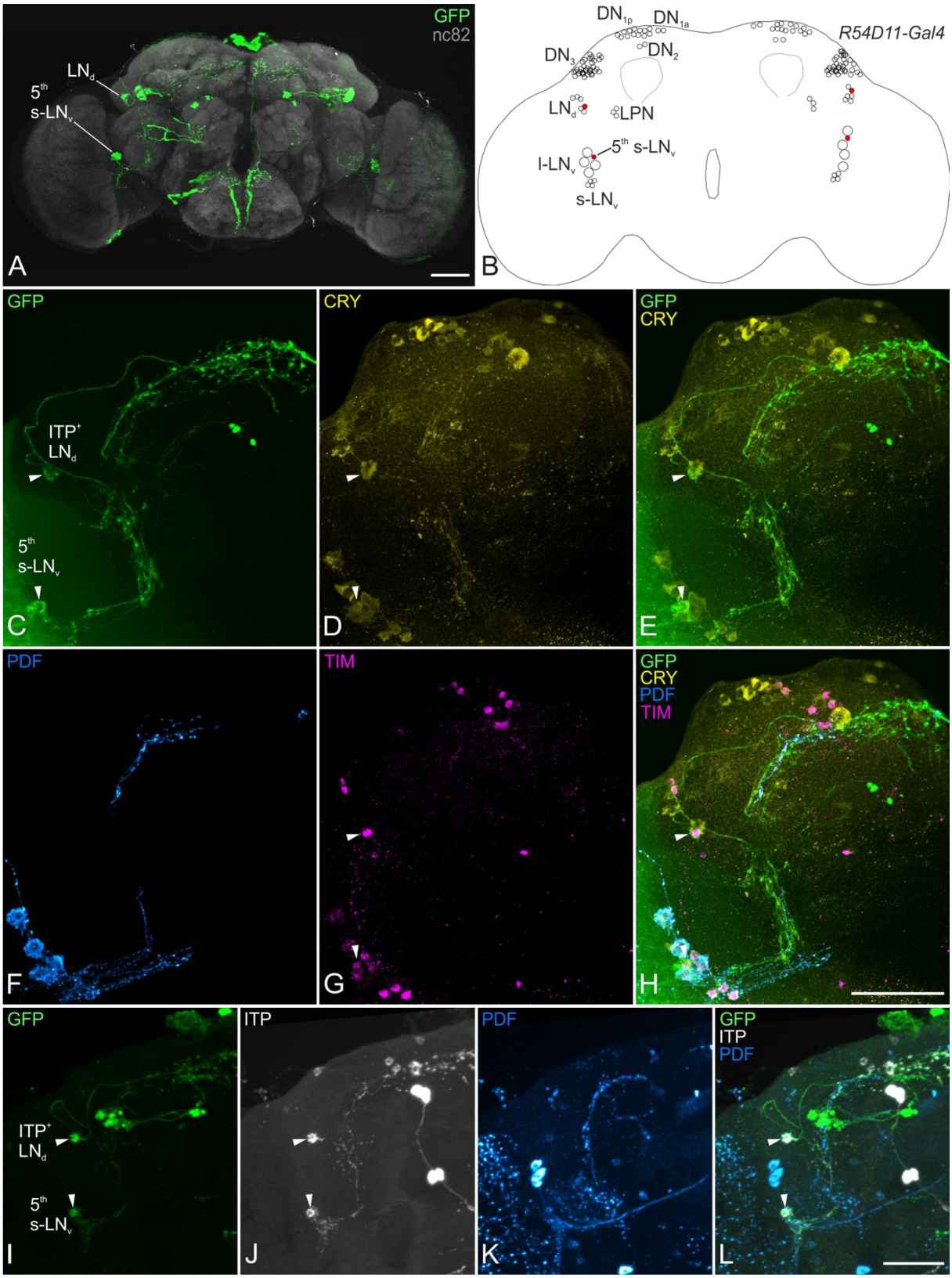

Fig. 15: Characterization of the *R54D11-Gal4* driver. (A) Antibody-labeling of myr-GFP (green) with nc82 neuropil staining (gray). (B) Overview of included clock neurons. The *R54D11-Gal4* line drives expression in the 5th s-LN$_v$ and one LN$_d$. (C-D) The lateral clock neurons both express the circadian photoreceptor CRY (arrowheads). (F-G) Co-labeling with PDF and TIM anti-sera and (H) merge of the

previous channels. (I-L) Triple staining for GFP and the clock components PDF and ITP. Scale bars = 50 µm.

3.2 The single-cell morphologies of the lateral clock neurons

3.2.1 The differences within the l-LN$_v$ cluster

The morphology of the PDF expressing lateral clock neurons have already been described in detail (Helfrich-Förster and Homberg, 1993; Helfrich-Förster, 1995; Helfrich-Förster *et al*., 2007). The M-cells (PDF expressing LN$_v$s) are a heterogeneous group of four small (s-LN$_v$s) and four large (l-LN$_v$s) ventrolateral neurons per brain-hemisphere. The two subgroups show different projection patterns, but are considered to be indistinguishable within the sub clusters of s-LN$_v$s and l-LN$_v$s.

The *Pdf-Gal4* driver line was used to address only the PDF expressing s- and l-LN$_v$s for analysis with the Flybow-reporter system. Since the projection pattern of PDF-cells is well known in respect to their location in the brain, I employed a commonly utilized PDF-antibody as a counterstain reagent instead of a neuropil-labeling compound, allowing to examine whether the overall network looks regular.

Out of 275 brains with FP expression in the s-LN$_v$s, only 14 cells were labeled individually. Here, I could not find any systematic morphological differences among them compared to the already known s-LN$_v$ projection pattern (described in detail by Helfrich-Förster *et al*., 2007). In contrast, the analysis of 166 single labeled l-LN$_v$s revealed a yet completely unknown morphological subclass of large ventrolateral clock neurons. One third of the analyzed l-LN$_v$s showed a restricted projection pattern on the surface of the ipsi- and contralateral ME compared to the so far described morphology (Fig. 16 C).

Due to the lack of further distinctive features, the l-LN$_v$ with its newly found characteristics will henceforth be referred to as “extra“ l-LN$_v$ (l-LN$_v$x) for the ease of discrimination. The majority of l-LN$_v$s (three out of four per hemisphere) show between four to five main projections on the surface of the ipsilateral ME, resulting from second order branching of the ipsilateral ME branch (yellow 3 in Fig. 16 K) and between two and four main projections on the surface of the contralateral side, which

are further subdividing towards the distal part of the ME (Fig. 16 A, B). Both hemispheres are connected via a single projection of each l-LN$_v$ that runs through the POC without additional branching in the central brain (Fig. 16 K).

The l-LN$_v$x shows the same initial branching pattern (shown in Fig. 16 K) as the other l-LN$_v$s, but innervates only the proximal area of the ME surfaces (Fig. 16 C, E). The two ME branches (blue 2 and yellow 3 in Fig. 16) bifurcate at the anteromedial edge of the ME, one branch runs ventrally, whereas the other projects dorsally along the medial ME surface (Fig. 16 C).

Both l-LN$_v$ types possess several fine fibers, originating from the first branching point, which invade the ipsilateral AME and proceed into the ME serpentine layer (Fig. 16 J). Furthermore, both l-LN$_v$ subclasses contribute to the ventral elongation of the ipsilateral AME (AME$_{vel}$, Fig. 16), whereas the projection in the AME$_{vel}$ of the l-LN$_v$x is not as far-reaching as the one of the remaining l-LN$_v$s (Fig. 16 A and C). Therefore, the AME$_{vel}$ of the l-LN$_v$x turns to the posterior part of the ME to a lesser extent compared to the residual l-LN$_v$s.

Since I also obtained brains in which one l-LN$_v$x was individually labeled among the other l-LN$_v$s (Fig. 16 E-H), it can be ruled out that optic lobe injury or impaired pathfinding caused the morphology of the newly described l-LN$_v$x. In these brains, the remaining l-LN$_v$s show their characteristic projection pattern without any abnormalities of the network on the surfaces of the ME (Fig. 16 F). In addition, the overall staining pattern against the PDF peptide was unaffected in brains with individually labeled l-LN$_v$x, showing that the overall network was intact and had not been damaged during dissection (Fig. 16 G).

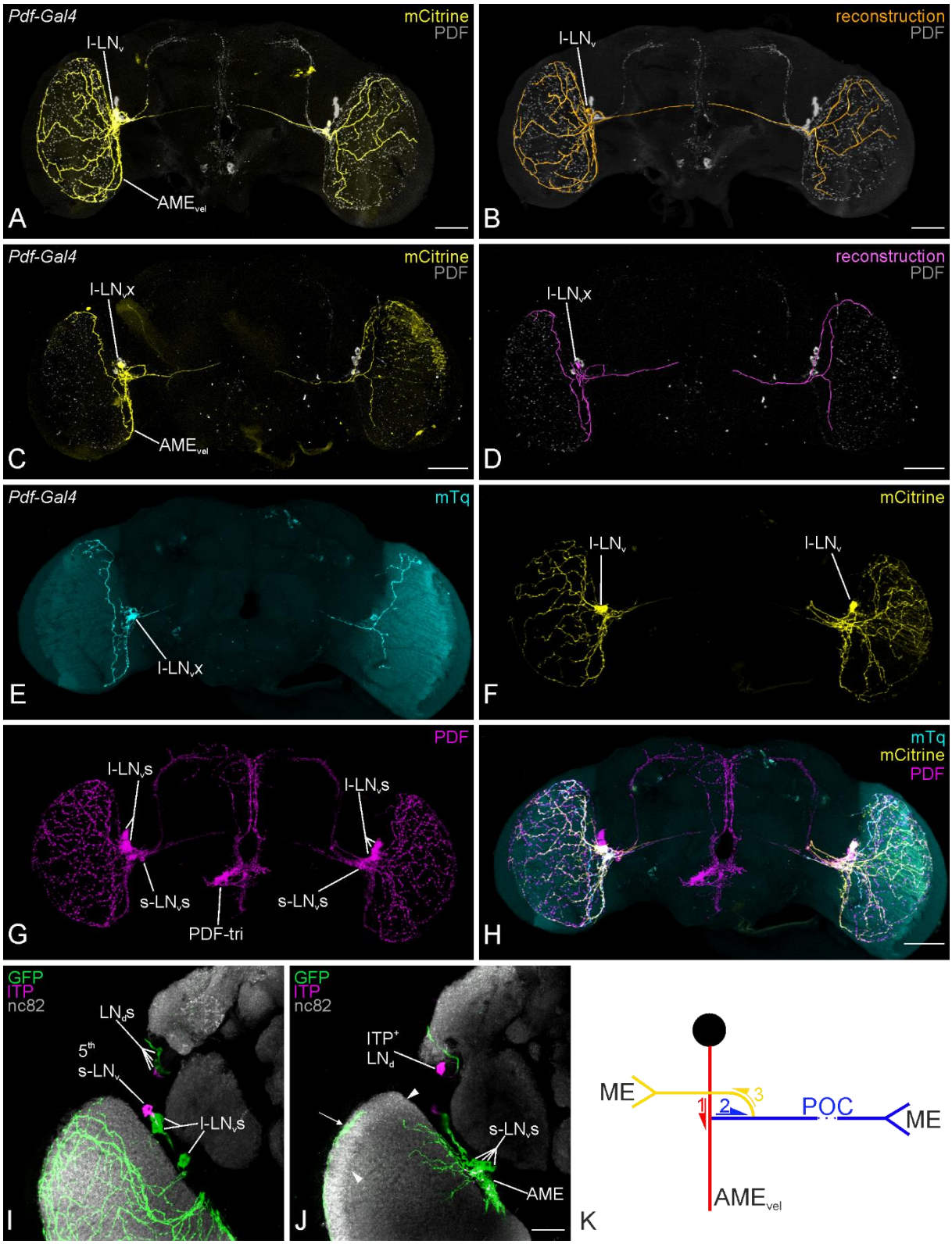

Fig. 16: Heterogenic morphology of the l-LN$_v$s. (A-B) Expression of mCitrine (yellow) in a single l-LN$_v$ and its reconstruction (orange) showing the already described morphology. (C-D) mCitrine expression (yellow) and reconstruction (magenta) of a single l-LN$_v$ showing the so far undescribed anatomy of a subtype of l-LN$_v$s ("extra" l-LN$_v$) and the morphological heterogeneity within this neuronal group. (E-H) Controlstaining for l-LN$_v$ heterogeneity. Flybow-reporter expression driven by *Pdf-Gal4*. (E) Single l-LN$_v$ expressing mTorquoise in the left brain-hemisphere showing the newly

found morphology. (F) Two l-LN$_v$s expressing mCitrine, one in each hemisphere, showing the already described projection pattern. (G) PDF staining showing the well-characterized projection pattern of PDF$^+$ LNs. (H) Merge of the previous channels. (I-J) Projections of the l-LN$_v$s are extensively invading the serpentine layer of the ME. The majority of l-LN$_v$ neurites run on the surface of the ME (I; arrow in J), but a remarkable proportion is invading the serpentine layer (J). The boundary between the inner and outer layers can be seen in the dorsal and distal area of the medulla (indicated with arrowheads in J). (K) Schematic representation of the initial branching pattern of l-LN$_v$s. The primary projection (red) runs ventrally from the soma (black sphere) along the medial edge of the ipsilateral ME and forms the ventral elongation of the accessory medulla (AME$_{vel}$). A secondary fiber (blue) branches off from the initial projection, runs through the posterior optic commissure (POC) and is thereby connecting both hemispheres, to eventually arborize onto the surface of the contralateral ME. The fiber network on the ipsilateral ME is built by the branches of a third side-projection (orange) which separates from the fiber that is running through the POC. Scale bars = 50 µm.

3.2.2 The morphology of the 5th s-LN$_v$

The *dvPdf-Gal4* and the *R54D11-Gal4* driver lines were used to unravel the projection pattern of the so far inconclusively described 5th s-LN$_v$. Using the *Flybow2.0B*-construct, I obtained eight individually labeled 5th s-LN$_v$s. Despite most analyzed samples showing only sparse labeling, the majority of specimen had more than one cell expressing the same fluorescence protein. Nonetheless, tracing the entire projections of a neuron was still feasible in brains in which only one additional cell had been labeled by the same reporter. Hereby, it was possible to analyze the morphology of in total 19 5th s-LN$_v$s.

The soma of the neuron is situated in the lateral cell body rind (LCBR), medially to the anterior part of the ME and lateral to the anterior ventrolateral protocerebrum (AVLP) (rAVLPl, Fig. 17 A; Fig. 18, upper panel). Only few fibers run onto the surface of the ME after invading the AME. Most projections run along the medial edge of the ME at the level of the serpentine layer, which is invaded by several fine fibers. The projections exit the AME along the initial part of the POC and run to the posterior side of the brain around the posterior ventrolateral protocerebrum (PVLP; Fig. 17; Fig. 18, upper panel). In the posterior brain, the main bundle leaves the POC and proceeds dorsally into the posterior lateral protocerebrum (PLP) where the fibers start to branch. The neurites leave the POC either as a fascicle or as separate fibers, but there is always one main branch, which is slightly thicker than the others (Fig. 18, upper panel). This main projection runs in parallel to the remaining fibers until it reaches

the ventromedial LH (Fig. 17 D). There, it turns and proceeds more anteriorly through the superior clamp (SCL), and from there into the superior lateral protocerebrum and superior medial protocerebrum (SLP and SMP, respectively). In the SMP the neurite turns even more anterior, runs through the middle dorsal commissure (MDC) into the contralateral SMP, and then turns back to the posterior part of the brain. From here, the main branch projects to the center of the contralateral SLP. The majority of varicose endings that branch off the dorsal main projection can be observed in the SMP of both hemispheres.

A fine neurite (1, Fig. 18, upper panel) separates from the main branch in the SCL and runs ventrally to the superior intermediate protocerebrum (SIP) into the ventrolateral SMP, where it usually reconnects with the main branch. A secondary neurite (2, Fig. 18, upper panel), which originates from the main projection in the lateral PLP, runs into the ventral LH and furcates into small fibers that terminate in the LH. Another secondary fiber (3, Fig. 18, upper panel) branches off from the main projection in the dorsolateral PLP, proceeding lateral via the PLP-LO fascicle (PLP-LOF) to the lobula (LO).

The remaining neurites, which run through the PLP project to the dorsal brain in parallel to the main branch (4, Fig. 18, upper panel). In the ventromedial LH, where the main branch turns to the anterior side, the other fibers proceed dorsal and run through the dorsolateral SCL into the SLP, where they end in close vicinity to the dorsal main branch.

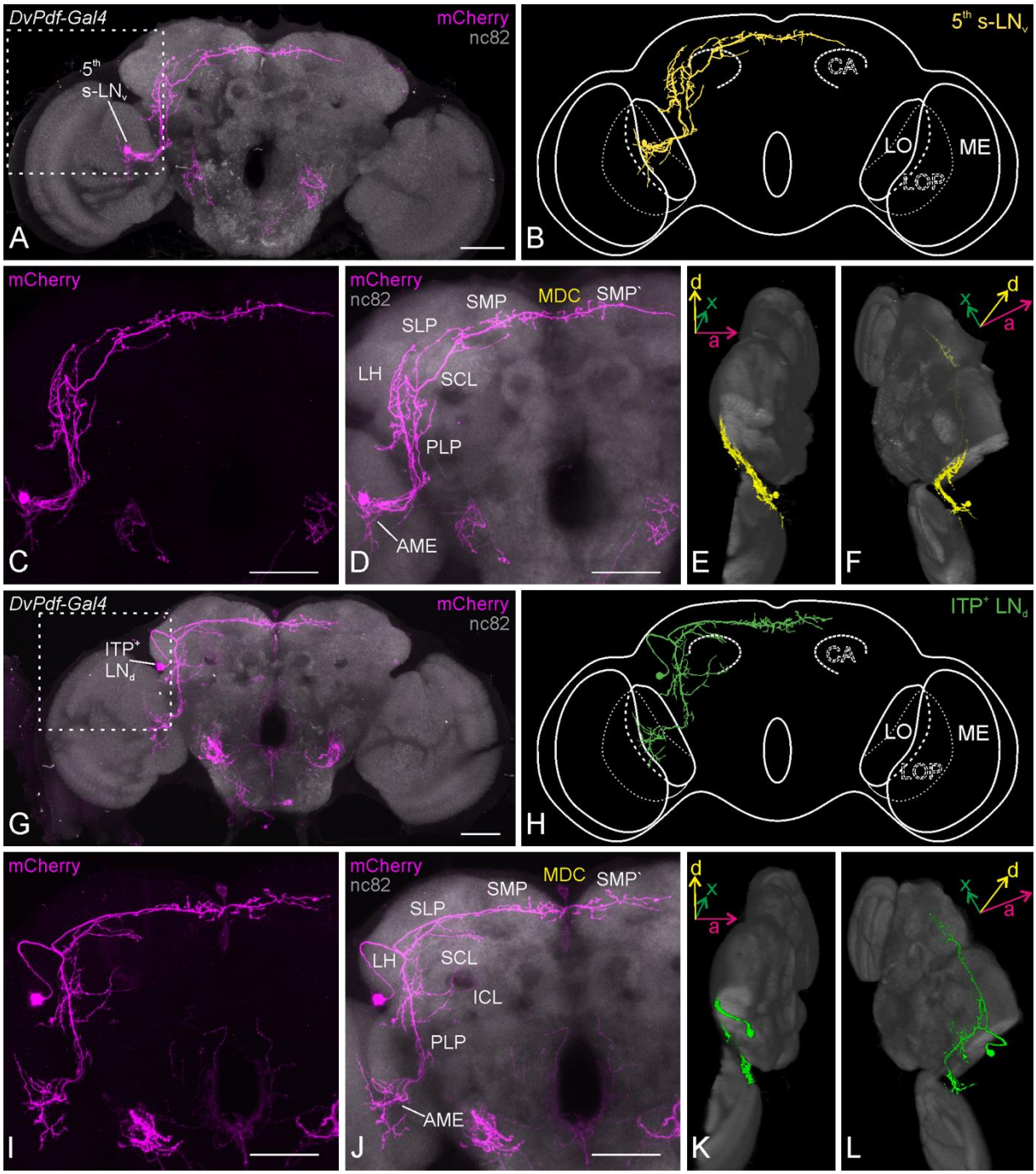

Fig. 17: Morphology of the 5th s-LNv and the ITP expressing LNd. (A) Overview of the 5th s-LNv expressing mCherry (magenta) and nc82 neuropil staining (gray) shown as maximum z-projection. The part that was cut out for the 3D view (E-F) is shown by the dashed square. (B) Scheme of the 5th s-LNv. (C-D) Magnification of maximum z-projection with average z-projected neuropil (gray). (E-F) Anterior-lateral (E) and posterior-lateral (F) view of the 5th s-LNv in the brain. The optic lobe of the left hemisphere was partly cut out (as indicated in A) for a nicer view on the soma and the initial branching. (G-L) Morphology of the CRY+ /ITP+ LNd. (G) Maximum z-projection of amplified mCherry expression (magenta) with nc82 neuropil staining (gray). The dashed square indicates the section that was cut out for the 3D view in K and L. (H) Schematic overview of the same neuron. (C-D) Magnification of the maximum z-projected neuron together with an average z-projection of the neuropil staining (gray). (E-F) Anterior-lateral (E) and posterior-lateral (F) view of the neuron and its location in the brain. The dorsal part of the left optic lobe was cut out (indicated in G) for improved visibility of the projections

running towards the optic neuropils. Orientation of the brain (E-F and K-L) is declared by the coordinate system. A, anterior; d, dorsal; x, lateral axis. ME, medulla; LO, lobula; LOP, lobula plate; CA, calyx; AME, accessory medulla; PLP, posterior lateral protocerebrum; LH, lateral horn; SCL, superior clamp; ICL, inferior clamp; SLP, superior lateral protocerebrum; SMP, superior medial protocerebrum; MDC, middle dorsal commissure; SMP`, contralateral superior medial protocerebrum. Scale bars = 50 µm.

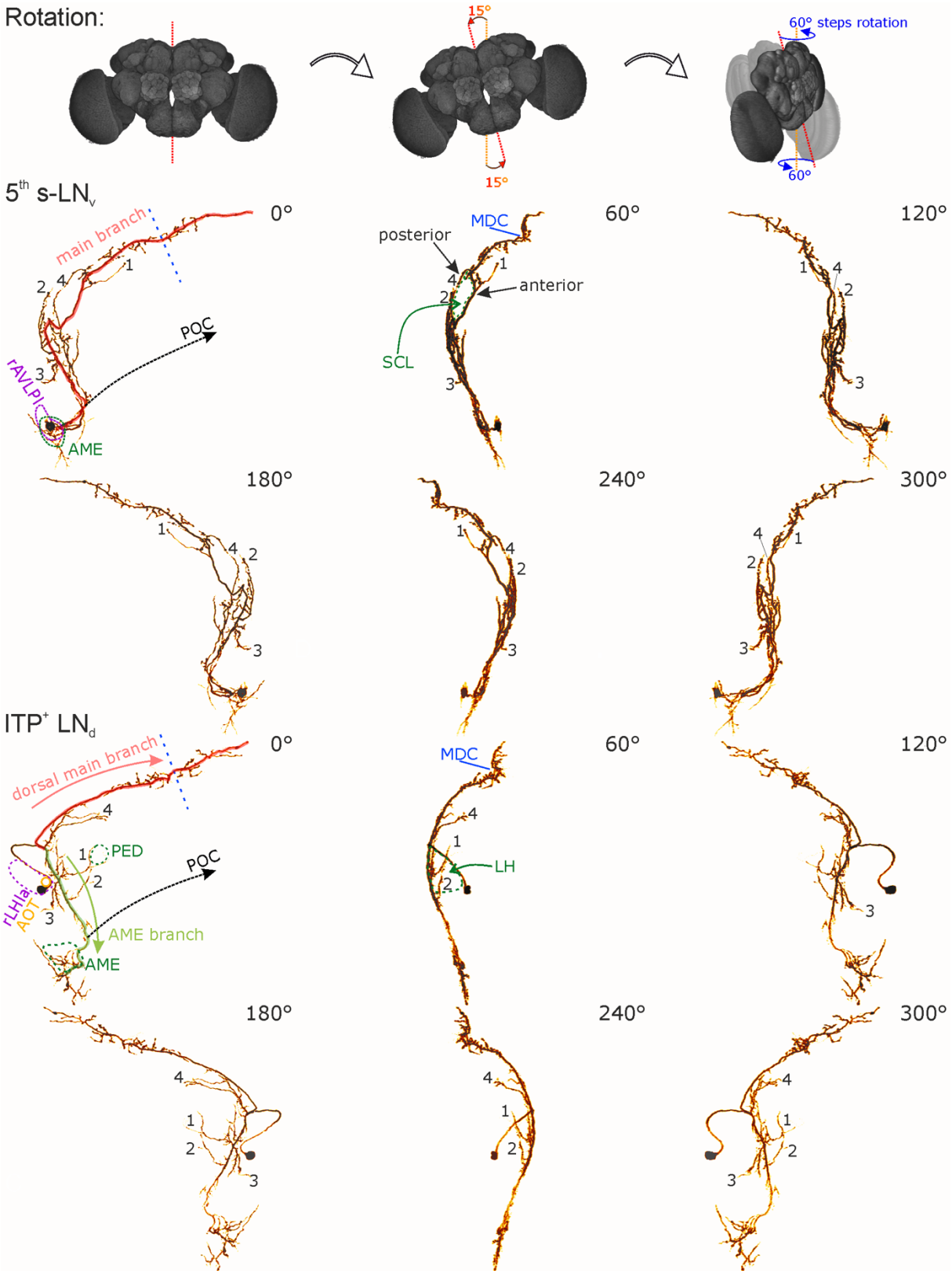

Fig. 18: Characteristic anatomical features of the ITP expressing LNs. Spatial visualization for easier comprehension of how the brain was tilted and rotated for the single-cell description (top panel). First, the brain was tilted by 15° in respect to the dorsoventral midline (orange). The hence resulting, slanted dorsoventral midline (red) was then rotated around the prior axis (orange) in 60° steps. 5th s-LNv single-cell projection pattern rotated and viewed from different angles in 60° steps

(middle panels). In the plane view (0°) the main branch was labeled (red) and characteristic branches were numbered for further description (see main text). For easier orientation, the dorsoventral midline is indicated (dashed blue line) and landmark fiber bundles are implied (POC, posterior optic tract). Included neuropil structures are shown in dark green. The location of the cell body is highlighted in purple (rAVLPl, cell body rind laterally to the anterior ventrolateral protocerebrum). In the dorsal brain, the main projection reaches into the contralateral hemisphere via the middle dorsal commissure (MDC). Rotated ITP$^+$ LN_d single-cell projection pattern (lower panels). The dorsal and ventral main projections were labeled (red and light green, respectively) and characteristic branches were numbered for detailed description (see main text). The dorsoventral midline (dashed blue line) and landmark fiber bundles are indicated (AOT, anterior optic tract; POC). Like the 5th s-LN_v, the LN_d's dorsal main projection is crossing the dorsoventral midline via the MDC (blue). AME, accessory medulla; SCL, superior clamp; PED, mushroom body peduncle; rLHla, cell body rind lateroanterior to the lateral horn.

3.2.3 The morphology of the ITP and CRY co-expressing LN_d

Two different *Gal4* lines were used to look at the arborization pattern of the only ITP expressing cell among the six LN_ds. The *dvPdf-Gal4* with a broad expression in the clock network and the *R54D11-Gal4* with a more restricted expression in only two clock neurons, the 5th s-LN_v and the LN_d of interest (Fig. 15). Previously, it was shown that the latter neuron has two main branches, one invading the superior neuropils of the brain and one running ventrally towards the AME (Helfrich-Förster *et al.*, 2007; Johard *et al.*, 2009). However, it was neither described whether it actually innervates the AME, nor if it is projecting into the contralateral hemisphere in the dorsal brain.

I obtained 12 single labeled ITP expressing LN_ds of individual brains. After adding sparsely labeled brains to my analysis, I was able to study the morphology of 31 cells in detail.

The cell body of the neuron is situated close by the boundary between the anterior and posterior ventrolateral protocerebrum, lateroanterior to the lateral horn (rLHla, Fig. 17 J; Fig. 18, lower panel). Dorsally of the soma runs the anterior optic tract (AOT) and the LH starts to expand on the posterior side (Fig. 17 J). Initially, the neuron projects medially around the AOT, then proceeds dorsally on the anterior surface of the LH. The fiber runs around the LH to the posterior surface of the neuropil, where it branches for the first time.

One main branch (AME branch, see Fig. 18, lower panel) descends towards the AME and passes through the PLP, where it vastly branches. Three smaller neurites separate from the ventral main branch in the dorsal PLP. Two projections run medially, from which one encompasses the peduncle (PED) of the ipsilateral mushroom body (MB). The dorsal projection (1, Fig. 18, lower panel) innervates the SCL, whereas the ventral one (2, Fig. 18, lower panel) runs into the inferior clamp (ICL). Another neurite proceeds more laterally (3, Fig. 18, lower panel) and reaches from the PLP into the dorsomedial part of the LO via the PLP-LOF. The AME branch leaves the PLP along the POC and projects along the posterior surface of the PVLP to the anterior part of the brain. In the anterior brain, at the level of the boundary between the PVLP and the AVLP, the ventral main projection invades the AME and proceeds into the serpentine layer and onto the surface of the ME.

The second main projection (dorsal main branch, Fig. 18, lower panel) originates from the initial branching in the LH and innervates the superior neuropils. The neurite runs in the posterior part of the brain and therefore only innervates the SLP and the SMP, but not the SIP. The fiber crosses the dorsoventral midline and reaches into the contralateral hemisphere via the MDC. In the contralateral brain-hemisphere, the neurite innervates the SMP and terminates a few microns after entering the SLP. The dorsal main branch shows varicose endings in the SMP of both brain-hemispheres, most of them are in close vicinity to the dorsoventral midline near the PI.

A second dorsal projection (Fig. 18, lower panel), which also originates from the initial branching point in the posterior LH, runs in parallel to the dorsal main branch, but slightly more ventral. The neurite branches into two fibers that leave the medial center of the LH. The fiber that runs more dorsally compared to the other, projects between the dorsal boundary of the SCL and the ventral boundary of the SLP, and terminates in the ventral part of the SLP. The ventral fiber runs in parallel but slightly more anterior in the brain. It also projects between the ventral SLP and the dorsal SCL, but it ends in the dorsomedial SCL, close to the posterior edge of the SIP.

3.2.4 The morphology of the two sNPF and CRY co-expressing LN_ds

The *R16C05-Gal4* driver line was used to disentangle the projections of the sNPF and CRY containing LN_ds from the remaining dorsolateral and dorsal clock neurons. In this driver line, only the two sNPF and CRY expressing LN_ds and the DN_{1a}s were addressed, and there was almost no further *Gal4* expression in the adult central brain (see Fig. 14 A). In total 101 sNPF/ CRY co-expressing LN_ds were analyzed, from which 17 were individually labeled.

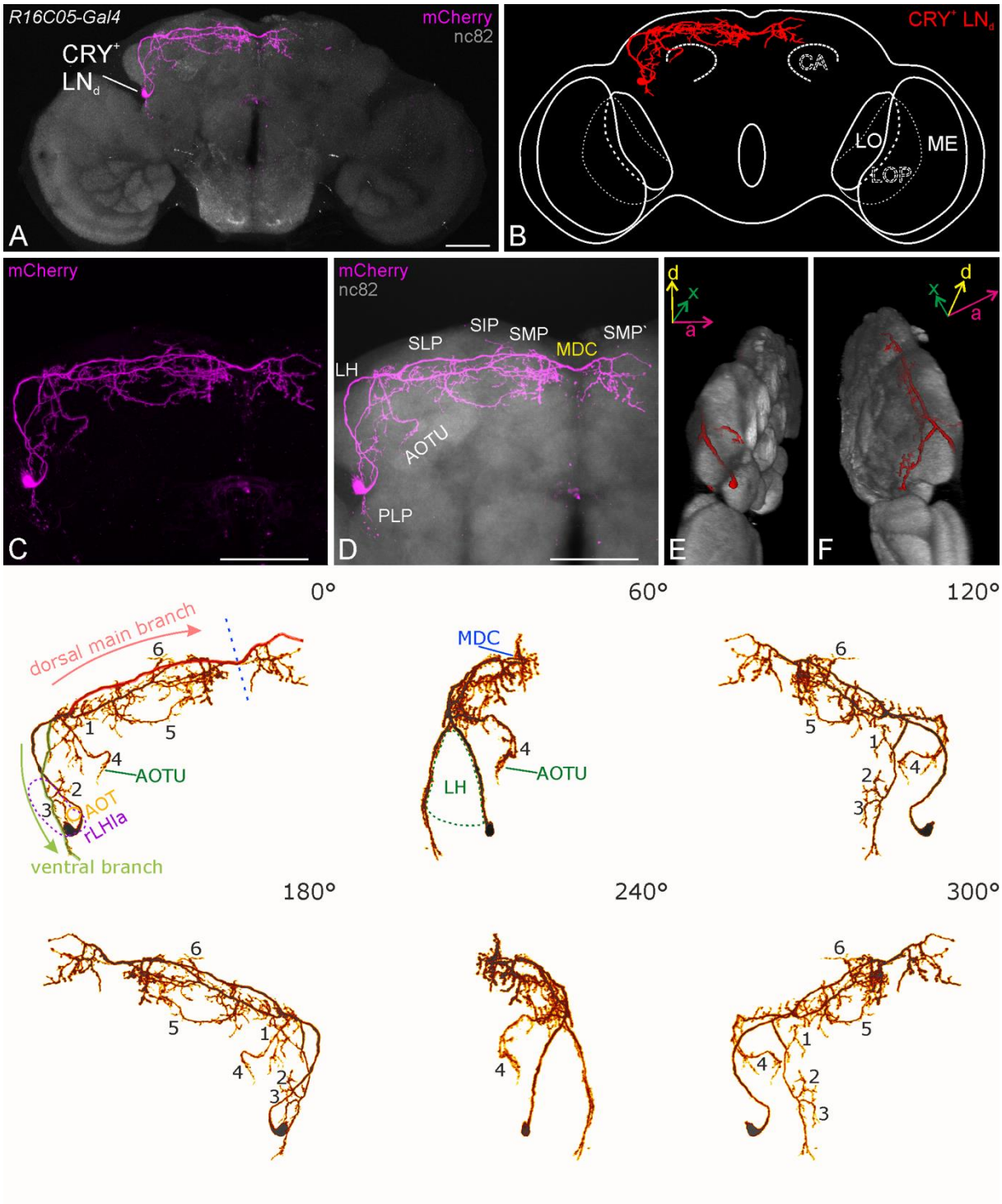

Fig. 19: Morphology of the two sNPF⁺/ CRY⁺ LNds. (A) Depiction of one of the two CRY⁺ but ITP⁻ LNds labeled with mCherry-antibody (magenta) shown together with a nc82 neuropil staining (gray) as maximum z-projection. (B) Schematic overview. (C-D) Magnification and average z-projected neuropil reference staining. (E-F) Anterior-lateral (E) and posterior-lateral (F) view on the 3D brain. The orientation is indicated by the coordinate system. Rotated single sNPF⁺/ CRY⁺ LNd (lower panel). For explanation on how the brain was rotated, see Fig. 18. The dorsal and ventral main branches are labeled (red and light green, respectively) and characteristic branches were numbered for further description in the main text. The dorsoventral midline is indicated (dashed blue line), and landmark fiber bundles are implied (AOT, anterior optic tract) for easier orientation. Additional information on

neuropil structures are shown in dark green, whereas the location of the cell body is highlighted in purple (rLHla). The dorsal main projection contributes to the MDC (blue) and passes into the contralateral hemisphere. A, anterior; d, dorsal; x, lateral axis. AOTU, anterior optic tubercle; AOT; anterior optic tract; ME, medulla; LO, lobula; LOP, lobula plate; CA, calyx; PLP, posterior lateral protocerebrum; LH, lateral horn; SLP, superior lateral protocerebrum; SIP, superior intermediate protocerebrum; SMP, superior medial protocerebrum; MDC, middle dorsal commissure; SMP`, superior medial protocerebrum of the contralateral hemisphere; rLHla, cell body rind lateroanterior to the lateral horn. Scale bars = 50 µm.

The two cell bodies of the CRY expressing LN_ds are located in close range to the other dorsolateral neurons and in most cases, the LN_ds form one distinct cluster. Therefore, the cell bodies of the two neurons are located in the rLHla as well, like the previously described LN_d. At first, the sNPF expressing cells project medially, too, encompassing the AOT, then turn dorsal to run on the surface of the LH to the posterior side of the brain (Fig. 19 D). On the posterior surface, the initial branch bifurcates at the dorsal boundary between the LH and the SLP.

One branch descends towards, but does not innervate the ipsilateral AME (ventral branch, Fig. 19, lower panel). It projects along the lateral edge of the PLP, terminating in close vicinity to the PLP-LOF. On its way ventral, the fiber sends three fine projections to more medially located areas.

The first branch (1, Fig. 19, lower panel) separates from the ventral branch on the posterior surface of the dorsal LH and terminates close to the dorsal main branch, after running through the LH.

The other two medial projections (2, 3, Fig. 19, lower panel) branch off from the ventral fiber at the dorsoventral level of the PED and invade the posterior ventrolateral LH and posterior dorsolateral PLP.

The main projection in the dorsal brain trifurcates on the posterior surface of the lateral SLP shortly after the initial branching. The thinner side branch (4, Fig. 19, lower panel) runs anteriorly on the surface of the SLP and passes into the anterior optic tubercle (AOTU).

Most projections remain in the dorsal part of the central brain (Fig. 19 A). After the trifurcation of the dorsal main branch, the two thicker main branches run in parallel

towards the dorsoventral midline. The more ventrally proceeding projection vastly branches in the SLP and SMP with most varicose terminals located at the ipsilateral, medial border of the SMP. This branch does not pass into the contralateral hemisphere. One projection branches off in the SLP and runs through the SCL into the SMP, terminating very close to the medial border of the ipsilateral SMP (5, Fig. 19, lower panel). Another side branch of the ventrally proceeding dorsal main projection separates in the lateral SMP and projects anteriorly and laterally to reach into the dorsomedial part of the SIP (6, Fig. 19, lower panel).

The more dorsally located main fiber hardly branches in the ipsilateral hemisphere. It crosses the dorsoventral midline via the MDC and innervates the medial- and center part of the contralateral SMP (Fig. 19 D).

3.2.5 The morphology of the three CRY lacking LN_ds

The projection pattern of the CRY absent LN_ds was analyzed by using the Flybow-reporter in combination with the *dvPdf-Gal4* driver, which includes all three CRY lacking cells (see Fig. 13). This combination provided 30 individually labeled non-CRY LN_ds and a total of 56 neurons for analysis (individually labeled cells and sparsely labeled brains).

The cell bodies of these neurons cluster with the other LN_ds, situated dorsally to the AVLP in the rLHla (Fig. 19, upper panel).

The initial projection runs around the AOT and proceeds dorsally on the anterior surface of the LH (Fig. 19, lower panel). It grows along the surface of the LH to the posterior side of the brain, where it turns medially to run into the superior neuropils (Fig. 19, lower panel).

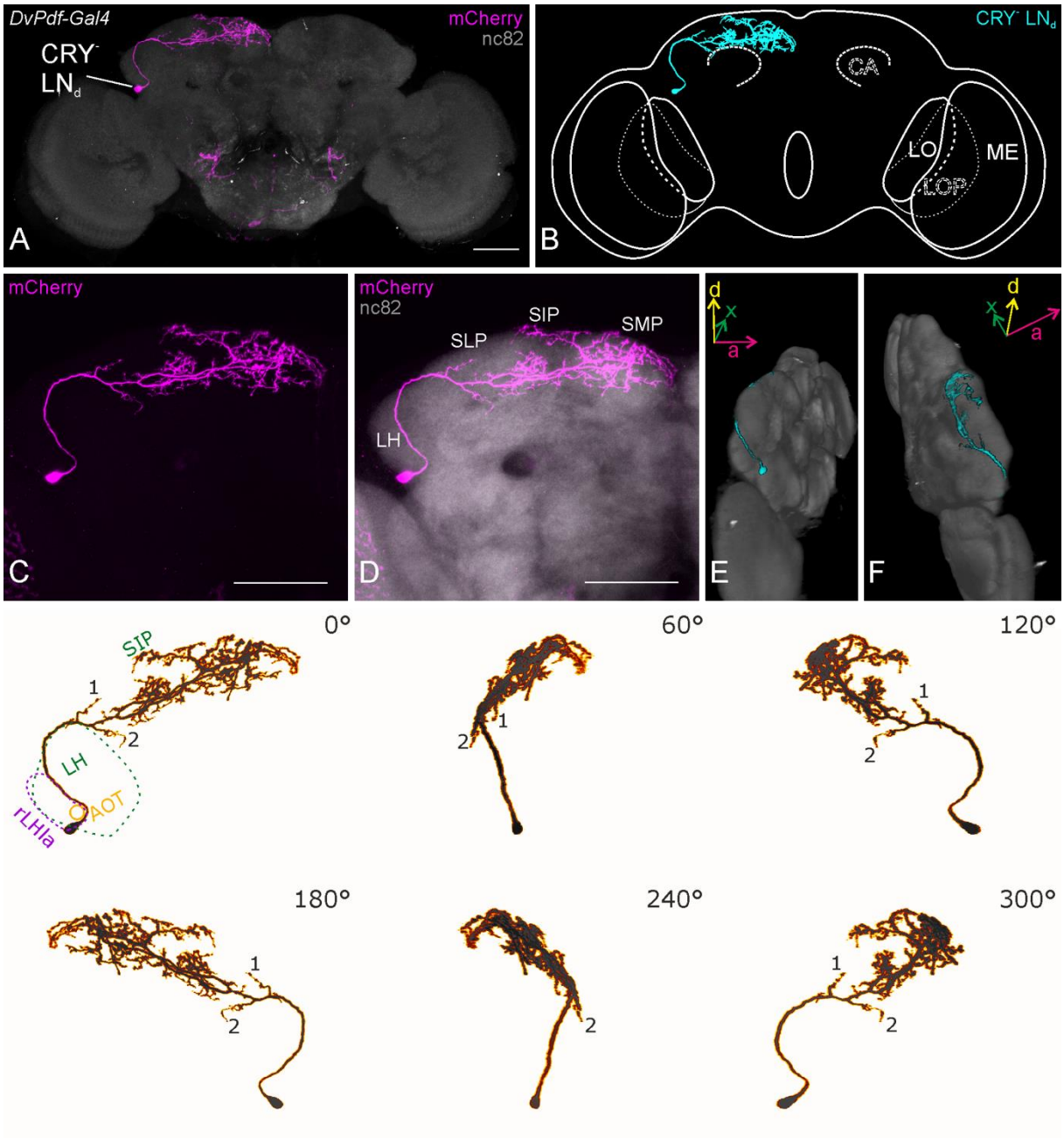

Fig. 20: Morphology of the three CRY lacking LN$_d$s. (A) Exemplary overview of one of the three CRY$^-$ LN$_d$s, labeled with an antisera against mCherry (magenta) and co-stained for the neuropils with nc82 (gray). Maximum z-projection of the neuron. (B) Scheme of a CRY$^-$ LN$_d$. (C-D) Maximum z-projected magnification and average z-projected neuropil staining for reference (gray). (E-F) Anterior-lateral (E) and posterior-lateral (F) view. Projection pattern rotated and viewed from different angles in 60° steps (lower panel; see Fig. 18 for information on rotation). Characteristic branches are numbered for further description in the main text and Landmark fiber bundles are implied in orange (AOT, anterior optic tract). Neuropil structures are shown in dark green and the location of the cell body is highlighted in purple (rLHla). The projections do not cross the dorsoventral midline and are restricted to the ipsilateral brain-hemisphere (see also A and D). A, anterior; d, dorsal; x, lateral axis. AOT, anterior optic tract; ME, medulla; LO, lobula; LOP, lobula plate; CA, calyx; PLP, posterior lateral protocerebrum; LH, lateral horn; SLP, superior lateral protocerebrum; SIP, superior intermediate protocerebrum; SMP, superior medial protocerebrum; MDC, middle dorsal commissure; SMP`,

superior medial protocerebrum of the contralateral hemisphere; rLHla, cell body rind lateroanterior to the lateral horn. Scale bars = 50 µm.

The first side branch (1, Fig. 20, lower panel) leaves the main projection at the posterior dorsolateral edge of the SLP and runs into the same neuropil. The second side branch (2, Fig. 20, lower panel) separates from the main branch slightly more posterior and medial as compared to the first. This fiber projects along the posterior boundary between the LH and the SLP, terminating in close vicinity to the calyx (CA).

The main tract bifurcates on the posterior surface of the SLP and continues in two fibers that run in parallel towards the dorsoventral midline (Fig. 19 D). The dorsal fiber does not ramify before it reaches into the SMP. Most of its branching occurs in the medial ipsilateral SMP, close to the dorsoventral border of the two hemispheres.

The more ventrally located main projection already starts to branch in the SLP, but most of the ramifications can be observed in the SMP (Fig. 19 D). Additionally, one projection separates from the ventral main branch in the SMP, turns laterally, and runs anterior into the dorsal SIP (Fig. 20).

The CRY lacking LN_ds are the only cells of the LN_d group, which do not cross the dorsoventral midline to pass into the contralateral brain-hemisphere (Fig. 19 A).

3.2.6 The estimated projection pattern of the LPN

With only one driver-line being available for the LPN (*clk856-Gal4*, see Fig. 8) and the fact that this line drives expression in more than 170 neurons, the LPN was the most challenging group in respect to the intended single-cell description. Factually, I was not able to reveal the entire projection pattern of this cell group, which was discovered in 2000 and remained obscure ever since (Kaneko and Hall, 2000). The employed *clk856-Gal4* driver includes all clock neurons, which rendered the single-cell approach with the Flybow-reporters virtually impossible. 38 brains contained labeled LPNs, though, and I was able to trace the projections until they reach the dorsal brain, where they overlapped with those of numerous other cells (Fig. 21 A-C).

The cell bodies were located in the posterior cell body rind, posterior to the PLP. Their neurites fasciculate and run dorsally towards the projections of the LNs and DNs in the posterior part of the dorsal brain. It seems that the fiber bundle disentangles in the region of the SMP and SLP, and the projections appear to run to the lateral and medial parts of the dorsal brain (Fig. 21 D).

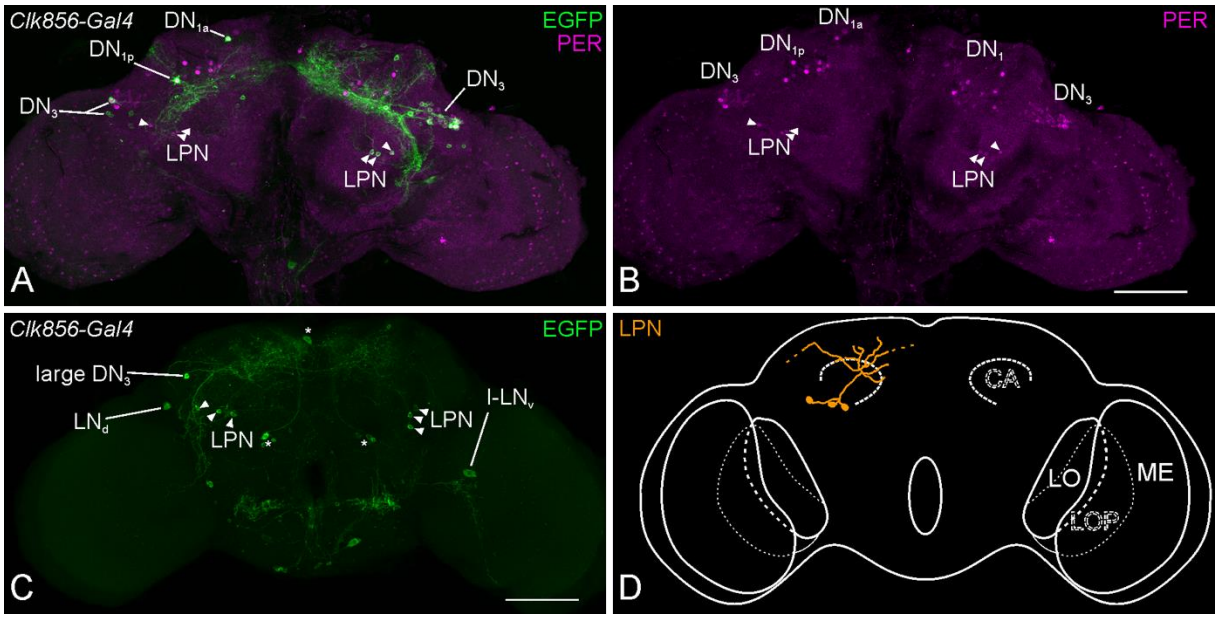

Fig. 21: Estimated projection pattern of the LPNs. (A) Flybow-reporter expression (EGFP, green) in different DN subgroups ($DN1_a$, DN_{1p}, DN_3) and the LPNs of the right hemisphere (arrowheads). Anti-PER immunostaining (magenta) was used for the identification of the clock neurons. (B) Same PER-staining as in (A), the LPNs are visible in the posterior brain (arrows). (C) In this exemplary brain, all LPNs (arrowheads) express the green Flybow-reporter (EGFP). (D) Estimated projection pattern of the LPNs, based on the observations made in 38 samples. All LPNs project dorsally towards the DN_1 and DN_2. In the dorsal part of the brain, fibers run medially and laterally, but the destination of those projections could not be identified (indicated by the dashed line) due to the overlap with the neurites of other cells.

3.3 Spatial relation of the lateral clock neurons that comprise the E-oscillator

The innervation pattern of each individually labeled neuron was described by reference to the nc82 neuropil staining (see Tab. 4). After analyzing their projection pattern, the most representative E-cells were registered to the Janelia Farm standard brain model (Fig. 22; Jenett *et al.*, 2012) to make them comparable to available data

from other sources. Besides the samples with individually labeled neurons, numerous brains had more than one cell tagged by a particular FP. These brains confirmed the results from the single-cell registrations to the template brain and further allowed to analyze the relation of the single clock cells in their native coordinate space.

Tab. 4: Innervation pattern of the E-cells

Neuropil/ Neuron	ME	AME	PLP	LH	SCL	ICL	AOTU	SLP	SIP	SMP	MDC	SMP'	SIP'	SLP'
sNPF$^+$ LN$_d$ (n=17)	-	-	17	17	17	-	17	17	17	17	17	17	-	-
ITP$^+$ LN$_d$ (n=12)	12	12	12	12	12	12	-	12	-	12	12	12	-	10
5th s-LN$_v$ (n=8)	8	8	8	8	8	-	-	8	-	8	8	8	-	8
CRY$^-$ LN$_d$ (n=30)	-	-	-	30	-	-	-	30	30	30	1	1	-	-

Abbreviations were used as previously described. Commissures are highlighted in gray. n = number of analyzed individually labeled cells.

The cells forming an oscillator subunit (E1-E3, see introduction) also show a similar projection pattern. Only the E2-subunit consists of neurons that are morphologically distinguishable from each other, mainly due to the location of their somata and partially because of single characteristic projections (Fig. 17 C, I). The overall innervation pattern of the two E2-cells only differs in the innervation of the ICL (Fig. 22 F). On the contrary, the remaining two E-oscillator units are each comprised of morphologically identical neurons (CRY$^+$ or CRY$^-$ LN$_d$s). The only criteria to further differentiate between the CRY-absent LN$_d$s, is the expression of neuropeptide F (NPF) by two out of the three neurons. All CRY expressing lateral E-cells are highly overlapping in the PLP and in the superior neuropils also with the CRY lacking LN$_d$s

(Fig. 22 E). The ITP expressing cells furthermore co-invade the AME with closely related fibers.

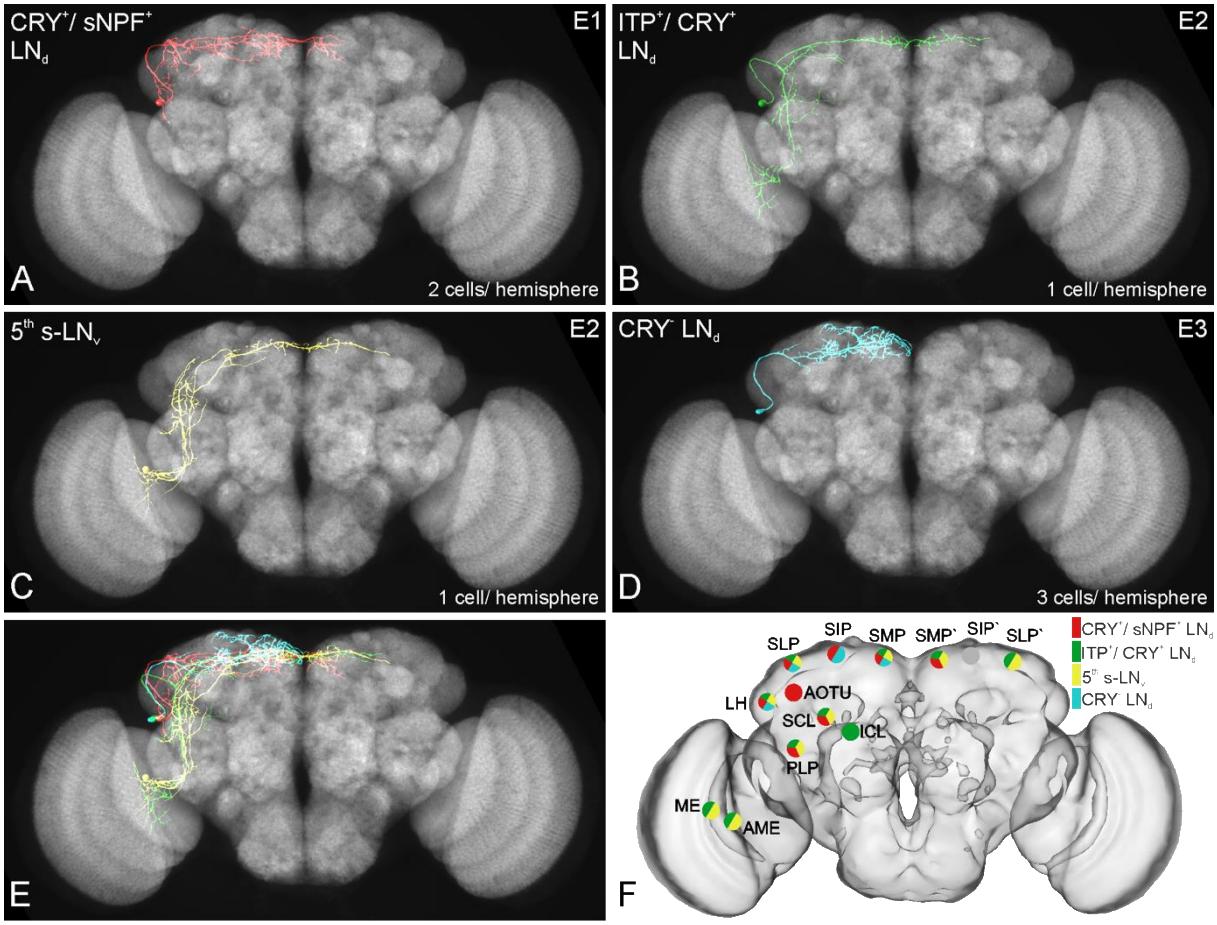

Fig. 22: Reconstructions and innervation map of the E-cells. Neuronal subgroups that build different E-oscillator subunits either show the same (E1 and E3) or highly comparable innervation patterns, even though they belong to different clock neuron subgroups (neurons of E2). (A-D) Exemplary reconstructions of the single-cell projection patterns of the lateral clock neurons that comprise the E-oscillator. (A) Two LN_ds per brain-hemisphere express the circadian photoreceptor Cryptochrome (CRY) and the short neuropeptide F precursor (sNPF). The two neurons comprise the E1-oscillator subunit and are not distinguishable from each other in respect to their morphology or neurochemical content. (B and C) The E2-oscillator is built by two neurons that belong to different clock neuron subclusters, and their cell bodies are located in discrete areas of the brain. The LN_d and the 5^{th} s-LN_v both co-express CRY and the ion transport peptide (ITP) and show a similar innervation pattern (see F), although they belong to different neuronal subgroups. There is only one cell of each neuron type per brain-hemisphere. (D) The E3-oscillator subunit consists of three CRY$^-$ LN_ds per brain-hemisphere that are morphologically equal. The only criteria for discrimination is the expression of neuropeptide F (NPF) by two of the three E3-cells. (E) Superposition of single E-cell subtypes onto the Janelia Farm standard brain. (F) Innervation map based on the projection pattern of individually analyzed lateral clock neurons. The same data underlies Table 3. ME, medulla; AME, accessory medulla; PLP, posterior lateral protocerebrum; ICL, inferior clamp; SCL, superior clamp; AOTU, anterior optic tubercle; LH, lateral horn; SLP, superior lateral protocerebrum; SIP, superior

intermediate protocerebrum; SMP, superior medial protocerebrum; SMP`, contralateral SMP; SIP`, contralateral SIP; SLP`, contralateral SLP.

3.4 Identification of putative in- and output sites of lateral clock neurons

After the single-cell characterization of the lateral clock neurons' morphology, I went on to use the obtained knowledge to identify putative in- and output sites. In order to label the pre- and postsynaptic projections, three different reporter lines were employed. The *UAS-DenMark* (Nicolaï *et al.* 2010) is a dendritic marker (Telencephalin, TLN) tagged with the red fluorescence protein mCherry and specifically labels the somatodendritic compartment. I used a presynaptic vesicle marker tagged with EGFP (*UAS-nSyb::EGFP*, neuronal Synaptobrevin::EGFP; Zhang Y.Q. *et al*., 2002) to unravel the putative input sites. For each condition, 10 brains were analyzed.

3.4.1 The ITP expressing cells

Reporter expression with *R54D11-Gal4/ pdf-Gal80* was only found in neurons of interest (ITP$^+$ LN_d and 5th s-LN_v) and in the subesophageal zone, belonging to non-clock neurons (Fig. 15 A). Due to the vast overlap of the projections stemming from the ITP expressing LN_d and the 5th s-LN_v, separation and assignment of the single projections was only possible in respect to the single-cell data and by going through the confocal stacks slice by slice. The nature of nSyb labeling hampered the segmentation and the assignment of the signal to specific projections, nevertheless, I was able to track some neurites from their origin at the cell body until they enter the superior neuropils. The two E2-cells presumably possess presynaptic sites in the AME and on the extensions reaching into the M7 margin of the ME (Fig. 23). I observed weak GFP expression in the PLP, most likely from neurites of both, 5th s-LN_v and the ITP producing LN_d. Almost no presynaptic vesicle marker was expressed in the lateral and intermediate superior neuropils, but strong labeling occurred in the SMP, where the projections of both hemispheres are vastly overlapping (Fig. 23 A).

Interpreting the signal from the TLN::mCherry reporter in *R54D11-Gal4* brains was easier, since I could easily follow the projections with reference to the single-cell morphology data. The addressed clock neurons (5^{th} s-LN_v and LN_d) both have postsynaptic terminals in the AME, although there are fewer fibers labeled as compared to the nSyb::GFP (Fig. 23 A, B). In the PLP and the SCL postsynaptic sites could be identified originating from both neuron types. The projections of the two neurons that contribute to the PLP-LOF could only be seen with the TLN::mCherry reporter, but not with nSyb::GFP (Fig. 23 A, B, left arrow in 9 C, D). Only neurites from the 5^{th} s-LN_v could be followed beyond the lateral neuropils into the superior part of the brain (indicated by the upper right arrow in Fig. 23 D).

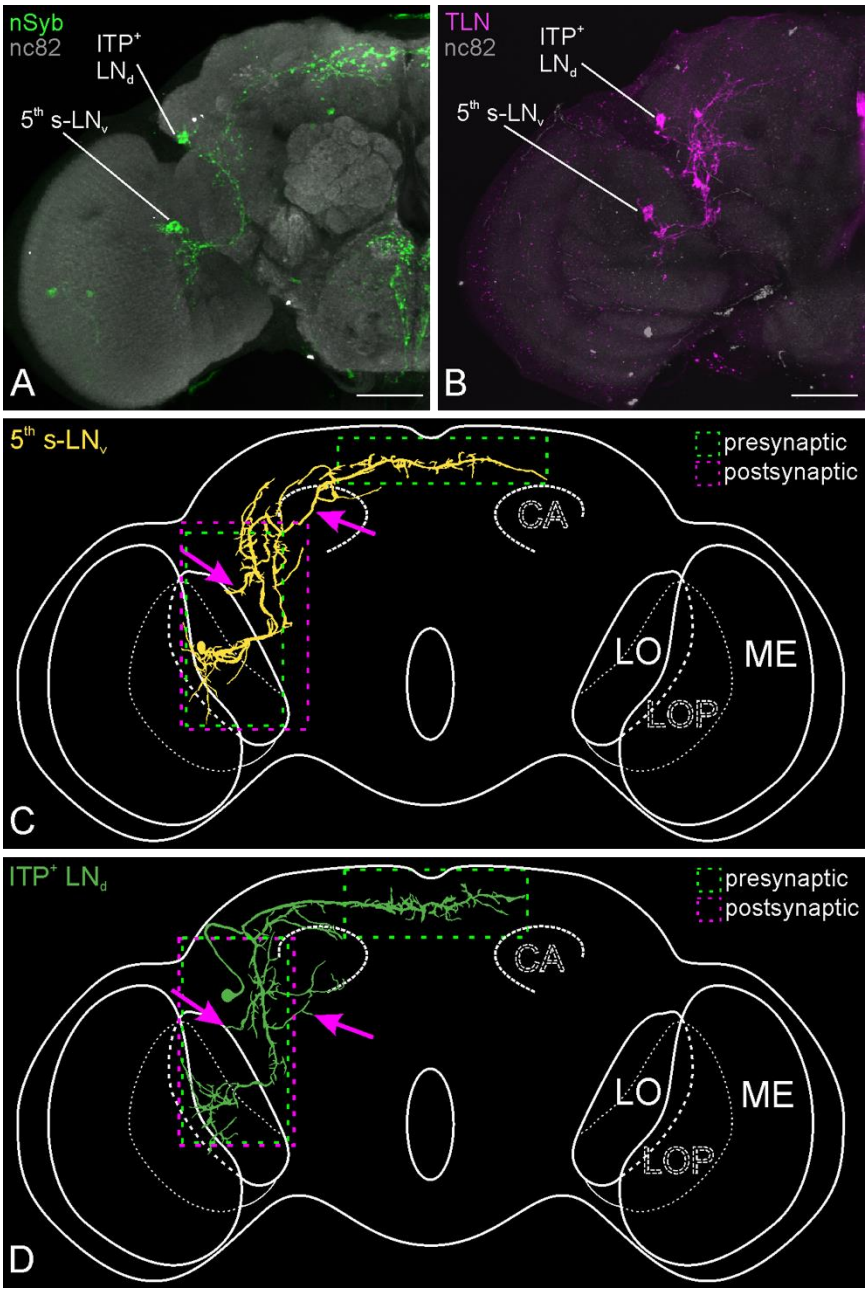

Fig. 23: Post- and presynaptic sites of the ITP expressing LN_d and the 5^{th} s-LN_v. (A) *UAS-nSyb* expression (green) of *R54D11-Gal4/ pdf-Gal80* shows putative presynaptic sites and (B) *UAS-DenMark* (TLN::mCherry, magenta) driven by the same *Gal4/ Gal80* combination the postsynaptic projections of the ITP^+ LN_d and the 5^{th} s-LN_v. (C-D) Schematic overview of the ITP^+ LN_d's (C) and the 5^{th} s-LN_v's polarity with presynaptic sites in green and postsynaptic sites in magenta. Scale bars = 50 µm.

3.4.2 The sNPF and CRY expressing LN_ds

With the *R16C05-Gal4* driver line and *UAS-nSyb::EGFP* only the presynaptic vesicles of two DN_{1a} and the two sNPF/ CRY co-expressing LN_ds were labeled (Fig. 24 A). The single-cell studies helped to disentangle and assign the projections of the different

neurons labeled by the synaptic markers. In the two LN_ds, the tagged presynaptic protein was found in the somata and in the initial projection running around the LH (Fig. 24 A). I observed weak expression in the projections in the SLP and PLP, but more strongly labeled vesicles in the AOTU (Fig. 24 A). The strongest labeling with nSyb::EGFP occurred in the terminals in the SMP, where the projections of the LN_ds of both hemispheres overlap (Fig. 24 A). Note, that the fibers, running through the MDC and connecting both hemispheres, are putatively also presynaptic (Fig. 24 A). The signal posterior to the AOTU, close to the mushroom body CA, and the fiber running through the PLP into the AME belongs to the DN_{1a} in the dorsal brain (Fig. 24 A). Labeling in the subesophageal zone belongs to non-clock neurons (see Fig. 14 A).

The postsynaptic reporter TLN::mCherry was localized in the complete ipsilateral projections of the sNPF and CRY expressing LN_ds (Fig. 24 B), indicating that some sites are pre- and postsynaptic. Reporter expression was observed in the somata and the somatodendritic compartment. The sNPF/ CRY producing LN_ds' postsynaptic projections can be seen in the PLP, LH and in the superior neuropils, as well as in the fiber that runs anteriorly into the AOTU (Fig. 24 B). Notably, there was no reporter signal in the MDC, suggesting that these cells possess postsynaptic sites only in the ipsilateral hemisphere (Fig. 24 B).

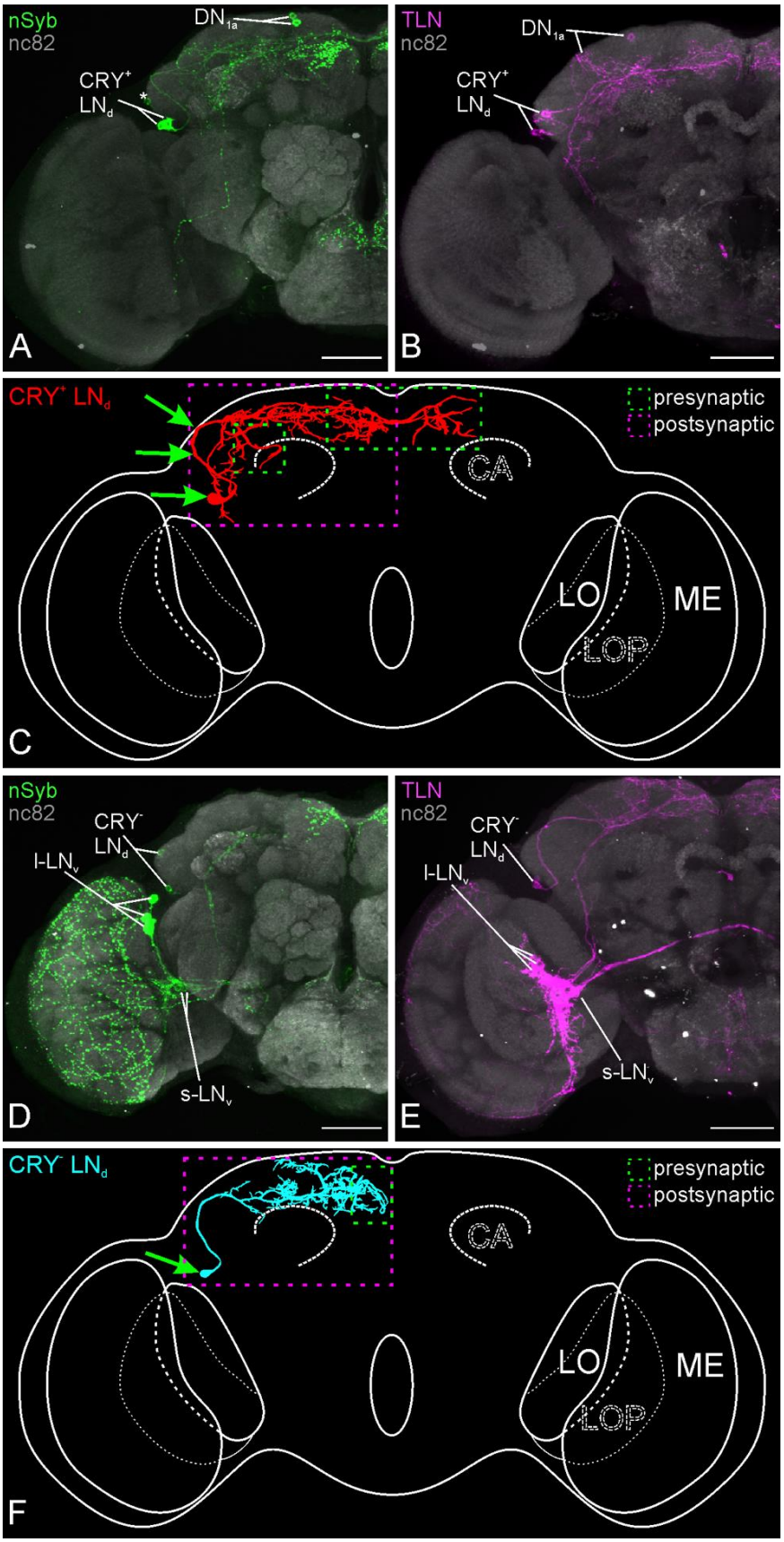

Fig. 24: Post- and presynaptic sites of the ITP lacking LN_ds and the DN_{1a}.

(A) Expression of *RI6C05-Gal4*/ *UAS-nSyb::EGFP* (green) to reveal putative presynaptic arborizations of the CRY$^+$ LN$_d$s and DN$_{la}$. (B) *RI6C05-Gal4*/ *UAS-DenMark* expression (*UAS-TLN::mCherry*, magenta) in the postsynaptic branches of the CRY$^+$ LN$_d$s and the DN$_{la}$. The soma of a non-clock cell can be seen at the lateral edge of the lateral horn (asterisk), but the marker expression in the neurites was too weak to interfere with the identification of clock cell projections. (C) Schematic overview of the polarity of CRY$^+$ LN$_d$s with postsynaptic sites in magenta and presynaptic sites in green. (D-F) Post- and presynaptic sites of the CRY$^-$ LN$_d$s. (D) *UAS*-nSyb (green) expression shows putative presynaptic sites in the brains of *dvPdf-Gal4*/ *cry-Gal80* flies and (E) *UAS-DenMark* (TLN; magenta) revealed the postsynaptic arborizations. *Cry-Gal80* did not sufficiently suppress the reporter expression in the PDF$^+$ LNs, but worked in the ITP$^+$ LN$_d$ and the 5th s-LN$_v$. (F) Schematic overview of the post- and presynaptic sites of the CRY$^-$ LN$_d$s in magenta and green, respectively. All scale bars = 50 µm.

3.4.3 The CRY lacking LN$_d$s

In order to analyze the putative in- and output sites of the CRY lacking LN$_d$s, I crossed the *dvPdf-Gal4* driver to the respective reporters and utilized the GAL4 repressor *cry-Gal80*, aiming at restricting the reporter expression only to the CRY absent cells. Unfortunately, the *cry-Gal80* construct does not sufficiently suppress the reporter expression in the PDF-cells (as reported in Guo *et al.*, 2014; Fig. 23 A, B). However, GAL4 repression worked for the remaining CRY expressing LNs (5th s-LN$_v$ and ITP$^+$ LN$_d$), which would otherwise impede the analysis due to the vast overlap of their projections. In the CRY lacking LN$_d$s, the presynaptic vesicle marker labeled the cytoplasm of the cells as well as the terminals in the SMP close to the dorsoventral midline (Fig. 24 D). In contrast to the presynaptic marker, labeling with the TLN::mCherry occurred over the entire neuronal structure, suggesting that they receive input from various dorsal clock neurons, which are branching in the superior neuropils (Fig. 24 E).

3.5 Comparison of estimated cell diameters

With nine out of 15 lateral clock neurons not only being named due to their location in the brain, but also after the relative size of their soma (s-LN$_v$s, l-LN$_v$s and 5th s-LN$_v$), I ascertained the maximal cell diameter of individually labeled clock neurons and compared them to each other (see Fig. 25). Surprisingly, the 5th s-LN$_v$ is considerably larger compared to the remaining, PDF expressing s-LN$_v$s (9.60±0.88 µm to 7.01±0.66

µm, see Fig. 25). However, it was very interesting to see that the 5th s-LNv and the ITP expressing LNd, which are a functional unit, have comparable cell diameters (9.60±0.88 µm and 9.44±1.11 µm, respectively). Solely the l-LNvs have been found to be significantly larger than the 5th s-LNv (11.07±1.42 µm to 9.60±0.88 µm). On the other hand, there was no statistical difference in cell diameters between the 5th s-LNv and the newly described l-LNvx (9.60±0.88 µm to 9.31±0.88 µm). The PDF producing s-LNvs fall in line with the dorsal neurons in the anterior brain (DN1a; 7.01±0.66 µm and 6.76±0.88 µm, respectively). The analysis of the cell diameters once again substantiates the heterogeneity of the dorsolateral clock neurons. Each subtype of LNds is showing a significantly different cell diameter compared to any other subtype of LNds (ITP+ LNd: 9.44±1.11 µm; CRY+ LNds: 8.15±1.14 µm; CRY- LNds: 7.52±0.97 µm).

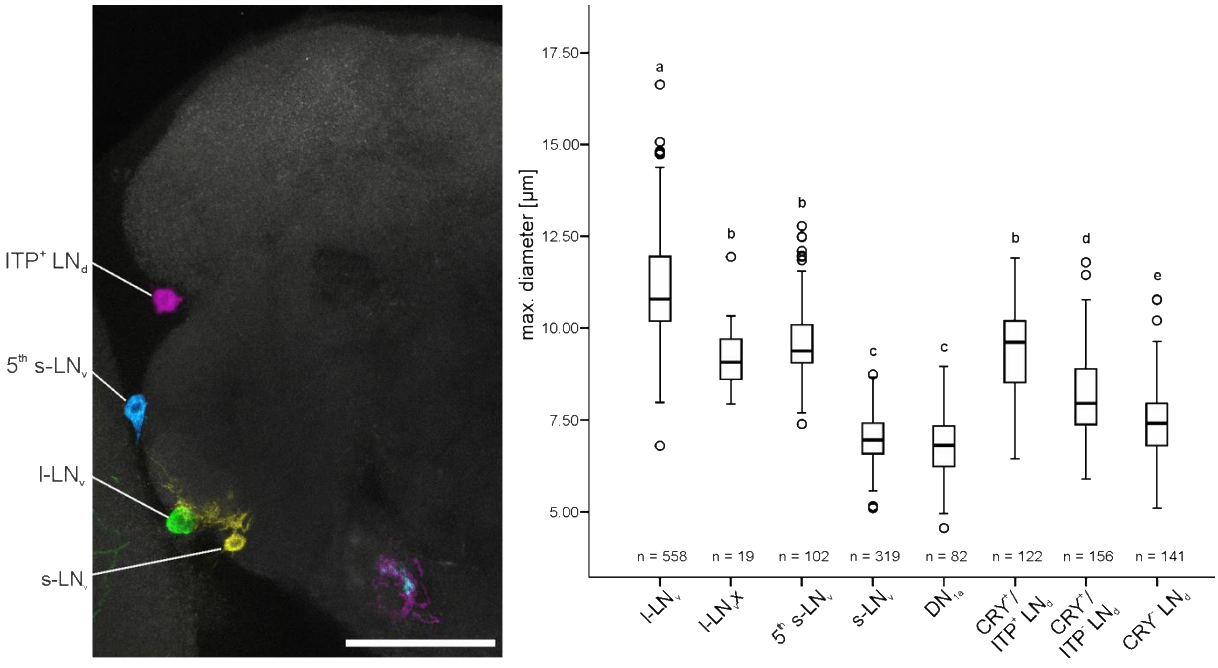

Fig. 25: Comparison of the estimated cell diameters of clock neurons. A one way ANOVA with post-hoc Bonferroni correction was performed for statistical testing. Contrary to the current nomenclature the 5th s-LNv shows the third largest cell diameter, surpassed in size only by the l-LNvs and the ITP+ LNd (not significant) and it is significantly larger than the PDF+ s-LNvs. Significant differences are indicated with different letters. The same letter means that there was no statistical disparity in cell diameter between the cell types. All indicated differences were highly significant with $p < 0.01$. Scale bar = 50 µm.

Comparing the estimated cell sizes, I noticed that particular cell types had membrane appendages at their cell bodies (Fig. 26 upper row). These membrane outgrowths were restricted to the CRY expressing E-cells and were consistently labeled with the DenMark reporter (Fig. 26). The smaller CRY lacking LN_ds had rather smooth somata-surfaces (Fig. 26).

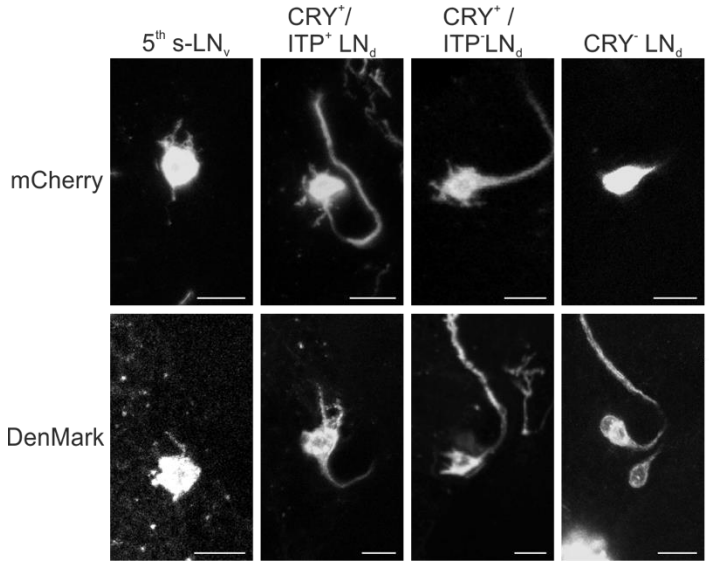

Fig. 26: Comparison of soma morphology of the E-cells. In contrast to the CRY^- LN_ds, the somata of all the CRY expressing E-cells show small appendages. The same appendages can be seen with DenMark expression, suggesting that these varicosities are likely postsynaptic. Scale bars = 10 µm.

3.6 The morphology of the dorsal clock neurons

Author declaration: The heat-shock protocol, dissection, and immunohistochemical staining of the samples, which were used to describe the DN_{1p}, DN_2, and most of the samples used for the DN_3 have been prepared by an undergraduate student (Nicolas Hagedorn) within the scope of an internship under my supervision. I obtained the confocal raw images for analysis, as well as interpretation of the data, which was exclusively my responsibility.

3.6.1 The morphology and assumed polarity of the DN_{1a}

Both DN_{1a} were included in the *R16C05-Gal4* driver line and could be analyzed on the single-cell level, due to the narrow expression of this driver (Fig. 8). The cell bodies are situated in the superior cell body rind dorsal to the SLP and both express CRY (Fig. 14 D, E; Fig. 27; Yoshii *et al.*, 2008). Initially, the DN_{1a} project ventrally and along the surface of the SLP into the posterior brain. The projections of both cells bifurcate at the level of the posterior boundary between LH and SLP and invade the posterior-most part of the LH. Here, the neurites of both DN_{1a} branch extensively and innervate the ventromedial region of the posterior LH (Fig. 27), closely related to the s-LN_v projections in the dorsal brain. Some fibers also run between the dorsolateral Kenyon cells of the MB, and both neurons send projections medially, which terminate dorsal to the Kenyon cells (KC) (Fig. 27 A, C, arrows).

It was interesting to see that out of 30 individually labeled DN_{1a} 11 did not project ventrally towards the AME (Fig. 27 C), suggesting the presence of two morphologically different cells. These 11 neurons also differed in respect to the shape and extent of arborizations in the posterior LH, further indicating that the two DN_{1a} are indeed not identical. One DN_{1a} rather innervates the medial part of the posterior LH, compared to the other, occupying more ventral regions of this neuropil (Fig. 27 A, C). The projections of the latter also terminate in this area and show bouton-like structures at their endings (Fig. 27 C, D). Roughly two-thirds (19 out of 30) of the analyzed DN_{1a} did not show these boutons along their rather thick neurites. These cells had one fiber, which leaves the posterior LH, proceeding ventrally through the PLP until it reaches and joins the POC (Fig. 27 A). Along this major fiber bundle, the ventral DN_{1a} projection invades the ipsilateral AME and often runs onto the surface or along the anteromedial edge of the ME (Fig. 27 A, B).

Due to the vast overlap of their arborizations in most parts, distinguishing the two neurons in the polarity staining was rather challenging/difficult (Fig. 24 A, B). I observed the signal of the post- and presynaptic markers in the posterior ventromedial LH, probably stemming from both DN_{1a} (Fig. 24 A, B; Fig. 27 E). The presynaptic vesicles in the projection to the AME were consistently and strongly

labeled (nSyb::EGFP), whereas only faint DenMark (TLN::mCherry) signal was found in that neurite (Fig. 24 A, B; Fig. 27 E).

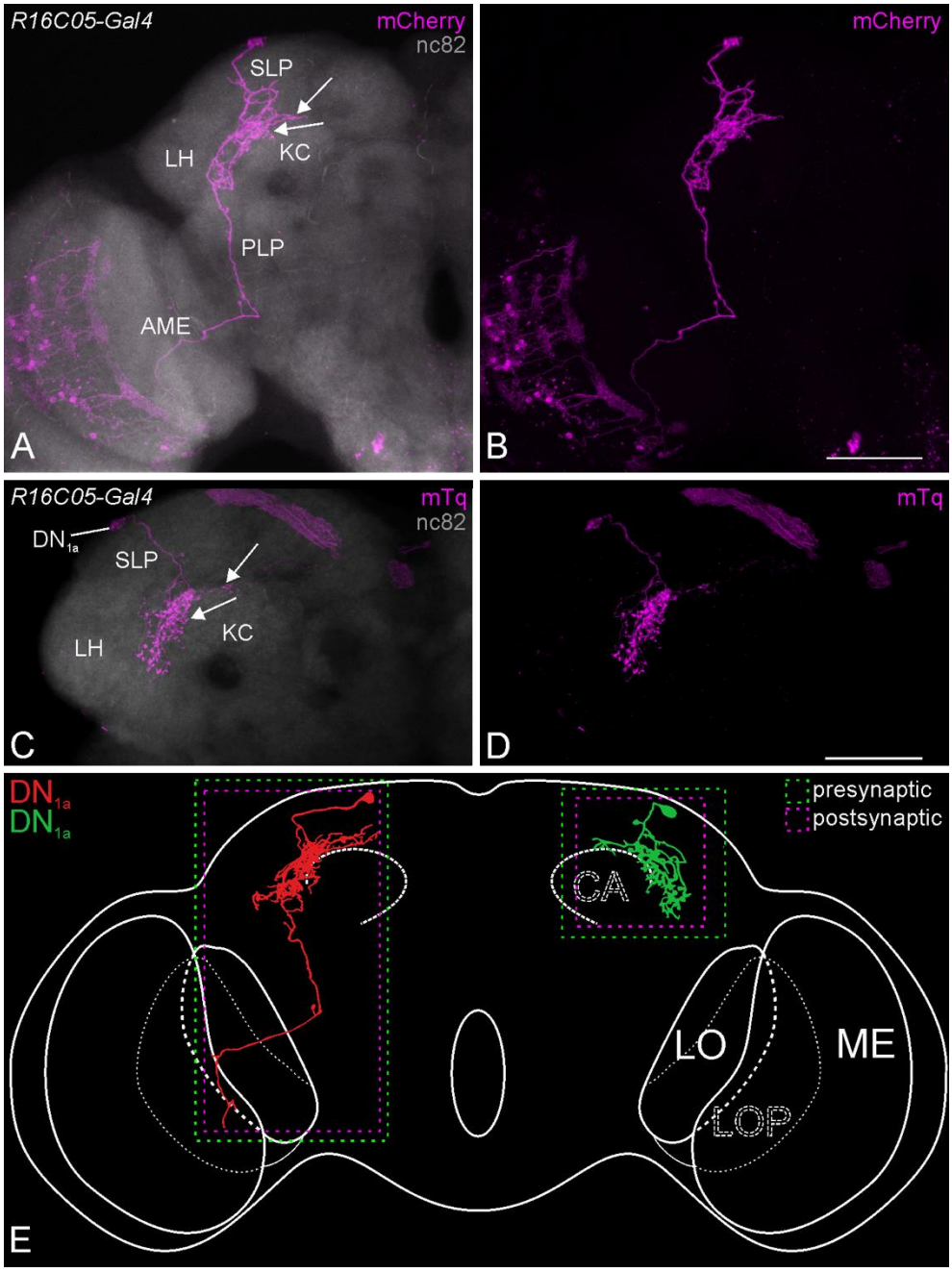

Fig. 27: DN_{1a}: The morphology of the two DN_{1a}. (A-B) Flybow-reporter expression (mCherrry, magenta) driven by *RI6C05-Gal4* and anti-nc82 neuropil staining (gray). Only one of the DN_{1a} is labeled together with several small cells in the optic lobe. A single fiber of this neuron projects from the ventromedial lateral horn (LH) through the posterior lateral protocerebrum into the accessory medulla (AME) and onto the surface of the medulla (ME). The arrows point to small processes, which run between the Kenyon cells (KC). (C-D) *RI6C05-Gal4* driven Flybow-expression (mTurquoise, mTq, magenta) in another anti-nc82 immunostained brain (gray). The labeled DNIa does not project

towards the AME and has bouton-shaped arborizations in the dorsolateral brain. The arrows indicate the fibers, which project between the KCs. (E) Assumptive post- and presynaptic regions of the two DN_{la}, based on the nSyb and DenMark reporters (shown in Fig. 24 A, B). LOP, lobula plate; LO, lobula; CA, mushroom body calyx; SLP, superior lateral protocerebrum. Scale bars = 50 µm.

3.6.2 The morphology of the DN_{lp}

The DN_{lp} are a demonstrably heterogeneous group in respect to CRY or PDFR expression (Shafer *et al.*, 2008; Yoshii *et al.*, 2008; Im and Taghert 2010). About half of the approximately 15 cells per brain-hemisphere express the intracellular blue-light receptor (Yoshii *et al.*, 2008), but whether those certainly relevant differences are also reflected in their morphology, yet remained elusive. The employed *clk4.1M-Gal4* line includes 8-10 out of the 15 DN_{lp} per hemisphere and addresses likewise CRY expressing and non-expressing cells. The different nature of the targeted cells in this driver line has been observed in CRY stainings and it is assumed that only the CRY lacking DN_{lp} cross the dorsoventral midline in the dorsal brain (Abyshek Chatterjee, personal communication, 2016). Whether this feature is an exclusion criterion for the distinction between CRY expressing and lacking DN_{lp} is not known.

I analyzed the DN_{lp} of 22 *clk4.1M-Gal4* brains in combination with the Flybow-reporter in order to reveal potential differences based on Chatterjee`s assumption. As it turned out, the modified Flp-recombinase has not been activated sufficiently, and only four brains showed individually labeled neurons. All DN_{lp} cell bodies are located in the posterior cell body rind posterior to the SLP (rSLPp). They further share the innervation of the posterior SMP and SLP, as well as of the posterior ventromedial LH and dorsal parts of the PLP (Fig. 28 A-F). In three brains, the projections of the individually labeled DN_{lp} did not run into the contralateral hemisphere (Fig. 28 A-D), whereas the remaining neuron crossed the dorsoventral midline via the MDC (Fig. 28 E, F). According to Chatterjee's observations, these neurons belong to the CRY expressing and CRY lacking DN_{lp}, respectively, though, it seems that there are at least four different morphological classes within the DN_{lp} subgroup (Fig. 28 G-J).

One of the presumably CRY expressing neurons projects anteriorly and transversely through the SIP into the anteriorlateral AOTU (arrowhead, Fig. 28 A). Additional

projections also run anteriorly, but more dorsally along the surface of the SLP (arrow, Fig. 28 A). A single fiber proceeds to the lateral-most part of the AOTU, overlapping with the arborizations, which run through the SIP (doublearrow, Fig. 28 A).

The second subclass of CRY expressing DN_{lp} does not project towards anterior brain regions, neither through the SIP, nor around the SLP. Compared to the previously described neuron, this DN_{lp} has more strongly labeled arborizations in the SMP than in the SLP (Fig. 28 A, C). Several neurites descend from the cell body ventrally towards the dorsomedial edge of the MB CA (Fig. 28 C). The projections remain in the posterior brain and run medially around the CA, on the surface of the SCL and ICL (arrowhead, Fig. 28 C). Finally, they terminate in close vicinity to the projections in the PLP (Fig. 28 C).

The presumably CRY lacking DN_{lp} consist of two subclasses, too (Fig. 28 I, J). One neuron was individually labeled (Fig. 28 E), whereas the presence of the fourth subtype (Fig. 28 J) has been concluded from the samples with varying numbers of visible cells. Like all DN_{lp}, both subclasses project ventrolaterally through the ventromedial LH into the PLP. In the superior neuropils, the CRY lacking DN_{lp} show less branching, compared to the CRY expressing cells (Fig. 28 A, C, E). Further, both CRY absent DN_{lp} project into the contralateral hemisphere, contributing to the MDC (Fig. I, J). However, only one of the CRY lacking DN_{lp} subclasses projects to more anterior brain regions (Fig. 28 J). Once again, the target area is the lateral part of the AOTU. Like in one of the CRY expressing DN_{lp}, the fibers run either transversely through the SIP or around the SLP into the AOTU (Fig. 28 J).

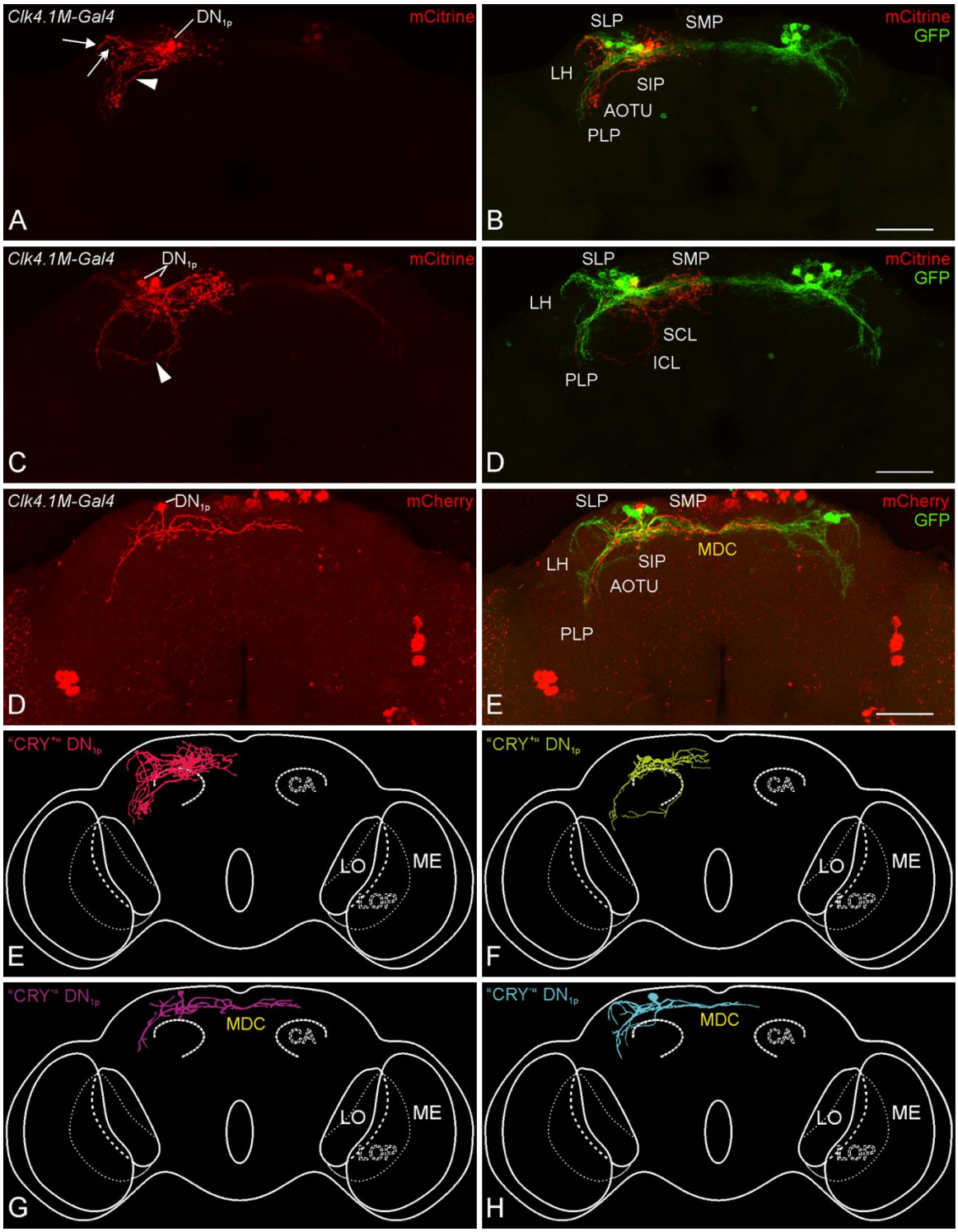

Fig. 28: The different morphologies within the DN_{1p}. *Clk4.1M-Gal4* driven Flybow-reporter expression (red and green) in different DN_{1p} (A-E). (A) Neuron with arborizations in the anterior brain. A single fiber (arrowhead) runs through the superior intermediate protocerebrum (SIP) and invades the lateral anterior optic tubercle (AOTU). Several more fibers (arrows) project dorsally around the superior lateral protocerebrum (SLP) to the anterior side. These projections also run into the lateral AOTU. (B) Overlay of the individually labeled neuron with several other DN_{1p}, which express the default GFP reporter (green). (C) Two separately labeled DN_{1p} (mCitrine, red) among ca. five GFP (green, D) expressing cells. Neither of the two neurons arborize in the anterior brain. Instead, there

are projections in the posterior brain (arrowhead, C), which run ventrally and turn lateral, encompassing the calyx (CA) of the ipsilateral mushroom body. (E) DN_{1p} expressing mCherry (red) and cell bodies of the l-LN_vs. The latter have been labeled with the PDF-C7-antibody (raised in mice), but the dye conjugated secondary probe was cross-reacting with the primary mCherry antibodies (raised in rats). The DN_{1p} does not have any arborizations towards anterior brain regions, but crosses the dorsoventral midline via a projection, which runs through the middle dorsal commissure (MDC, F). (G-J) Schematic depiction of the four identified DN_{1p} subclasses. Unpublished data from Abyshek Chatterje indicates that only the CRY lacking DN1p project via the MDC into the contralateral hemisphere (I, J). SMP, superior medial protocerebrum; LH, lateral horn; SCL, superior clamp; ICL, inferior clamp; PLP, posterior lateral protocerebrum; ME, medulla; LO, lobula; LOP, lobula plate. Scale bars = 50 μm.

3.6.3 The morphology of the DN_2

In order to analyze the arborizations of the two DN_2, we used the *clk206-Gal4* driver in combination with *cry-Gal80*, aiming to restrict the Flybow-expression exclusively to the three CRY absent LN_ds and the DN_2. Unfortunately, GAL4 was not sufficiently suppressed in the s-LN_vs and DN_{1a}, and only the 5th s-LN_v was excluded by the use of Gal80. None of the 17 analyzed brains contained individually labeled DN_2, but all additionally marked neurons have been described on the single-cell level in previous sections. Hence, I was able to assign certain structures of the overall expression pattern specifically to the DN_2.

Their somata are situated in the rSLPp, close to the terminals of the s-LN_vs in the dorsal brain (arrowheads, Fig. 29 A, B). From there, projections run laterally and medially, overlapping with the neurites of other clock neurons in the superior neuropils (Fig. 29 C). The projections towards the medial brain pass the dorsoventral midline into the contralateral hemisphere (MDC, Fig. 29), probably reaching as far as the contralateral DN_2 cell bodies. The remaining fibers in the lateral brain bifurcate near the posterior boundary between the SLP and LH. Two projections turn ventrally and terminate in the ventromedial LH, whereas another pair of fibers runs dorsally around the SLP, eventually invading the anteriorlateral part of the AOTU (arrows, Fig. 29 A, B).

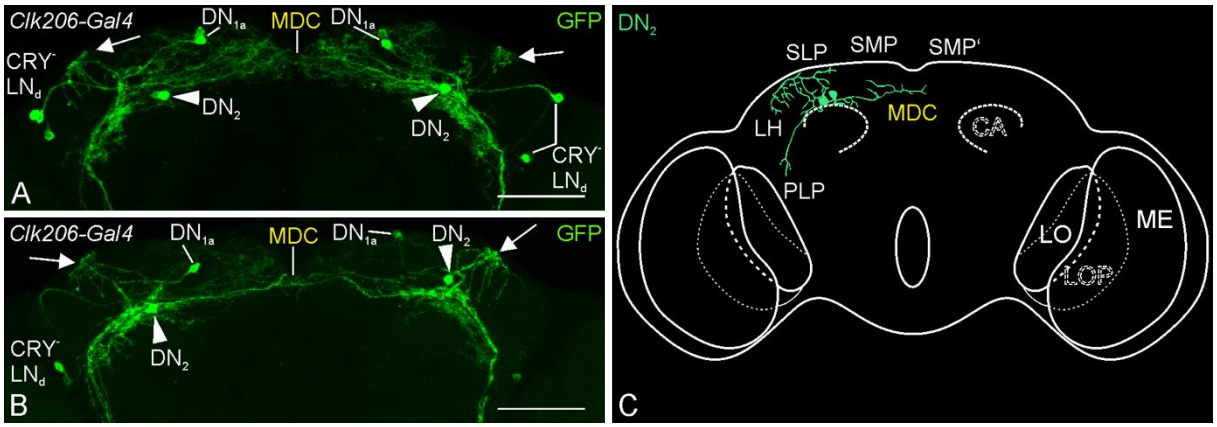

Fig. 29: The morphology of the DN_2. (A, B) Flybow-reporter expression (GFP, green) in dorsal clock neurons driven by *clk206-Gal4*/ *cry-Gal80*. In addition to the DN_2 (arrowheads), one or both DN_{1a} and between two and three CRY^- LN_ds per hemisphere were consistently labeled with GFP. As previously described, neither the DN_{1a} nor the CRY^- LN_ds project anteriorly around the superior lateral protocerebrum (SLP). Therefore, the arborizations seen in this region (arrows) have to originate from the DN_2. The few fibers, which add to the middle dorsal commissure (MDC) arise from the DN_2, too, following the same reasoning. The s-LN_vs' projections to the superior neuropils can be seen in the lateral brain, overlapping with the arborizations of the DN_{1a}. (C) Schematic overview of the DN_2 arborization pattern. The projections through the MDC might also run further, probably up until to the DN_2 cell bodies of the contralateral side. SMP, superior medial protocerebrum; CA, calyx; ME, medulla; LO, lobula; LOP, lobula plate. Scale bars = 50 µm.

3.6.4 The morphology of the DN_3

Comprising approximately 40 cells, the DN_3 group is by far the largest clock neuron cluster in the brain of the adult fly. The studies of Helfrich-Förster and her colleagues have already revealed that there are larger and smaller DN_3 cell bodies, and that some of them are situated more anteriorly in the brain compared to the others (Helfrich-Förster, 2003; Shafer *et al.*, 2006; Helfrich-Förster *et al.*, 2007). This is in line with my observations, which I made by analyzing 43 brains, in which the Flybow-reporters were expressed under the control of the pan-clock-neuronal *clk856-Gal4* driver (Fig. 8). The somata of approximately 15 DN_3 are located posterior to the LH (rLHp), whereas the remaining cells reside more anteriorly in the dorsal and lateral cell body rind (rLHd and rLHl, respectively). The majority of DN_3 possess rather small cell bodies and only around four neurons have larger somata. Half of the larger cells reside among the small posterior DN_3, while the other two are amidst the more anteriorly located neurons of this group (Fig. 30 A). Interestingly, the DN_3 projections resemble the arborization pattern of the combined E2- and E3-cells in large parts (Fig. 22 B, C,

D; Fig. 30 A). Originating from the cell bodies in the dorsolateral brain, the projections initially run along the posterior boundary between the LH and the SLP (Fig. 30 A). The first branching occurs on the posterior surface at the level of the trijunction between the LH, SLP and SCL (arrow, Fig. 30 A). Some neurites run ventrally, pass through the PLP, and join the fibers of the POC to further project to the ipsilateral AME (Fig. 30 A). Numerous side-branches separate from the ventrolateral main bundle, including projections that contribute to the PLP-LOF, analogous to the ITP expressing LNs (Fig. 30 A). In the dorsal brain, a proportion of the projections run via the MDC and SAC (superior arch commissure) into the contralateral hemisphere (Fig. 30 A). The remaining dorsal projections turn anteriorly at the LH-SLP-SCL trijunction, briefly contribute to the posterior component of the superior lateral longitudinal fascicle, and invade the anterior and posterior part of the SMP (arrowheads, Fig. 30 A).

I observed a slightly different arborization pattern in brains in which the larger DN_3 were not labeled (Fig. 30 C). In these brains, the two hemispheres are connected exclusively via the MDC, missing additional projections through the SAC (Fig. 30 A and C). However, the lack of projections, which pass through the PLP into the AME, is the more apparent difference. The arborizations from the small DN_3 terminate in the dorsal PLP, suggesting that the branching in the PLP and the connection to the AME are exclusive features of the four large DN_3 (Fig. 30 A, C, D, E).

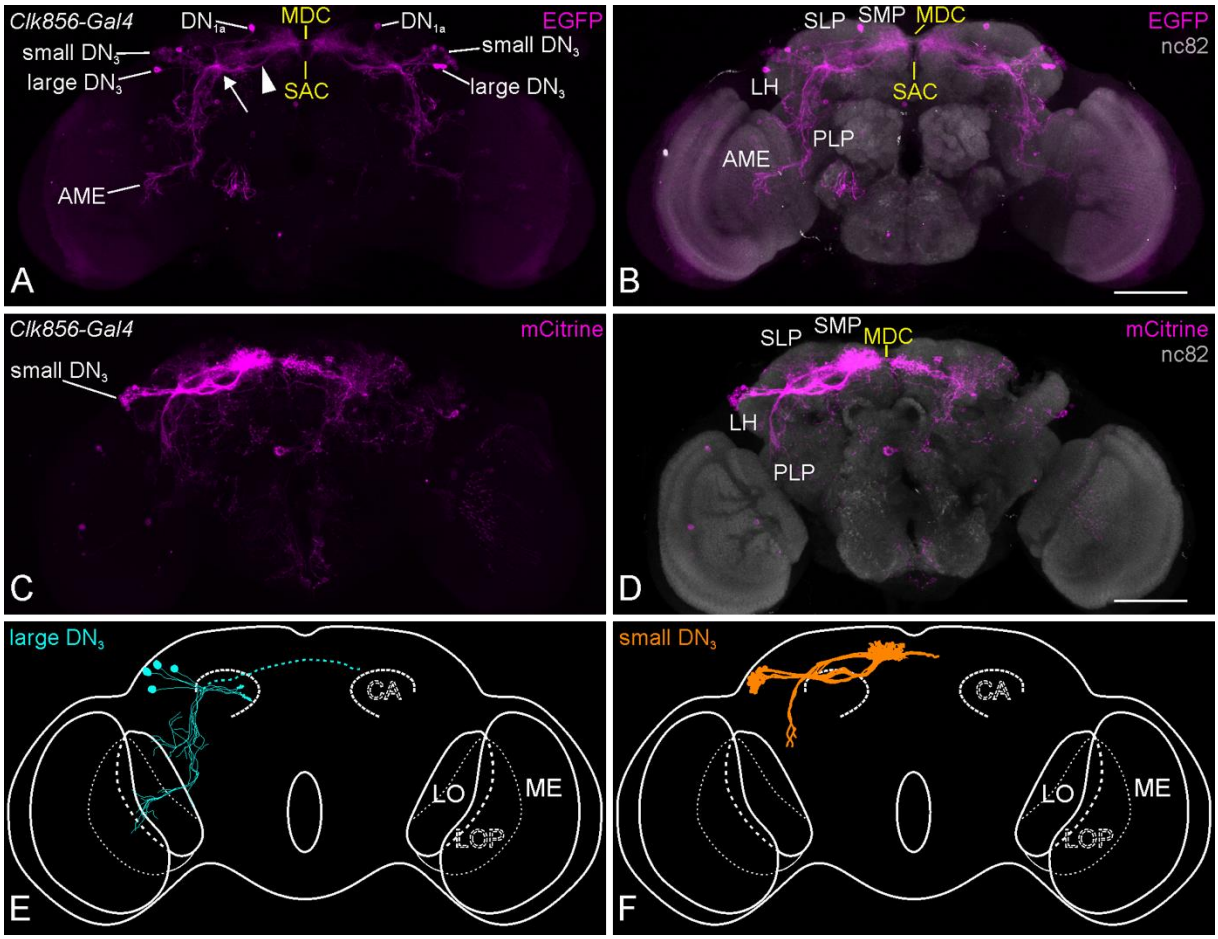

Fig. 30: The morphology of the DN$_3$ subclasses. Two exemplary brains, which express the Flybow-reporters in different subsets of DN$_3$. (A-B) Fibers in the accessory medulla (AME) could only be observed in brains, in which the larger DN$_3$ were labeled. Likewise, the projections through the superior arch commissure (SAC) are absent in brains, in which the large DN$_3$ are not labeled. (B) Overlay with neuropil counterstaining (nc82, gray). (C) Arborization pattern of the small DN$_3$. The projections of these cells in the posterior lateral protocerebrum (PLP) do not invade the AME. The fibers run through the middle dorsal commissure (MDC), but not via the SAC into the contralateral hemisphere. (E-F) Estimated projection pattern of the large and small DN$_3$. All DN$_3$ have arborizations in the dorsal brain, but contribution to the SAC is unique to the larger cells. The overlap with projections from other neurons (mainly small DN$_3$) made further analysis of the DN$_3$ arborization pattern in the dorsal brain impossible (indicated by dashed line, E).

3.6.5 Spatial relationship of the dorsal clock neurons

As shown in previous studies, the arborizations of the DNs vastly overlap in the dorsal brain. Together with the projections of the LNs, they form a brain-wide circadian clock network, innervating numerous neuropils simultaneously (compare Tab. 4 to Tab. 5 and Fig. 22 F to Fig. 31).

Tab. 5: Innervation pattern of the DNs

Neuropil/ Neurontype	ME	AME	PLP	LH	SCL	ICL	KC	AOTU	SLP	SIP	SMP	MDC	SAC	SMP'
DN_{1a} (n=30)*	19	19	19	30	30	-	30	-	30	-	-	-		-
"CRY^{+}" DN_{1p} (n=22)	-	-	✓	✓	✓/-	✓/-	-	✓/-	✓	✓/-	✓	-	-	-
"CRY^{-}" DN_{1p} (n=22)	-	-	✓	✓	-	-	-	✓/-	✓	✓/-	✓	✓	-	✓
DN_2 (n=17)	-	-	✓	✓	-	-	-	✓	✓	-	✓	✓		✓
small DN_3 (n=43)	-	-	✓	✓	✓	-	-	-	✓	-	✓	✓	-	✓
large DN_3 (n=43)	✓	✓	✓	✓	✓	-	-	-	✓	-	✓	✓	✓	✓

Abbreviations were used as previously described. Commissures are highlighted in gray. n = number of analyzed brains/ *individually labeled cells. Tick marks indicate innervation and the presence of neuronal subclasses (✓/-).

All DNs conjointly innervate the PLP, LH and SLP (Tab. 5, Fig. 31). Except for the DN_1, all DNs contribute to the MDC and run into the contralateral SMP. The DN_3 and one DN_{1a} are the only DNs, projecting ventrally to invade the AME. Further, the arborization pattern of the large DN_3 in the lateral brain highly resembles the one of the 5^{th} s-LN_v. Notably, not only the sNPF/ CRY expressing LN_ds project dorsally around the SLP into the AOTU (Tab. 4, Fig. 22 F), the DN_2 and some DN_{1p} take the same route, likewise innervating the lateral-most AOTU.

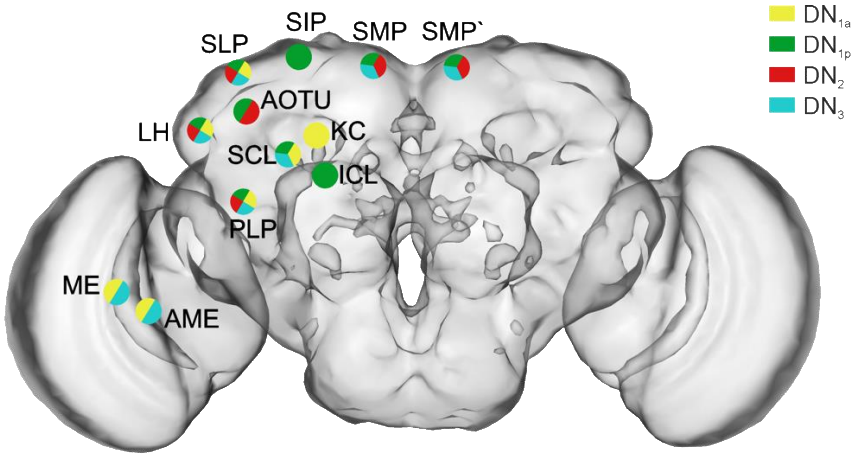

Fig. 31: Innervation map of the DNs. Based on the projection pattern of individually labeled dorsal clock neurons and the analysis of numerous brains, in which neurons of different DN subsets were fluorescence-labeled. The same data underlies Tab. 5. ME, medulla; AME, accessory medulla; PLP, posterior lateral protocerebrum; ICL, inferior clamp; SCL, superior clamp; AOTU, anterior optic tubercle; LH, lateral horn; SLP, superior lateral protocerebrum; SIP, superior intermediate protocerebrum; SMP, superior medial protocerebrum; SMP`, contralateral SMP.

3.7 Long-term luciferase imaging of living brain explants

As already mentioned in Material and Methods (section 2.8), the brain culturing protocol was adapted from Saskia Eck (Eck, 2016) and adjusted to meet the requirements for an inverted microscope setup. In particular, I omitted the agarose embedding, mainly due to two reasons: First, the embedded brains float in the agarose until it turns solid. Therefore, the brains can never be plane in focus. Even more importantly, the objective's restricting traveling range limits the free working distance to only a few hundred micrometers above the glass bottom. Most of the agarose-embedded brains are trapped out of focus range and cannot be imaged with an inverted setup. Second, the brains were swelling over the course of several days after the embedding, rendering long-term imaging of a particular focal plane impossible.

These drawbacks were bypassed by coating the glass bottom dishes with Poly-L-Lysine. Hereby, the brains were adherent to the coated glass surface, producing the minimum working distance possible. Changing the culturing protocol did not affect the viability of the explanted brains, which expressed cytoplasmic GFP in all clock neurons. 12 out of 15 samples looked vital and healthy after 21 days in vitro (DIV), and

two out of the five brains of the longest culture did not die until it was contaminated on DIV43. In accordance with the protocol, half of the medium was substituted on every second day ensuring the maximum period possible. However, preliminary imaging trials have demonstrated that refreshing the medium introduces inevitable motion artifacts, which should be avoided concerning the objective of long-term recordings. Consequently, I evaluated the viability of brain cultures, which were maintained without exchanging the medium, to define a reasonable time-period for the PER-LUC recordings. For this purpose, I monitored the fluorescence of cytoplasmatically expressed GFP in *repo-Gal4* expressing glial cells of 36 explanted brains. Glial cells are a convenient indicator of the general condition and state of health of brain explants, since glia is essential for neuronal survival and suppression of cell death (Buchanan and Benzer, 1993; Xiong and Montell, 1995; Volkenhoff *et al.*, 2015). The brains looked healthy for 7-9 days, and on average lived for three more days until they died (Fig. 32 A-C). This time-period is sufficiently long to record several circadian cycles, while the brain is still in pristine condition (see "2.9.2 Bioluminescence imaging" for time table).

The measurement of the PER-LUC oscillations were carried out with *w; Pdf::mRFP1; BG-luc* flies (see 2.3 Fly strains and genetic crosses). With no fluorescence light source being available for the bioluminescence imaging setup, I had to adjust the focal plane solely by reference to the brightfield image and the bioluminescence signal, emitted by the clock neurons. As a result, I focused on the l-LN_vs on account of the fact that they are closely located to the brain surface, relatively large in size and hence, could be easily identified (Fig. 32 D, E). The specifity of the luciferase reporter has been verified by anti-Luciferase antibody-stainings and imaging the native *Pdf*::mRFP1 signal with a confocal microscope (Fig. 32 F-H). Following the successful recording of at least four cycles of PER-LUC oscillation, the respective brains were subjected to IHC to identify the neurons, which had been recorded, and for further assessment of the condition of the brains (Fig. 32 I-K). The staining protocol was carefully executed so the brains would not detach from the glass surface, maintaining their original orientation for the ease of the subsequent allocation. On the downside, the confocal scans had to be obtained by only using the 10-fold air objective, since the higher

magnification lenses were too bulky to fit into the culturing dish. As a consequence, the autofluorescence which is caused by residual culturing medium weighs disproportionately more heavily (Fig. 32 I-K). It is nevertheless remarkable that projections of the s- and l-LN_vs could be labeled after keeping the brains for seven days in culture without refreshing the medium.

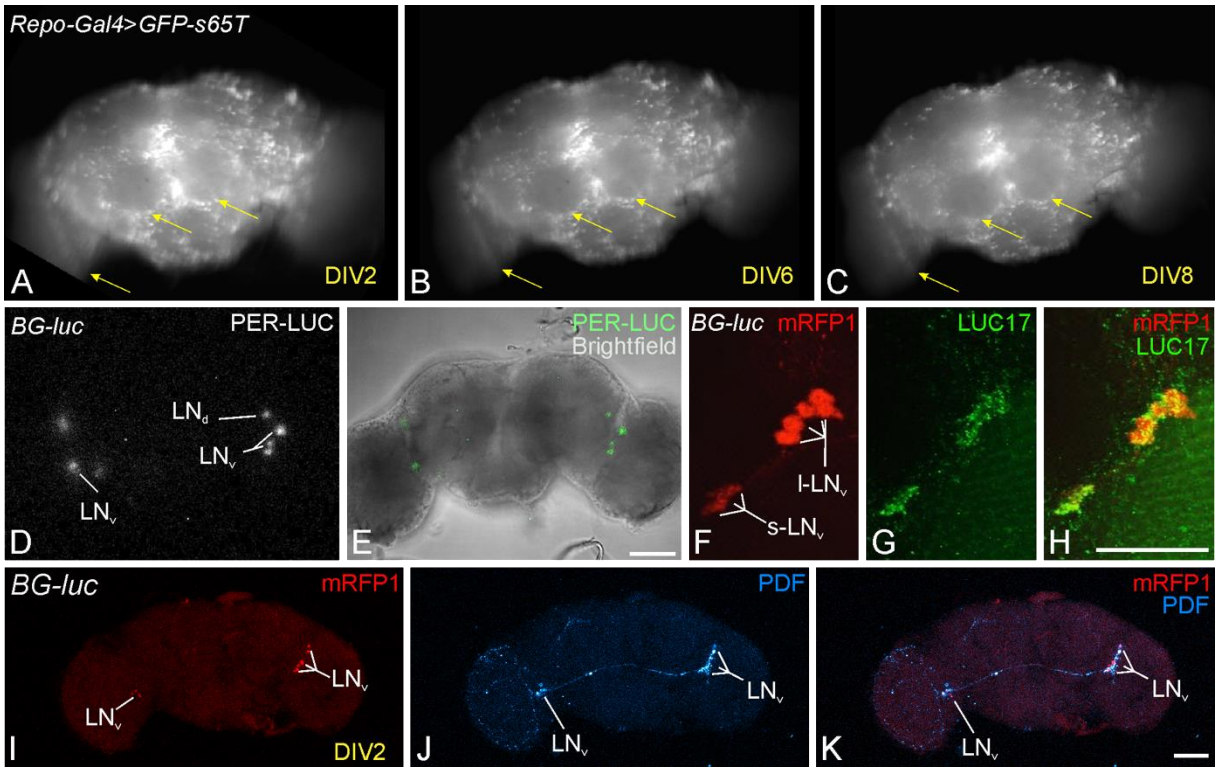

Fig. 32: The establishment of long-term measurements of PER-LUC bioluminescence rhythms. The viability of *repo-Gal4/ UAS-GFP-S65T* brain explants was monitored with a fluorescence stereomicroscope to determine how long the brain cultures could survive, if the medium was not refreshed (A-C). Judging by eye, only a negligible number of GFP expressing glial cells had vanished over the course of the first six days in culture and prominent neuropil boundaries still looked defined (A, B; arrows). On the 7-9th day in vitro (DIV), the boundaries began to blur (medulla, antennal lobes; arrows), even though most glial cells still looked healthy (C). Single time-point of a PER-LUC bioluminescence measurement (D) and an overlay with the brightfield image of the brain (E). The relative large size and the stereotypic localization in the anterior brain make the l-LN_vs the easiest group to record from. (F-H) Confocal scans of the native RFP expression (F) in the PDF expressing LNs of the test flies (*w; Pdf::RFP1; BG-luc*), counterstained with a Luciferase-antibody (LUCI7; G). (I-K) Successfully imaged brains can be processed for immunohistochemistry. Native RFP expression in PDF neurons (I) and anti-PDF staining (J) of a brain, which had been kept in culture for seven days, prior to the IHC procedure. The brain had been mounted on the specimen slide 10 days post-dissection and was subsequently imaged with the 10-fold magnification objective. Scale bars = 50 µm.

A total sum of more than 400 cultures were prepared in order to establish the bioluminescence assay in our lab. Each culture dish contained up to six brains, which were simultaneously and continuously monitored (Fig. 33 A, B). Depending on the orientation and adherence of the brains to the coated glass surface, it is possible to record different neuronal subgroups in the individual brains of the same culture (*e.g.* LNs in brains with their anterior side on the glass surface and DNs in brains, which were placed with the posterior side facing down). Eventually, I was able to record the PER-LUC bioluminescence rhythms of individual clock neurons over the course of five days (Fig. 33 C, D). The analysis of the obtained data with the provided MATLAB script (see "2.10 Analysis of the bioluminescence recordings") identified rhythms in the circadian range. The period lengths estimated by MESA were always shorter than the ones obtained with autocorrelation analysis (Fig. 33 C, D). In some cases, both methods failed to detect rhythmicity, even though the oscillations appeared clearly rhythmic (Fig. 33 C, upper panel). The period lengths of these signals were estimated by manually measuring the peak-to-peak intervals. Even though the underlying rhythms might not be significant, the manually calculated periods once again range between 20 and 28 h, demonstrating that the recording of bioluminescence rhythms was successfully established.

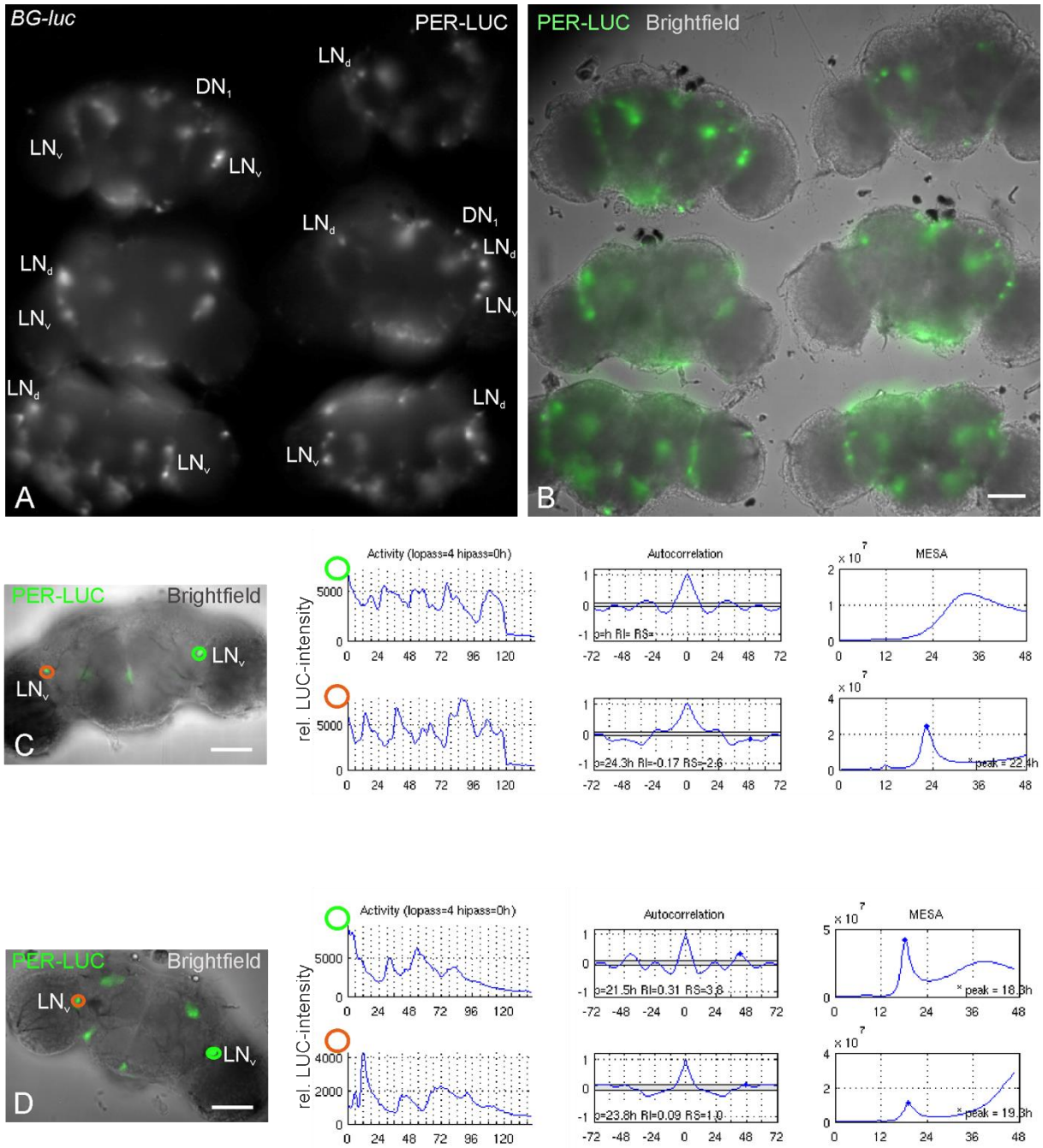

Fig. 33: PER-LUC long-term recordings of cultured brains. Average t-projected luminescence signal of a five day long recording (A) and merge with the brightfield image (B). Up to six brains can be monitored simultaneously in one culture dish. (C-D) Two exemplary brains and analysis of the measured PER-LUC oscillations of lateral neurons. For correct assignment of the plots, a color code was used to highlight the recorded cells (green and orange circles). The first column next to the recorded brains shows the lowpass filtered bioluminescence intensity over time (in hours). The middle column consists of the respective correlograms of the autocorrelation analysis. Gray lines indicate the 5% significance level. Detected rhythms were further analyzed for period length (p) and rhythmicity index (RI). The results of the MESA are shown in the rightmost column. The peaks of the correlograms indicate the estimated period lengths (x-axis). Scale bars = 50 µm

4 Discussion

4.1 The l-LN$_v$s are a heterogenic group of clock neurons

The classification of the l-LN$_v$s as M-oscillators is a controversially discussed fact (*e.g.* Beuchle *et al.*, 2012; Abruzzi *et al.*, 2015), tough, the release of high levels of PDF which acts directly on E-cells to control the phasing of the evening activity peak independently from s-LN$_v$ signaling (Cusumano *et al.* 2009; Potdar and Sheeba, 2012; Schlichting *et al.*, 2016), as well as the described role of l-LN$_v$s in the control of sleep and arousal (Parisky *et al.*, 2008; Sheeba *et al.*, 2008; Gmeiner *et al.*, 2013) justifies this subsumption.

Utilizing the Flybow-multicolor technique, I am the first to demonstrate that the current subdivision of M-cells into s- and l-LN$_v$s is yet too simplified, and therefore introduced the term l-LN$_v$x for a newly described morphological subclass of l-LN$_v$s. My results indicate that there is only one l-LN$_v$x opposing to three regular l-LN$_v$s per brain-hemisphere. Either l-LN$_v$ subtype shows a similar initial branching pattern, which has already been assumed by Park and Griffith (2006) based on fluorescence dye-fills. However, the small number of backfilled neurons in their study could not reveal the presence of the l-LN$_v$x and my approach using membrane targeted FPs is considerably superior in order to expose the neuronal structure in its entirety. Likewise, I am the first to show that l-LN$_v$ and l-LN$_v$x projections, originating from the primary ventral branch, are extensively invading the serpentine layer of the ipsilateral ME and that these projections co-localize with fibers from the ITP-expressing E-cells (5th s-LN$_v$ and one LN$_d$). The E-cell-, as well as the l-LN$_v$ neurites in this region were responsive to n-Syb and DenMark labeling, supporting the findings of Schlichting *et al.* (2016), who were the first to demonstrate a direct functional link between the l-LN$_v$s and the E-cells in the adjacently located AME. In the same study, the authors conclude that l-LN$_v$ PDF-signaling to the NPF and ITP expressing E-cells becomes more important for proper timing of the E-activity peak with increasing day-

lengths, suggesting a functional relevant disparity between s- and l-LN_v secreted PDF (Schlichting *et al.*, 2016). Hence, they provided evidence for an important link between the neurons, on which the first part of my study focused on (l-LN_vs and E-cells).

Due to the shared initial branching and projection pattern, both l-LN_v subclasses contribute to the ipsilateral AME_{vel}, even though the individual l-LN_vs project further along the ventral edge to the posterior side and thereby proceed towards the distal ME more often. The strikingly different projection pattern on the surface of the ipsi- and contralateral ME is the more apparent disparity. The regular l-LN_vs project in the accustomed manner (Helfrich-Förster *et al.*, 2007), forming a network that covers the surface of the ME of both hemispheres. As already described by Helfrich-Förster and peers (2007), the main target area of the l-LN_vs is the distal ME, where the fibers are densely running along the lateral edge. In contrast, the l-LN_vx exclusively invades the dorsomedial and ventromedial surface of the ME, indicating that these cells might have a unique function among the l-LN_vs. This assumption still needs to be verified, but there are several indicators (resting membrane potential, spontaneous action potential firing rate, and membrane excitability upon light illumination) suggesting that one l-LN_v per brain-hemisphere exhibits significantly different electrophysiological properties compared to the others (Edgar Buhl, personal communication of unpublished data, 2017). This indication strengthens the necessity of anatomical single-cell studies to provide valuable reference and to push our understanding of complex neuronal networks, not only on the anatomical, but also on the functional level.

4.2 The functional heterogeneity of the LNs is reflected in their morphology

With the help of the widely utilized antibody against synthetic crustacean PDH, the anatomy of the PDF expressing LN_vs could be described early on, and they were the first clock neurons in *Drosophila* with a revealed projection pattern (Helfrich-Förster and Homberg, 1993; Helfrich-Förster, 1995). In contrast, the morphology of the LN_ds

remained elusive for more than one additional decade, until Helfrich-Förster and her colleagues provided the first decent description of *Drosophila*'s clock network (Helfrich-Förster *et al.*, 2007; Yoshii *et al.*, 2008; Johard *et al.*, 2009). Whether the CRY expressing LN_ds make contact with other clock neurons in the AME is a central question that remained unanswered by previous studies and therefore was one of my main interests. I further endeavored to clarify potential morphological differences among the CRY expressing LN_ds, according to the different functions they are attributed with (Rieger *et al.*, 2006; Shafer *et al.*, 2006; Yao and Shafer, 2014).

My results demonstrate that the functional subdivision of the LN_ds is highly reflected in their morphology. The projections of the two ITP lacking, CRY producing LN_ds (those are the sNPF co-expressing LN_ds, Johard *et al.*, 2009), which are strongly coupled to the s-LN_v output via PDFR signaling (Yao and Shafer, 2014), do not reach far enough ventrally to possibly invade the AME and cannot make direct contact with other clock cells there. My findings further indicate that there is no structural difference between the two sNPF expressing cells.

According to the current working model of peptidergic unit composition of *Drosophila*'s clock, the ITP expressing LN_d is assigned to another oscillator unit (E2), which also includes the 5^{th} s-LN_v. The two ITP expressing clock neurons have never been shown separately before, and I was surprised by their remarkable resemblance, as it was generally assumed that the 5^{th} s-LN_v would look like the PDF containing s-LN_vs. Instead, the two ITP clock cells (5^{th} and one LN_d) show an almost identical projection pattern, reflecting their functional similarity. My results clearly demonstrate that out of all LN_ds, solely the ITP expressing one invades the AME, and that innervation of the AME is an exclusive feature of the ITP expressing E2-subunit.

For the CRY lacking LN_ds it has already been assumed that they would not project ventrally towards the AME. However, with the current study I demonstrated for the first time that a) the CRY lacking LN_ds' projections are indeed restricted exclusively to the superior neuropils, b) there is no systematic morphological difference between those neurons and c) these are the only E-cells that do not cross the dorsoventral midline into the contralateral hemisphere.

Overall, this is the first work providing clear evidence for a morphological subdivision of the E-oscillator, in line with the already described functional subunits.

4.3 The 5th s-LN$_v$: a LN$_d$ in disguise

Although the 5th s-LN$_v$ has always stood out from the other s-LN$_v$s, as it is the only one without PDF expression, it has been assumed that all s-LN$_v$s share a similar projection pattern. This assumption has now proven to be false and the soma size on its own, already discriminates the 5th from the other s-LN$_v$s. As I discussed the morphological and functional similarities of the 5th s-LN$_v$ and the ITP expressing LN$_d$ in the previous section, this raises the question whether the 5th s-LN$_v$ might in fact belong to the LN$_d$s rather than to the s-LN$_v$s.

The presence of the 5th s-LN$_v$ was first described by Kaneko *et al*. (1997), who found the cell in third instar larvae (L3) by using a *per-lacz* reporter. In the discussion of their paper, the authors state that the "[...] fifth LN could correspond to part of either the LN$_d$ or LN$_v$ cluster in pupae and adults" (Kaneko *et al*., 1997). However, given the fact that the LN$_d$s did not express the *lacz* reporter before 60% of the metamorphosis had been completed, the authors finally concluded that the 5th LN is more likely an s-LN$_v$ (Kaneko *et al*., 1997). Based on this initial report, the 5th s-LN$_v$ was quickly referred to as such by other authors. In this way, the cell got assigned to the s-LN$_v$s only because the LN$_d$s lacked *per-lacz* reporter expression in larvae, assuming that the dorsal cluster has not yet developed at this stage. More recent studies, by contrast, showed that all pacemaker neurons except for the l-LN$_v$s are already differentiated and expressing CLK and CYC in the late L3 larval stage (Liu *et al*., 2015). The reason why *per* is not expressed in the so-called late pacemaker neurons (LN$_d$s, LPN, DN$_{1p}$, DN$_3$) of the L3 stage, even though the transcriptional activators CLK and CYC are already present, still needs to be clarified (Liu *et al*., 2015). Nevertheless, these findings deprive the basis of initially classifying the 5th LN$_v$ as a s-LN$_v$, since the LN$_d$s are already differentiated, too. With their CLK-GFP reporter Liu *et al.* (2015) could also show that the 5th s-LN$_v$ and the LN$_d$s are spatially closely related throughout larval development. In the early pacemaker neurons (DN$_{1a}$, DN$_2$ and all s-LN$_v$s

including the 5th), CLK expression starts during early embryogenesis and initiates rhythmic per expression in late embryos and L1 larvae, which persists throughout development and adulthood (Kaneko *et al*., 1997; Kaneko and Hall, 2000; Helfrich-Förster *et al*., 2007; Houl *et al*., 2008;). The first LN_ds appear to express CLK-GFP around the transition from the L2 to L3 stage (Liu *et al*., 2015). In late L3 larvae, all late pacemakers were detected (except l-LN_vs; Liu *et al*., 2015), but rhythmic *per* expression cannot be demonstrated before 50-90% of the pupal development is completed (Kaneko *et al*., 1997; Kaneko and Hall., 2000). As soon as the LN_ds start to express the CLK-GFP reporter, it is no longer possible to precisely differentiate the 5th s-LN_v from the LN_ds, since these cells localize in one common cluster (Liu *et al*., 2015). In fact, they stay together until the LN_ds migrate dorsally after 20-30% of pupal development is completed (Helfrich-Förster *et al*., 2007). It is reasonable to assume that the 5th s-LN_v does not migrate dorsally because of its initial innervation target, which is the ipsilateral AME. It would be pointless to migrate along with the LN_ds and then project all the way back to invade the AME. In contrast, the s-LN_vs are clearly definable from the LN_ds at all times (Kaneko *et al*., 1997; Kaneko and Hall, 2000; Helfrich-Förster *et al*., 2007; Liu *et al*., 2015), which might indicate a common developmental origin of the 5th s-LN_v and the LN_ds. I further reevaluated the report of Helfrich-Förster *et al*. (2007) in respect to my new findings that only the ITP expressing LN_d invades the AME. Considering this, it becomes apparent that the neuron, which they described to be the first LN_d to extend its projections during metamorphosis (Fig. 6 C in Helfrich-Förster *et al*., 2007), is the ITP expressing LN_d. This would mean that the two ITP expressing clock neurons are the first E-cells, which take up their function as circadian oscillators. This is plausible, since the E2-cells are the stronger oscillators of the E units, yet more independent from the M-cell output to be able to sufficiently track dusk (Rieger *et al*. 2006; Yao and Shafer, 2014). In conclusion, neurochemical content (Helfrich-Förster, 1995; Kaneko *et al*., 1997), observed function (Rieger *et al*., 2006; Yao and Shafer, 2014), as well as developmental studies (Helfrich-Förster et al., 2007; Liu *et al*., 2015) already argue against classifying the 5th LN_v as a s-LN_v, since this might imply similarities with the PDF expressing cells and confuse newcomers in the field. So far, it has been assumed

that the 5th s-LNv would at least look like the PDF containing s-LNvs, justifying the nomenclature despite all this. However, the findings of my study, which revealed the morphological differences of the 5th s-LNv to the PDF cells on one hand, and the striking similarities with the ITP expressing LNd on the other, opens the discussion whether the naming of the 5th s-LNv is still applicable. This becomes even more questionable with respect to my measurements of the clock neuron somata-sizes. I demonstrated that, once again, the 5th s-LNv is more comparable to the ITP expressing LNd and significantly larger than the s-LNvs. Actually, the 5th s-LNv is on average the same size as the l-LNvx and only slightly smaller than the other l-LNvs. This means even the relative cell size of the 5th s-LNv argues against naming it "small". In terms of classical nomenclature, which referred to the size and location of the cell body, the 5th s-LNv would have to be called "5th l-LNv" correctly. This, however, would be as misleading as the current nomenclature, and further, changing it would be incomprehensive for longer-established chronobiologists. To nonetheless emphasize the unique character of the 5th s-LNv and to differentiate them from the other LNvs, I propose to refer to this neuron as the "5th LNv", since this would correctly name the location without implying any further commonalities with other LNvs. The designation "5th" would still be correct in various respects, as it is one of the five early LNv pacemaker neurons. As there are four l-LNvs and four s-LNvs, it would still be the "5th" neuron, regardless of which cluster it would have theoretically been assigned to.

After all, this did not truly answer the question whether the 5th s-LNv could be a disdained LNd. To clarify this, one has to investigate whether these neurons derive from the same progenitor cell or not. However, according to the location, the 5th would then still be a LNv. Therefore, it seems more important to point out the obvious differences to the other s-LNvs, which could easily be achieved by simply omitting the wrongly added "small", changing it to "5th LNv".

4.4 The heterogeneity of the DNs

Although the DNs are not capable of driving behavioral rhythmicity on their own under constant conditions (Helfrich-Förster, 1998; Blanchardon *et al.*, 2001; Velerie *et al.*, 2003), they contribute to various aspects of circadian regulation.

The DN_{1p} and DN_{1a}, the latter being the same neurons as the two *per* expressing larval DN_1 (Kaneko *et al.*, 1997; Kaneko and Hall, 2000; Klarsfeld *et al.*, 2004; Shafer *et al.*, 2006), are demonstrably among the downstream targets of the s-LN_vs (Shafer *et al.*, 2008; Cusumano *et al.*, 2009; Zhang Y. *et al.*, 2010; Zhang L. *et al.*, 2010). It is reported that a particular subset of 16-20 DN_{1p}, the ones which are addressed by the *clk4.1M-Gal4* line, rescue morning anticipatory behavior under 12:12 h high light LD cycles (500 lux during the day) in otherwise per^0 mutant flies, whereas they are sufficient to restore the evening activity under 12:12 h temperature cycles of 29:20 °C (thermophase:cryophase (TC); Zhang Y. *et al.*, 2010). Given this functional diversity and the relatively high number of the DN_1 cells, I expected to find several different morphologies in the mentioned cluster. As I could demonstrate, the DN_{1p} already seem to consist of at least four different subclasses of neurons, conceivably reflecting their different functions, as it holds true for the LN_ds, too. However, assignment of discrete functions in accordance to their different morphologies remains to be established. More unexpectedly, I ascertained the presence of two disparate DN_{1a} with the main difference being that only one of them projects ventrally towards the AME. This indicates that even the small group of only two DN_{1a} may be functionally diverse, which is, as yet, completely unproven.

The DN_2 consist of only two neurons per brain-hemisphere, which express *per* already in the larval stages (Kaneko *et al.*, 1997). Under LD cycles, the PER oscillations of the larval DN_2 are in antiphase to all other clock neurons (Kaneko *et al.*, 1997). The phasing of the DN_2 in LD cycles depends on the PDF signaling of the s-LN_vs, while in return, the DN_2 take control over the s-LN_vs in TC cycles (Picot *et al.*, 2009). In adults, the DN_2 show the same phasing as the remaining clock neurons (Kaneko *et al.*, 1997; Kaneko and Hall, 2000) and they are demonstrably sufficient to generate daytime temperature preference rhythms (TPR; Kaneko *et al.*, 2012; Tang *et al.*, 2017).

Unfortunately, I was not able to look at the arborizations of the two neurons separately and therefore cannot judge whether they are morphologically identical or not. Given the importance of daytime TPR in ectotherm animals (Stevenson, 1985), which is comparable with the body temperature rhythm of mammals (Refinetti and Menaker, 1992), it is possible that these cells might have developed redundantly, just like the s-LN_vs.

The DN_3 are among the late pacemakers, which start *per* expression during pupal development (Kaneko *et al.*, 1997; Kaneko and Hall; 2000). It has already been reported, that there are smaller and larger DN_3, and that two of the latter reside more anteriorly in the dorsal brain (Helfrich-Förster, 2003; Shafer *et al.*, 2006; Helfrich-Förster *et al.*, 2007). Hence, I expected to find different arborization patterns among the cells comprising the DN_3. Indeed, the small and large DN_3 project differently, and it is likely that further disparities will be revealed, by the time when the DNs have been fully analyzed. Considering that the DN_3 represent about 50% of the clock neurons, and that their projections cover almost the complete innervation pattern of the remaining network, longs for a functional characterization of this heterogenic group, which still needs to be provided. Recent observations made by the group of Ralf Stanwesky suggest a role for the sensory integration of temperature cues into the circadian system (Harper *et al.*, 2016).

4.5 The network and its putative connections

Even before this study, it has been well established that the clock neurons form a vastly overlapping network (Helfrich-Förster, 2003; Helfrich-Förster *et al.*, 2007), which integrates multisensory inputs (*e.g.* light and temperature cues) from the environment (Helfrich-Förster *et al.*, 2002; Yoshii *et al.*, 2002; Yoshii *et al.*, 2005; Busza *et al.*, 2007; Yoshii *et al.*, 2008; Velerie *et al.*, 2007; Picot *et al.*, 2009; Sehadova *et al.*, 2009; Yoshii *et al.* 2009; Kaneko *et al.*, 2012; Buhl *et al.*, 2016; Harper *et al.*, 2016; Tang *et al.*, 2017). Although *Drosophila*'s clock has been shown to have an implication on the fly's metabolism (Xu et al., 2008; Xu et al., 2011), sleep (Hendricks *et al.*, 2000; Shaw *et al.*, 2000; Hendricks *et al.*, 2003), the control of locomotor

rhythms (Konopka and Benzer, 1971; Handler and Konopka, 1979; Helfrich and Engelmann, 1983), the gating of eclosion and metamorphosis (Pittendrigh and Skopik, 1970; Konopka and Benzer, 1971; Hamblen-Coyle *et al.*, 1992; Sehgal *et al.*, 1994; Myers *et al.*, 2003), as well as on learning and memory (Lyons and Roman, 2009; Fropf *et al.*, 2014; Chouhan *et al.*, 2015), the coverage of specific connections to downstream neurons of the circadian network still lags behind. So far, only six studies have been able to identify specific target neurons, reporting their implication in the control of rest:activity- (Pirez *et al.*, 2013; Cavanaugh *et al.*, 2014) and wakefulness:sleep–cycles (Cavanaugh et al., 2016; Cavey *et al.*, 2016; King *et al.*, 2017), metabolic regulation (Barber *et al.*, 2016), and the coupling of the peripheral clock of prothoracic gland (PG) to the central pacemaker in the brain (Selcho *et al.*, 2016). In the upcoming years, the research focus will increasingly shift from the already well-described input pathways and clock network properties to the outputs and its underlying circuits.

I identified several neuropils, in which clock neuron projections went so far unnoticed or have not been analyzed in great detail (SCL, ICL, AOTU, ME serpentine layer). These neuropils are candidate regions for the possible localization of downstream neurons or their arborizations, which has to be investigated more closely.

The clamp (SCL and ICL) contains fibers of some DN_{1p} and the two ITP expressing clock cells (LN_d and 5^{th} s-LN_v). Additionally, the posteriorly located neuropil gets densely innervated by fibers, stemming from *fruitless* and *doublesex* expressing neurons, which belong to the courtship circuit (Cachero *et al.*, 2010; Rideout *et al.*, 2010; Robinett *et al.*, 2010; Yu *et al.*, 2010; Zhou *et al.*, 2015). Courtship and mating behavior is controlled by the circadian clock and depends on the expression of the clock genes (Sakai and Ishida, 2001; Tauber *et al.*, 2003; Manoli *et al.*, 2005; Fuji *et al.*, 2007). Since the increased evening locomotor activity correlates with reduced courtship and mating frequency (Sakai and Ishida, 2001; Fuji *et al.*, 2007), it is conceivable that the E-cells might signal onto the courtship neurons in the clamp.

The *fruitless* expressing courtship neurons additionally arborize into the AOTU (Manoli *et al.*, 2005), a neuropil, in which projections from the clock neurons have not yet been reported. With the help of membrane targeted 10-fold reporters, I was

able to provide evidence that different clock neuron subgroups (sNPF$^+$/CRY$^+$ LN$_d$s, DN$_2$ and various DN$_{1p}$) invade the lateralmost AOTU, suggesting yet another location where interaction between clock cells and courtship neurons are possible.

Interestingly, the AOTU is demonstrably an integral part of the polarization vision pathway of many insects, which enables them to navigate via sun compass orientation (reviewed by el Jundi *et al.*, 2014). To compensate for the changes of solar elevation and the hereby resulting sensory conflicts, the sky compass requires information from the circadian clock, which might get integrated at the level of the AOTU and CX in locusts, cockroaches, and honeybees (reviewed by el Jundi *et al.*, 2014). For *Drosophila*, the insect with the best-studied circadian clock, no polarization vision pathway had been described until Omoto *et al.* (2017) identified the anterior visual pathway (AVP) as the underlying neural substrate. The AVP is a three-legged pathway, connecting the serpentine layer of the medulla to the lateral-most AOTU, the AOTU to the bulb, and the bulb to the ellipsoid body of the CX (Omoto *et al.*, 2017). Strikingly, I discovered clock neuron arborizations in two out of the four structures, particularly in the serpentine layer of the ME, stemming from the l-LN$_v$s and ITP expressing E2-neurons (5th s-LN$_v$, one LN$_d$), and in the lateral-most AOTU, originating from the DN$_{1p}$, DN$_2$ and E1-neurons (sNPF$^+$ LN$_d$s). The mere fact that this is the only physical overlap of the circadian network with the sky compass pathway in the fly, highly recommends further examination of this observation in order to possibly reveal the functional link of the two systems.

En route for the AOTU, the clock neuron fibers (DN$_{1p}$, DN$_2$, E1 cells) run close by the dendrites of the prothoracicotropic hormone (PTTH) producing cells, which reportedly couple the central pacemaker to the PG clock (Selcho *et al.*, 2016). A PDF independent link from the s-LN$_v$s to the PTTH neurons via sNPF has already been demonstrated (Selcho *et al.*, 2016), but since the E1-neurons (2 CRY$^+$ LN$_d$s) are likewise expressing sNPF, a contribution of those cells cannot be ruled out completely.

Further, two of the initially mentioned reports specified distinct cell populations in the PI as downstream targets of the DN$_{1p}$ (Cavanaugh *et al.*, 2014; Barber *et al.*, 2016; King *et al.*, 2017), confirming a long-suspected connection (Kaneko and Hall, 2000;

Helfrich-Förster, 2003; Helfrich-Förster *et al.*, 2007). The PI is considered the *Drosophila* equivalent of the mammalian hypothalamus (de Velasco *et al.*, 2007), housing a variety of discrete populations of neurosecretory cells (Rowell, 1976; Zaretsky and Loher, 1983; Homberg *et al.*, 1991a,b; Veelaert *et al.*, 1998; Siegmund and Korge, 2001; de Velasco *et al.*, 2007). In 2014, Cavanaugh *et al.* identified six PI neurons and their output molecule (DH44) as an integral part of the pathway controlling rest:activity rhythms. They further noted that the DH44 expressing cells are entirely complementary to the *Drosophila* insulin-like peptide (DILP2) producing cells in the PI (Cavanaugh *et al.*, 2014), which demonstrably contribute to the regulation of sleep and metabolism (Rulifson *et al.*, 2002; Broughton *et al.*, 2005; Crocker *et al.*, 2010). Two years later, the same group demonstrated a functional link between the DN_{1p} and DILP2 cells, which regulates rhythmic expression of metabolic genes in the fat body via DILP2 signaling (Barber *et al.*, 2016). My results indicate that most other clock neurons directly target the abovementioned or other cells of the PI, too. Except for the PDF neurons and the DN_{1a}, all clock cells possess varicose arborizations in the SMP, close by the dendrites of the PI neurons. Particularly the analysis of putative in- and output sites, showing the presynaptic nature of the E-cells' projections in that region, furthermore suggests the PI as a target of multiple clock neurons. Since the s-LN_vs (Fernández *et al.*, 2008; Sivachenko *et al.*, 2013; Gorostiza *et al.*, 2014; Petsakou *et al.*, 2015) and the DN_2 (Tang *et al.*, 2017) are reported to undergo activity-dependent circadian remodeling, it is likely, that also other clock neurons experience neuronal circadian plasticity. I controlled this effect in my study by collecting and fixing all samples at a particular time-point (ZT23). However, to obtain the complete picture of possible innervations throughout the day, a time-series analysis is required.

In conclusion, the anatomical study with single-cell resolution not only provided new insights into the clock network, but also yielded various candidate regions in the brain where potential downstream connections to other systems might be revealed in the future.

4.6 Establishment of a method for the long-term recording of PER-LUC bioluminescence rhythms of the clock neurons of isolated brains

Luciferase based reporters for *Drosophila* have been and continue to be highly beneficial in chronobiological studies. Luciferase has a short reporter half-life and does not require light excitation, which would affect the molecular oscillations of the clock (Brandes *et al.*, 1996; Stanewsky *et al.*, 1997). Thus, bioluminescence reporters are well-suited to study the clock and its implications in living animals or cultivated tissues (heads, legs, wings), and consequently contributed to a broader understanding of clock protein regulation and aspects of entrainment (Brandes *et al.*, 1996; Plautz *et al.*, 1997; Stanewsky *et al.*, 1997; Stanewsky *et al.*, 1998; McDonald *et al.*, 2001; Stanewsky *et al.*, 2002; Glaser and Stanewsky, 2005; Peschel *et al.*, 2009; Sehadova *et al.*, 2009).

Classically, luciferase based experiments were carried out in plate-reading scintillation counters, allowing a high sample throughput and the monitoring of individual flies or fly tissues over a period of up to two weeks (Brandes *et al.*, 1996; Stanewsky *et al.*, 1997; Stanewsky *et al.*, 2002). Complying to strict hygienic measures during the cultivation procedure even allowed the long-term recording of isolated brains (Glaser and Stanewsky, 2005). In 2010, advances in CCD technology and brain culturing protocols allowed a first proof of concept for circadian bioluminescence imaging with single-cell resolution (Sellix *et al.*, 2010). Nonetheless, reaching the same spatial resolution, quality level, and value as comparable immunohistochemical approaches remained inconceivable (reviewed by Tataroglu and Emery, 2014). This did not change until the group of Todd Holmes demonstrated the practical implementation of the method in the context of an elaborated study, by showing the network-wide response to light pulses with whole-circuit bioluminescence imaging (Roberts *et al.*, 2015). At that time, I was already testing my own protocol for the luminescence imaging of single clock neurons. In contrast to the previous studies, I relied on a commercially available system (LV200, Olympus life science, Tokio, Japan), allowing others to adapt my protocol without changes if they decide to use the same setup.

First, I demonstrated that the brain cultures are vital for up to 9 days, even if the medium was not refreshed. Subsequently, I successfully established the recording of PER-LUC bioluminescence rhythms at single-cell resolution in our lab. Although I was able to measure s-LN_vs and LN_ds, too, I mainly focused on the l-LN_vs, as these are the largest clock neurons and hence easier to find than the other clock cells. At first, I was surprised to find the PER-LUC signal oscillating, since the l-LN_vs are the only clock neurons which do not show consistent PER cycling in DD (Yang and Sehgal, 2001; Shafer *et al.*, 2002; Peng Y. *et al.*, 2003; Klarsfeld *et al.*, 2004). Roberts *et al.* (2015) likewise reported PER-LUC cycling in the l-LN_vs of their preparations and reasoned that this is likely due to the missing inhibitory aminergic input from the visual system (Schlichting *et al.*, 2016) and the loss of feedback from other peripheral tissues after the dissection. This raises the question of whether the brain culture model is too artificial to reliably reflect the true processes, which are taking place in the intact animal. Hence, Roberts *et al.* (2015) additionally verified their findings with immunohistochemistry, showing that the luciferase imaging approach can indeed provide new insights into the properties of the circadian network. Besides, several other studies successfully used brain cultures to investigate the fly's circadian clock, demonstrating the value of an ex-vivo model (Glaser and Stanewsky, 2005; Ayaz *et al.*, 2009; Sehadova *et al.*, 2009; Mezan *et al.*, 2016; Sabado *et al.*, 2017). In the end, one has to decide on a study-to-study basis whether the culturing approach is applicable to answer the formulated scientific question.

Considering that circadian bioluminescence imaging approaches with single-cell resolution are still in its very early stages, it is conceivable and possible that this technique might partially replace the laborious immunohistochemical methods of chronobiological studies in *Drosophila*. Classically, in order to assess the clock protein cycling of individual neurons, one has to sacrifice and process a considerable number of flies in an immunohistochemical time-series experiment (reviewed by Helfrich-Förster, 2005). The staining intensity and localization of the clock proteins at different time-points provides insights into the temporal occurrence and abundance of the clock gene products (*e.g.* Eck *et al.*, 2016). This method, however, relies on averaging the intensity values of many samples at a given time-point and only

represents “snapshots” of the current state of the molecular oscillation. In contrast, bioluminescence imaging approaches enable us to follow the clock protein oscillations of individual brains over a period of several days. Further development of this method would consequently reduce the number of required animals and simultaneously increase the temporal resolution of time-series analyses.

Long-term circadian imaging of individual brains will further allow the examination of network properties by manipulating specific clock neurons and consecutive monitoring of the circuit-wide response. Versatile thermo- and optogenetic tools are already available for the timely precise manipulation of the membrane excitability via temperature or light, respectively (reviewed by Owald *et al.*, 2015). Thermogenetic tools are probably less appropriate, since temperature fluctuations of more than ±1 °C reliably evoked motion artifacts in my bioluminescence recordings. Furthermore, the luciferase activity itself is also temperature dependent and proper controls are necessary when TC cycles are used. Optogenetic tools are theoretically better suited and are even more precise in terms of their activation, compared to the temperature triggered candidates. Unfortunately, no light activated tool has been reported so far which could reliably phase-shift the molecular oscillations of the clock neurons. However, due to the high interest in the rapidly expanding field of optogenetics, it is likely that suitable tools for the application in bioluminescence imaging experiments will be available in the near future.

5 Outlook

The results of this thesis represent the most detailed anatomical description of the circadian clock network of *Drosophila melanogaster*. For the first time, the lateral neurons were assessed and described on the single-cell level, providing new insights about their morphology, shifting the focus to brain areas that have so far been ignored by the chronobiological fly-community. The here provided detailed anatomical description will help to select specific driver lines (*Gal4* and split-*Gal4*) to target and study the function of individual clock cells in more detail. Moreover, the identification of the putative in- and output sites of the LNs provides a major indication where additional downstream target neurons might be located.

However, the discrepancy in the detail of the anatomical description of the lateral compared to the dorsal neurons is not only due to the high amount of time that is needed for such studies, but mainly reasoned by the lack of suitable driver lines. There are numerous *Gal4* lines available to address the lateral neurons in all kinds of combinations, but only few lines restrict the expression to the DNs. Even though it would have eventually been possible to dissect the dorsal network with the Flybow-reporters, the lack of sparsely expressing drivers for the DNs made the characterization of the in- and output sites impossible.

Gummadova *et al.* (2009) studied the regulatory elements of the *clock* promotor and generated several driver lines bearing the *Gal4* under the control of different regulatory sequences. This resulted in a set of drivers with expression in different subsets of lateral and dorsal clock neurons. Some of these lines were used in this thesis, but the majority, especially those that showed a restricted expression in the DNs, had been lost due to a climate chamber incident prior to stock center donation.

Since the DNs are high in number and conventional *Gal4* lines include far too many neurons to efficiently dissect the dorsal network even with the Flybow-system, I suggest to make use of the ever expanding collection of split-*Gal4* lines. I further

recommend the chemical labeling method described by (Kohl *et al.*, 2014), for which multicolor labeling reporters were realized and became publicly available just recently (Sutcliffe *et al.*, 2017). By using this protocol, the time needed for sample preparation (dissection, staining, mounting) can be drastically reduced from five days to only two hours, allowing a considerably higher sample throughput. I am confident that the combination of suitable split-*Gal4* lines with the multicolor chemical labeling approach will contemporarily reveal the single-cell anatomy and polarity of the DNs and LPNs in the near future, too.

As already discussed above, further directions could also be the investigation of the circadian plasticity of the network or the functional examination of the presumed downstream connections (*e.g.* sky compass pathway).

6 References

Abruzzi, K., Chen, X., Nagoshi, E., Zadina, A., Rosbash, M. (2015) Chapter Seventeen-RNA-seq Profiling of Small Numbers of *Drosophila* Neurons. *Methods Enzymol*, 551, 369-386.

Akten, B., Jauch, E., Genova, G.K., Kim, E.Y., Edery, I., Raabe, T., Jackson, F.R. (2003) A Role for CK2 in the *Drosophila* Circadian Oscillator. *Nat Neurosci*, 6, 251-257.

Allada, R., White, N.E., So, W.V., Hall, J.C., Rosbash, M. (1998). A Mutant *Drosophila* Homolog of Mammalian Clock Disrupts Circadian Rhythms and Transcription of Period and Timeless. *Cell*, 93, 791-804.

Ashmore, L.J., Sathyanarayanan, S., Silvestre, D.W., Emerson, M.M., Schotland, P., Sehgal, A. (2003) Novel Insights Into the Regulation of the timeless Protein. *J Neurosci*, 23, 7810-7819.

Awasaki, T., Kao, C.F., Lee, Y.J., Yang, C.P., Huang, Y., Pfeiffer, B.D., Luan, H., e*t al.* (2014) Making *Drosophila* Lineage-restricted Drivers Via Patterned Recombination in Neuroblasts. *Nat Neurosci*, 17, 631-637.

Ayaz, D., Leyssen, M., Koch, M., Yan, J., Srahna, M., Sheeba, V., Fogle, K.J., *et. al* (2008) Axonal Injury and Regeneration in the Adult Brain of *Drosophila*. *J Neurosci*, 28, 6010–6021.

Bae, K., Lee, C., Hardin, P.E., Edery, I. (2000) dCLOCK is Present in Limiting Amounts and Likely Mediates Daily Interactions Between the dCLOCK-CYC Transcription Factor and the PER-TIM Complex. *J Neurosci*, 20, 1746–1753.

Bahn J.H., Lee, G., Park, J.H. (2009) Comparative Analysis of Pdf-mediated Circadian Behaviors Between *Drosophila melanogaster* and *D. virilis*. *Genetics*, 181, 965-975.

Barber, A.F., Erion, R., Holmes, T.C., Sehgal, A. (2016) Circadian and Feeding Cues Integrate to Drive Rhythms of Physiology in *Drosophila* Insulin-producing Cells. *Genes Dev*, 30, 2596-2606.

Bargiello, T.A., Jackson, F.R., Young, M.W. (1984) Restoration of Circadian Behavioural Rhythms by Gene Transfer in *Drosophila*. *Nature*, 312, 752-754.

Bargiello, T.A., Young, M.W. (1984) Molecular Genetics of a Biological Clock in *Drosophila*. *Proc Natl Acad Sci USA,* 81, 2142-2146.

Beuchle, D., Jaumouille, E., Nagoshi, E. (2012) The Nuclear Receptor unfulfilled is Required for Free-Running Clocks in *Drosophila* Pacemaker Neurons. *Curr Biol*, 22, 1221-1227.

Blanchardon, E., Grima, B., Klarsfeld, A., Chélot, E., Hardin, P. E., Préat, T., Rouyer, F. (2001) Defining the Role of *Drosophila* Lateral Neurons in the Control of Circadian Rhythms in Motor Activity and Eclosion by Targeted Genetic Ablation and PERIOD Protein Overexpression. *Eur J Neurosci*, 13, 871-888.

Blau, J., Young, M.W. (1999) Cycling vrille Expression is Required for a Functional *Drosophila* Clock. *Cell*, 99, 661-671.

Boulina, M., Samarajeewa, H., Baker, J.D., Kim, M.D., Chiba, A. (2013) Live Imaging of Multicolor-labeled Cells in *Drosophila*. *Development*, 140, 1605-1613.

Brand, A.H., Perrimon, N. (1993) Targeted Gene Expression as a Means of Altering Cell Fates and Generating Dominant Phenotypes. *Development*, 118, 401-415.

Brandes, C., Plautz, J.D., Stanewsky, R., Jamison, C.F., Straume, M., Wood, K.V., Kay, A.S., *et al.* (1996) Novel Features of *Drosophila* period Transcription Revealed by Real-time Luciferase Reporting. *Neuron*, 16, 687-692.

Broughton, S.J., Piper, M.D., Ikeya, T., Bass, T.M., Jacobson, J., Driege, Y., Martinez P., *et al*. (2005) Longer Lifespan, Altered Metabolism, and Stress Resistance in *Drosophila* from Ablation of Cells Making Insulin-like Ligands. *Proc Natl Acad Sci USA,* 102, 3105–3110.

Buchanan, R.L., Benzer, S. (1993) Defective Glia in the *Drosophila* Brain Degeneration Mutant Drop-dead. *Neuron*, 10, 839-850.

Buhl, E., Bradlaugh, A., Ogueta, M., Chen, K.F., Stanewsky, R., Hodge, J.J. (2016) Quasimodo Mediates Daily and Acute Light Effects on *Drosophila* Clock Neuron Excitability. *Proc Nat Acad Sci*, 113, 13486-13491.

Busza, A., Murad, A., Emery, P. (2007) Interactions Between Circadian Neurons Control Temperature Synchronization of *Drosophila* Behavior. *J Neurosci*, 27, 10722-10733.

Cachero, S., Ostrovsky, A.D., Yu, J.Y., Dickson, B.J., Jefferis, G.S.X.E. (2010) Sexual Dimorphism in the Fly Brain. *Curr Biol*, 20, 1589–1601.

Cavanaugh, D.J., Geratowski, J.D., Wooltorton, J.R., Spaethling, J.M., Hector, C.E., Zheng, X., Johnson, E.C., *et al*. (2014) Identification of a Circadian Output Circuit for Rest: Activity Rhythms in *Drosophila*. *Cell*, 157, 689-701.

Cavanaugh, D.J., Vigderman, A.S., Dean, T., Garbe, D.S., Sehgal, A. (2016) The *Drosophila* Circadian Clock Gates Sleep Through Time-of-day Dependent Modulation of Sleep-promoting Neurons. *Sleep*, 39, 345-356.

Cavey, M., Collins, B., Blau, J. (2016) Circadian Rhythms in Neuronal Activity Propagate Through Output Circuits. *Nat Neurosci,* 19, 587–95

Chouhan, N.S., Wolf, R., Helfrich-Förster, C., Heisenberg, M. (2015) Flies Remember the Time of Day. *Curr Biol*, 25, 1619-1624.

Crocker, A., Shahidullah, M., Levitan, I. B., Sehgal, A. (2010) Identification of a Neural Circuit That Underlies the Effects of Octopamine on Sleep:wake Behavior. *Neuron*, 65, 670–681.

Curtin, K.D., Huang, Z.J., Rosbash, M. (1995) Temporally Regulated Nuclear Entry of the *Drosophila* period Protein Contributes to the Circadian Clock. *Neuron*, 14, 365-372.

Cusumano, P., Klarsfeld, A., Chélot, E., Picot, M., Richier, B., Rouyer, F. (2009) Modulated Visual Inputs and Cryptochrome Define Diurnal Behavior in *Drosophila*. *Nat Neurosci*, 12, 1431-1437.

Cyran, S.A., Buchsbaum, A.M., Reddy, K.L., Lin, M.C., Glossop, N.R., Hardin, P.E., Young, M.W. *et al*. (2003) vrille, Pdp1, and dClock Form a Second Feedback Loop in the *Drosophila* Circadian Clock. *Cell*, 112, 329-341.

Darlington, T.K., Wager-Smith, K., Ceriani, M.F., Staknis, D., Gekakis, N., Steeves, T.D., Weitz, C.J. (1998) Closing the Circadian Loop: CLOCK-induced Transcription of its Own Inhibitors per and tim. *Science*, 280, 1599-1603.

De Mairan J.J. d'Ortous (1729) Observation Botanique. *Histoire de l'Academie Royale des Sciences*, 35–36. (in French)

De Candolle A.P. (1832) Physiologie Végétale. Bechet Jeune, Paris. (in French)

De Velasco, B., Erclik, T., Shy, D., Sclafani, J., Lipshitz, H., McInnes, R., Hartenstein, V. (2007) Specification and Development of the Pars Intercerebralis and Pars Lateralis, Neuroendocrine Command Centers in the *Drosophila* Brain. *Dev Biol*, 302, 309-323.

Dircksen, H., Zahnow, C.A., Gaus, G., Keller, R., Rao, K.R., Riehm J.P. (1987) The Ultrastructure of Nerve Endings Containing Pigmentdispersing Hormone (PDH) in Crustacean Sinus Glands: Identification by an Antiserum Against Aynthetic PDH. *Cell Tissue Res,* 250, 377–387.

Dircksen, H., Tesfai, L.K., Albus, C., Nässel, D.R. (2008) Ion Transport Peptide Splice Forms in Central and Peripheral Neurons Throughout Postembryogenesis of *Drosophila melanogaster*. *J Comp Neurol*, 509, 23-41.

Dowse, H.B. (2009) Analyses for Physiological and Behavioral Rhythmicity. *Methods Enzymol*, 454, 141-174.

Dowse, H.B. (2013) Maximum Entropy Spectral Analysis for Circadian Rhythms: Theory, History and Practice. *J Circadian Rhythms*, 11, 6.

Eck, S. (2016) The Impact of Thermogenetic Depolarizations of Specific Clock Neurons on *Drosophila melanogaster's* Circadian Clock. *Doctoral Thesis*, University of Würzburg.

Eck, S., Helfrich-Förster, C., Rieger, D. (2016) The Timed Depolarization of Morning and Evening Oscillators Phase Shifts the Circadian Clock of *Drosophila*. *J Biol Rhythms,* 31, 428-442.

el Jundi, B., Pfeiffer, K., Heinze, S., Homberg, U. (2014) Integration of Polarization and Chromatic Cues in the Insect Sky Compass. *J Comp Physiol,* 200, 575-589.

Emery, P., So, W.V., Kaneko, M., Hall, J.C., Rosbash, M. (1998) CRY, a *Drosophila* Clock and Light-regulated Cryptochrome, is a Major Contributor to Circadian Rhythm Resetting and Photosensitivity. *Cell*, 95, 669-679.

Evans, C.J., Olson, J.M., Ngo, K.T., Kim, E., Lee, N.E., Kuoy, E., Patananan, A.N., *et al.* (2009) G-TRACE: Rapid Gal4-based Cell Lineage Analysis in *Drosophila*. *Nat Methods*, 6, 603-605.

Ewer, J., Frisch, B., Hamblen-Coyle, M.J., Rosbash, M., Hall, J.C. (1992) Expression of the period Clock Gene Within Different Cell Types in the Brain of *Drosophila* Adults

and Mosaic Analysis of these Cells' Influence on Circadian Behavioral Rhythms. *J Neurosci*, 12, 3321-3349.

Fernandez, M.P., Berni, J., Ceriani, M.F. (2008) Circadian Remodeling of Neuronal Circuits Involved in Rhythmic Behavior. *PLoS Biol*, 6, e69.

Foster, R.G., Helfrich-Förster, C. (2001) The Regulation of Circadian Clocks by Light in Fruitflies and Mice. *Phil Trans R Soc B*, 356, 1779-1789.

Frisch, B., Hardin, P.E., Hamblen-Coyle, M.J., Rosbash, M., Hall, J.C. (1994) A Promoterless period Gene Mediates Behavioral Rhythmicity and Cyclical per Expression in a Restricted Subset of the *Drosophila* Nervous System. *Neuron*, 12, 555-570.

Fropf, R., Zhang, J., Tanenhaus, A.K., Fropf, W.J., Siefkes, E., Yin, J.C. (2014) Time of Day Influences Memory Formation and dCREB2 Proteins in *Drosophila*. *Front Sys Neurosci*, 8, 1-10.

Fujii, S., Krishnan, P., Hardin, P., Amrein, H. (2007) Nocturnal Male Sex Drive in *Drosophila*. *Curr Biol*, 17, 244-251.

Gekakis, N., Saez, L., Delahaye-Brown, A.M., Myers, M.P., Sehgal, A., Young, M.W., Weitz, C.J. (1995) Isolation of timeless by PER Protein Interaction: Defective Interaction Between timeless Protein and Long-Period Mutant PER^{L}. *Science*, 5237, 811-815.

Glaser, F.T., Stanewsky, R. (2005) Temperature Synchronization of the *Drosophila* circadian clock. *Curr Biol*, 15, 1352-1363.

Glossop, N.R., Lyons, L.C., Hardin, P.E. (1999) Interlocked Feedback Loops within the *Drosophila* Circadian Oscillator. *Science*, 286, 766-768.

Gmeiner, F., Kołodziejczyk, A., Yoshii, T., Rieger, D., Nässel, D.R., Helfrich-Förster, C. (2013) GABAB Receptors Play an Essential Role in Maintaining Sleep During the Second Half of the Night in *Drosophila melanogaster*. *J Exp Biol*, 216, 3837-3843.

Golic, K.G., Lindquist, S. (1989) The FLP Recombinase of Yeast Catalyzes Site-specific Recombination in the *Drosophila* Genome. *Cell*, 59, 499-509.

Golic, K.G. (1991) Site-specific Recombination Between Homologous Chromosomes in *Drosophila*. *Science*, 252, 958-962.

Gorostiza, E.A., Depetris-Chauvin, A., Frenkel, L., Pírez, N., Ceriani, M.F. (2014) Circadian Pacemaker Neurons Change Synaptic Contacts Across the Day. *Curr Biol*, 24, 2161-2167.

Grima, B., Lamouroux, A., Chelot, E., Papin, C. (2002) The F-box Protein Slimb Controls the Levels of Clock Proteins period and timeless. *Nature*, 420, 178-182.

Grima, B., Chélot, E., Xia, R., Rouyer, F. (2004) Morning and Evening Peaks of Activity Rely on Different Clock Neurons of the *Drosophila* Brain. *Nature*, 431, 869-873.

Gummadova, J.O., Coutts, G.A., Glossop, N.R.J. (2009) Analysis of the *Drosophila* Clock Promoter Reveals Heterogeneity in Expression Between Subgroups of Central Oscillator Cells and Identifies a Novel Enhancer Region. *J Biol Rhythms*, 24, 353-367.

Guo, F., Cerullo, I., Chen, X., Rosbash, M. (2014) PDF Neuron Firing Phase-shifts Key Circadian Activity Neurons in *Drosophila*. *Elife*, 3, e02780

Hadjieconomou, D., Rotkopf, S., Alexandre, C., Bell, D.M., Dickson, B.J., Salecker, I. (2011) Flybow: Genetic Multicolor Cell Labeling for Neural Circuit Analysis in *Drosophila melanogaster*. *Nat Methods*, 8, 260-266.

Hamblen-Coyle, M.J., Wheeler, D.A., Rutila, J.E., Rosbash, M., Hall, J. C. (1992) Behavior of period-altered Circadian Rhythm Mutants of *Drosophila* in Light: Dark Cycles (Diptera: *Drosophilidae*). *J Insect Behav*, 5, 417-446.

Hampel, S., Chung, P., McKellar, C.E., Hall, D., Looger, L.L., Simpson, J.H. (2011) *Drosophila* Brainbow: A Recombinase-based Fluorescence Labeling Technique to Subdivide Neural Expression Patterns. *Nat Methods*, 8, 253-259.

Handler, A.M., Konopka, R.J. (1979) Transplantation of a Circadian Pacemaker in *Drosophila*. *Nature*, 279, 236-238.

Hardin, P.E., Hall, J.C., Rosbash, M. (1990) Feedback of the *Drosophila period* Gene Product on Circadian Cycling of its Messenger RNA Levels. *Nature*, 343, 536-540.

Hardin, P.E. (2011) Molecular Genetic Analysis of Circadian Timekeeping in *Drosophila*. *Adv Genet*, 74, 141-173.

Harper, R.E., Dayan, P., Albert, J.T., Stanewsky, R. (2016) Sensory Conflict Disrupts Activity of the *Drosophila* Circadian Network. *Cell Rep*, 17, 1711-1718.

Helfrich, C., Engelmann, W. (1983) Circadian Rhythm of the Locomotor Activity in *Drosophila melanogaster* and its Mutants 'Sine Oculis' and 'Small Optic Lobes'. *Physiol Entomol*, 8, 257-272.

Helfrich-Förster, C., Homberg, U. (1993) Pigment-dispersing Hormone-immunoreactive Neurons in the Nervous System of Wild-type *Drosophila melanogaster* and of Several Mutants with Altered Circadian Rhythmicity. *J Comp Neurol*, 8, 177-190.

Helfrich-Förster, C. (1995) The Period Clock Gene is Expressed in Central Nervous System Neurons which also Produce a Neuropeptide that Reveals the Projections of Circadian Pacemaker Cells within the Brain of *Drosophila melanogaster*. *Proc Natl Acad Sci USA*, 92, 612-616.

Helfrich-Förster, C. (1998) Robust Circadian Rhythmicity of *Drosophila melanogaster* Requires the Presence of Lateral Neurons: A Brain-Behavioral Study of Disconnected Mutants. *J Comp Physiol*, 182, 435-453.

Helfrich-Förster, C. (2000) Differential Control of Morning and Evening Components in the Activity Rhythm of *Drosophila melanogaster* – Sex-specific Differences Suggest a Different Quality of Activity. *J Biol Rhythms*, 15, 135-154.

Helfrich-Förster, C., Edwards, T., Yasuyama, K., Wisotzki, B., Schneuwly, S., Stanewsky, R., Meinertzhagen, I.A., *et al.* (2002) The Extraretinal Eyelet of *Drosophila*: Development, Ultrastructure, and Putative Circadian Function. *J Neurosci*, 22, 9255-9266.

Helfrich-Förster, C. (2003) The Neuroarchitecture of the Circadian Clock in the Brain of *Drosophila melanogaster*. *Microsc Res Tech*, 62, 94-102.

Helfrich-Förster, C., Shafer, O.T., Wülbeck, C., Grieshaber, E., Rieger, D., Taghert, P. (2007) Development and Morphology of the Clock-gene-expressing Lateral Neurons of *Drosophila melanogaster*. *J Comp Neurol*, 500, 47-70.

Hendricks, J.C., Finn, S.M., Panckeri, K.A., Chavkin, J., Williams, J.A., Sehgal, A., Pack, A.I. (2000) Rest in *Drosophila* is a Sleep-like State. *Neuron*, 25, 129-138.

Hendricks, J.C., Lu, S., Kume, K., Yin, J.C.P., Yang, Z., Sehgal, A. (2003) Gender Dimorphism in the Role of Cycle (BMAL1) in Rest, Rest Regulation, and Longevity in *Drosophila melanogaster*. *J Biol Rhythms*, 18, 12-25.

Hermann-Luibl, C., Yoshii, T., Senthilan, P.R., Dircksen, H., Helfrich-Förster C. (2014) The Ion Transport Peptide is a New Functional Clock Neuropeptide in the Fruit Fly *Drosophila melanogaster*. *J Neurosci*, 34, 9522-9536.

Hofbauer, A. (1991) Eine Bibliothek monoklonaler Antikörper gegen das Gehirn von *Drosophila melanogaster*. *University of Würzburg, Würzburg*.

Hofman, M.A., Fliers, E., Goudsmit, E., Swaab, D.F. (1988) Morphometric Analysis of the Suprachiasmatic and Paraventricular Nuclei in the Human Brain: Sex Differences and Age-dependent Changes. *J Anat*, 160, 127-143.

Homberg, U., Davis, N.T., Hildebrand, J.G. (1991a) Peptide-immunocytochemistry of Neurosecretory Cells in the Brain and Retrocerebral Complex of the Spinx Moth *Manduca sexta*. *J Comp Neurol*. 303, 35–52.

Homberg, U., Wurden, S., Dircksen, H., Rao, K.R. (1991b) Comparative Anatomy of Pigment Dispersing Hormone-immunoreactive Neurons in the Brain of Orthopteroid Insects. *Cell Tissue Res*, 266, 343–357.

Houl, J.H., Ng, F., Taylor, P., Hardin, P.E. (2008) CLOCK Expression Identifies Developing Circadian Oscillator Neurons in the Brains of *Drosophila* Embryos. *BMC Neurosci*, 9, 119.

Hunter-Ensor, M., Ousley, A., Sehgal, A. (1996) Regulation of the *Drosophila* Protein timeless Suggests a Mechanism for Resetting the Circadian Clock by Light. *Cell*, 84, 677-685.

Im, S.H., Taghert, P.H. (2010) PDF Receptor Expression Reveals Direct Interactions Between Circadian Oscillators in *Drosophila*. *J Comp Neurol*, 518, 1925-1945.

Ito, K., Awano, W., Suzuki, K., Hiromi, Y., Yamamoto, D. (1997) The *Drosophila* Mushroom Body is a Quadruple Structure of Clonal Units Each of Which Contains a Virtually Identical Set of Neurones and Glial Cells. *Development*, 24, 761-771.

Ito, K., Shinomiya, K., Ito, M., Armstrong, J. D., Boyan, G., Hartenstein,V., Harzsch, S., *et al.* (2014) A Systematic Nomenclature for the Insect Brain. *Neuron*, 81, 755–765.

Jefferis, G.S., Potter, C.J., Chan, A.M., Marin, E.C., Rohlfing, T., Maurer, C.R., Luo, L. (2007) Comprehensive Maps of *Drosophila* Higher Olfactory Centers: Spatially Segregated Fruit and Pheromone Representation. *Cell*, 128, 1187-1203.

Jenett, A., Rubin, G.M., Ngo, T.T., Sheperd, D., Murphy, C., Dionne, H., Pfeiffer, B.D., *et al.* (2012) A *Gal4*-driver Line Resource for *Drosophila* Neurobiology. *Cell Rep*, 2, 991-1001.

Johard, H.A., Yoshii, T., Dircksen, H., Cusumano, P., Rouyer, F., Helfrich-Förster, C., Nässel, D.R. (2009) Peptidergic Clock Neurons in *Drosophila*: Ion Transport Peptide and Short Neuropeptide F in Subsets of Dorsal and Ventral Lateral Neurons. *J Comp Neurol*, 516, 59-73.

Kanca, O., Caussinus, E., Denes, A.S., Percival-Smith, A., Affolter, M. (2014) Raeppli: A Whole-tissue Labeling Tool for Live Imaging of *Drosophila* Development. *Development*, 141, 472-480.

Kaneko, M., Helfrich-Förster, C., Hall, J. C. (1997) Spatial and Temporal Expression of the period and timeless Genes in the Developing Nervous System of *Drosophila*: Newly Identified Pacemaker Candidates and Novel Features of Clock Gene Product Cycling. *J Neurosci*, 17, 6745-6760.

Kaneko, M., Hall, J.C. (2000) Neuroanatomy of Cells Expressing Clock Genes in *Drosophila*: Transgenic Manipulation of the period and timeless Genes to Mark the Perikarya of Circadian Pacemaker Neurons and their Projections. *J Comp Neurol*, 422, 66-94.

Kaneko, H., Head, L.M., Ling, J., Tang, X., Liu, Y., Hardin, P.E., Emery, P. *et al.* (2012) Circadian Rhythm of Temperature Preference and its Neural Control in *Drosophila*. *Curr Biol*, 22, 1851-1857.

King, A.N., Barber, A.F., Smith, A.E., Dreyer, A.P., Sitaraman, D., Nitabach, M.N., Cavanough, D.J., *et al.* (2017) A peptidergic Circuit Links the Circadian Clock to Locomotor Activity. *Curr Biol*, 27, 1915-1927.

Klarsfeld, A., Malpel, S., Michard-Vanhée, C., Picot, M., Chélot, E., Rouyer, F. (2004) Novel Features of Cryptochrome-Mediated Photoreception in the Brain Circadian Clock of *Drosophila*. *J Neurosci*, 24, 1468-1477.

Kloss, B., Price, J.L., Saez, L., Blau, J., Rothenfluh, A., Wesley, C.S., Young, M.W. (1998) The *Drosophila* Clock Gene double-time Encodes a Protein Closely Related to Human Casein Kinase Iε. *Cell*, 94, 97-107.

Kloss, B., Rothenfluh, A., Young, M.W., Saez, L. (2001) Phosphorylation of period is Influenced by Cycling Physical Associations of double-time, period, and timeless in the *Drosophila* Clock. *Neuron*, 30, 699-706.

Ko, H.W., Jiang, J., Edery, I. (2002) Role for Slimb in the Degradation of *Drosophila* Period Protein Phosphorylated by Doubletime. *Nature*, 420, 673-678.

Kohl, J., Ng, J., Cachero, S., Ciabatti, E., Dolan, M.J., Sutcliffe, B., Tozer, A., *et al*. (2014) Ultrafast Tissue Staining with Chemical Tags. *Proc Natl Acad Sci USA*, 111, 3805-3814.

Konopka, R.J., Benzer, S. (1971) Clock Mutants of *Drosophila melanogaster*. *Proc Natl Acad Sci USA,* 68, 2112-2116.

Konopka, R.J., Pittendrigh, C., Orr, D. (1989) Reciprocal Behaviour Associated with Altered Homeostasis and Photosensitivity of *Drosophila* Clock Mutants. *J Neurogen*, 6, 1-10.

Lai, S.L., Lee, T. (2006) Genetic Mosaic with Dual Binary Transcriptional Systems in *Drosophila*. *Nat Neurosci*, 9, 703–709.

Lee, C., Parikh, V., Itsukaichi, T., Bae, K., Edery, I. (1996) Resetting the *Drosophila* Clock by Photic Regulation of PER and a PER-TIM Complex. *Science*, 271, 1740.

Lee, C., Bae, K., Edery, I. (1998) The *Drosophila* CLOCK Protein Undergoes Daily Rhythms in Abundance, Phosphorylation, and Interactions with the PER-TIM Complex. *Neuron*, 21, 857-867.

Lee, C., Bae, K., Edery, I. (1999) PER and TIM Inhibit the DNA Binding Activity of a dCLOCK-CYC/dBMAL1 Heterodimer Without Disrupting Formation of the Heterodimer: A Basis for Circadian Transcription. *Mol Cell Biol*, 19, 5316-5325.

Lee, T., Luo, L. (1999) Mosaic Analysis with a Repressible Cell Marker for Studies of Gene Function in Neuronal Morphogenesis. *Neuron,* 22, 451-461.

Lee, T., Luo, L. (2001) Mosaic Analysis with a Repressible Cell Marker (MARCM) for *Drosophila* Neural Development. *Trends Neurosci*, 24, 251-254.

Lin, J.M., Kilman, V.L., Keegan, K., Paddock, B., Emery-Le, M., Rosbash, M., Allada, R. (2002) A Role for Casein Kinase 2alpha in the *Drosophila* Circadian Clock. *Nature*, 420, 816-820.

Liu, T., Mahesh, G., Houl, J.H., Hardin, P.E. (2015) Circadian Activators are Expressed Days Before They Initiate Clock Function in Late Pacemaker Neurons from *Drosophila*. *J Neurosci*, 35, 8662-8671.

Livet, J., Weissman, T. A., Kang, H., Draft, R. W., Lu, J., Bennis, R. A., Sanes, J.R. *et al.* (2007) Transgenic Strategies for Combinatorial Expression of Fluorescent Proteins in the Nervous System. *Nature*, 450, 56-62.

Lue, N.F., Chasman, D.I., Buchman, A.R., Kornberg, R.D. (1987) Interaction of GAL4 and GAL80 Gene Regulatory Proteins in Vitro. *Mol Cell Biol*, 7, 3446–51.

Lyons, L.C., Roman, G. (2009) Circadian Modulation of Short-term Memory in *Drosophila*. *Learn Mem*, 16, 19-27.

Manoli, D.S., Foss, M., Villella, A., Taylor, B.J., Hall, J.C., Baker, B.S. (2005) Male-specific Fruitless Specifies the Neural Substrates of *Drosophila* Courtship Behaviour. *Nature,* 436, 395–400.

Martinek, S., Inonog, S., Manoukian, A.S., Young, M.W. (2001) A Role for the Segment Polarity Gene shaggy/GSK-3 in the *Drosophila* Circadian Clock. *Cell*, 105, 769-779.

McDonald, M.J., Rosbash, M., Emery, P. (2001) Wild-type Circadian Rhythmicity is Dependent on Closely Spaced E boxes in the *Drosophila* timeless Promoter. *Mol Cell Biol*, 21, 1207–1217.

Menet, J.S., Abruzzi, K.C., Desrochers, J., Rodriguez, J., Rosbash, M. (2010) Dynamic PER Repression Mechanisms in the *Drosophila* Circadian Clock: From on-DNA to off-DNA. *Gen Dev*, 24, 358-367.

Mezan, S., Feuz, J.D., Deplancke, B., Kadener, S. (2016) PDF Signaling Is an Integral Part of the *Drosophila* Circadian Molecular Oscillator. *Cell Rep*, 17, 708–719.

Moore, R.Y., Lenn, N.J. (1972) A Retinohypothalamic Projection in the Rat. *J Comp Neurol*, 146, 1-14.

Myers, M.P., Wager-Smith, K., Rothenfluh-Hilfiker, A., Young, M.W. (1996) Light-induced Degradation of TIMELESS and Entrainment of the *Drosophila* Circadian Clock. *Science*, 271, 1736.

Myers, E.M., Yu, J., Sehgal, A. (2003) Circadian Control of Eclosion Interaction between a Central and Peripheral Clock in *Drosophila melanogaster*. *Curr Biol*, 13, 526-533.

Nellen, D., Burke, R., Struhl, G., Basler, K. (1996) Direct and Long-Range Action of a DPP Morphogen Gradient. *Cell*, 85, 357-368.

Nicolaï, L.J., Ramaekers, A., Raemaekers, T., Drozdzecki, A., Mauss, A.S., Yan, J., Landgraf, *et al.* (2010) Genetically Encoded Dendritic Marker Sheds Light on Neuronal Connectivity in *Drosophila*. *Proc Natl Acad Sci USA*, 107, 20553-20558.

Omoto, J.J., Keleş, M.F., Nguyen, B.C.M., Bolanos, C., Lovick, J.K., Frye, M.A., Hartenstein, V. (2017) Visual Input to the *Drosophila* Central Complex by Developmentally and Functionally Distinct Neuronal Populations. *Curr Biol*, 27, 1098-1110.

Owald, D., Lin, S., Waddell, S. (2015) Light, Heat, Action: Neural Control of Fruit Fly Behaviour. *Phil Trans R Soc B*, 370, 20140211.

Parisky, K.M., Agosto, J., Pulver, S.R., Shang, Y., Kuklin, E., Hodge, J.J., Kang, K. *et al.* (2008) PDF Cells are a GABA-responsive Wake-promoting Component of the *Drosophila* Sleep Circuit. *Neuron*, 60, 672-682.

Park, D., Griffith, L.C. (2006) Electrophysiological and Anatomical Characterization of PDF-positive Clock Neurons in the Intact Adult *Drosophila* Brain. *J Neurophysiol*, 95, 3955-3960.

Peng, Y., Stoleru, D., Levine, J.D., Hall, J.C., Rosbash, M. (2003) *Drosophila* Free-running Rhythms Require Intercellular Communication. *PLoS Biol*, 1, e13.

Peng, H., Ruan, Z., Long, F., Simpson, J.H., Myers, E.W. (2010) V3D Enables Real-time 3D Visualization and Quantitative Analysis of Large-scale Biological Image Data Sets. *Nat Biotechnol*, 28, 348-353.

Peng, H., Bria, A., Zhou, Z., Iannello, G., Long, F. (2014a) Extensible Visualization and Analysis for Multidimensional Images Using Vaa3D. *Nat Protoc*, 9, 193-208.

Peng, H., Tang, J., Xiao, H., Bria, A., Zhou, J., Butler, V., Zhou, Z., *et al.* (2014b) Virtual Finger Boosts Three-dimensional Imaging and Microsurgery as well as Terabyte Volume Image Visualization and Analysis. *Nat Commun*, 5, 4342.

Peschel, N., Chen, K.F., Szabo, G., Stanewsky, R. (2009) Light-dependent Interactions Between the *Drosophila* Circadian Clock Factors cryptochrome, jetlag, and timeless. *Curr Biol*, 19, 241-247.

Petsakou, A., Sapsis, T.P., Blau, J. (2015) Circadian Rhythms in rho1 Activity Regulate Neuronal Plasticity and Network Hierarchy. *Cell*, 162, 823–835.

Pfeiffer B.D., Jenett, A., Hammonds, A.S., Ngo, T.T., Misra, S., Murphy, C., Scully, A., *et al.* (2008) Tools for Neuroanatomy and Neurogenetics in *Drosophila*. *Proc Natl Acad Sci USA*, 105, 9715-9720.

Pfeiffer, B.D., Ngo, T.T., Hibbard, K.L., Murphy, C., Jenett, A., Truman, J.W., Rubin, G.M. (2010) Refinement of Tools for Targeted Gene Expression in *Drosophila*. *Genetics*, 186, 735-755.

Picot, M., Klarsfeld, A., Chélot, E., Malpel, S., Rouyer, F. (2009) A Role for Blind DN2 Clock Neurons in Temperature Entrainment of the *Drosophila* Larval Brain. *J Neurosci*, 29, 8312-8320.

Pignoni, F., Zipursky, S.L. (1997) Induction of *Drosophila* Eye Development by Decapentaplegic. *Development*, 124, 271-278.

Pittendrigh, C.S. (1960) Circadian Rhythms and the Circadian Organization of Living Systems. *Cold Spring Harb Symp Quant Biol,* 25, 159–184.

Pittendrigh, C.S., Skopik, S.D. (1970) Circadian Systems, V. The Driving Oscillation and the Temporal Sequence of Development. *Proc Natl Acad Sci*, 65, 500-507.

Pittendrigh, C.S., Daan S. (1976) A Functional Analysis of Circadian Pacemakers in Nocturnal Rodents. *J Comp Neurol*, 106, 291-331.

Pírez, N., Christmann, B.L., Griffith, L.C. (2013) Daily Rhythms in Locomotor Circuits in *Drosophila* Involve PDF. *J Neurophysiol*, 110, 700-708.

Plautz, J.D., Straume, M., Stanewsky, R., Jamison, C.F., Brandes, C., Dowse, H.B., Hall, J.C. (1997) Quantitative Analysis of *Drosophila* period Gene Transcription in Living Animals. *J Biol Rhythms*, 12, 204-217.

Potdar, S., Vasu, S. (2012) Large Ventral Lateral Neurons Determine the Phase of Evening Activity Peak Across Photoperiods in *Drosophila melanogaster*. *J Biol Rhythms*, 27, 267-279.

Potter, C. J., Tasic, B., Russler, E.V., Liang, L., Luo, L. (2010) The Q System: A Repressible Binary System for Transgene Expression, Lineage Tracing, and Mosaic Analysis. *Cell*, 141, 536-548.

Price, J.L., Dembinska, M.E., Young, M.W., Rosbash, M. (1995) Suppression of PERIOD Protein Abundance and Circadian Cycling by the *Drosophila* Clock Mutation timeless. *EMBO J*, 14, 4044-4049.

Price, J.L., Blau, J., Rothenfluh, A., Abodeely, M., Kloss, B., Young, M.W. (1998) Double-time is a Novel *Drosophila* Clock Gene that Regulates PERIOD Protein Accumulation. *Cell*, 94, 83-95.

Reddy, P., Zehring, W.A., Wheeler, D.A., Pirrotta, V., Hadfield, C., Hall, J.C., Rosbash, M. (1984) Molecular Analysis of the Period Locus in *Drosophila melanogaster* and Identification of a Transcript Involved in Biological Rhythms. *Cell*, 38, 701-710.

Refinetti, R., Menaker, M. (1992) Body Temperature Rhythm of the Tree Shrew, *Tupaia belangeri*. *J Exp Zool A Ecol Genet Physiol*, 263, 453-457.

Reischig, T., Stengl, M. (2003) Ectopic Transplantation of the Accessory Medulla Restores Circadian Locomotor Rhythms in Arrhythmic Cockroaches (*Leucophaea maderae*). *J Exp Biol*, 206, 1877-1886.

Renn, S.C., Park, J.H., Rosbash, M., Hall, J.C., Taghert, P.H. (1999) A *pdf* Neuropeptide Gene Mutation and Ablation of PDF Neurons Each Cause Severe Abnormalities of Behavioral Circadian Rhythms in *Drosophila*. *Cell*, 99, 791–802.

Rideout, E.J., Dornan, A.J., Neville, M.C., Eadie, S., Goodwin, S.F. (2010) Control of Sexual Differentiation and Behavior by the doublesex Gene in *Drosophila melanogaster*. *Nat Neurosci*, 13, 458-466.

Rieger, D., Stanewsky R., Helfrich-Förster, C. (2003) Cryptochrome, Compound Eyes, Hofbauer-Buchner Eyelets, and Ocelli Play Different Roles in the Entrainment and Masking Pathway of the Locomotor Activity Rhythm in the Fruit Fly *Drosophila melanogaster*. *J Biol Rhythms*, 18, 377-391.

Rieger, D., Shafer, O.T., Tomioka, K., Helfrich-Förster, C. (2006) Functional Analysis of Circadian Pacemaker Neurons in *Drosophila melanogaster*. *J Neurosci*, 26, 2531–2543.

Rieger, D., Wülbeck, C., Rouyer, F., Helfrich-Förster, C. (2009) *Period* Gene Expression is Sufficient for Rhythmic Activity of *Drosophila melanogaster* under Dim Light Conditions. *J Biol Rhythms*, 24, 271-282.

Rieger, D., Peschel, N., Dusik, V., Clotz, S., Helfrich-Förster, C. (2012) The Ability to Entrain to Long Photoperiods Differs Between 3 *Drosophila melanogaster* Wild-type Strains and is Modified by Twilight Simulation. *J Biol Rhythms*, 21, 37-47.

Roberts, L., Leise, T.L., Noguchi, T., Galschiodt, A.M., Houl, J.H., Welsh, D.K., Holmes, T.C. (2015) Light Evokes Rapid Circadian Network Oscillator Desynchrony Followed by Gradual Phase Retuning of Synchrony. *Curr Biol*, 25, 858-867.

Robinett, C.C., Vaughan, A.G., Knapp, J.M., Baker, B.S. (2010) Sex and the Single-Cell. II. There is a Time and Place for Sex. *PLoS Biol*, 8, e1000365.

Roenneberg T., Merrow M. (2005) Circadian Clocks: The Fall and Rise of Physiology. *Nat Rev*, 6, 965-971.

Rohlfing, T., Maurer, C.R. (2003) Nonrigid Image Registration in Shared-memory Multiprocessor Environments with Application to Brains, Breasts, and Bees. *IEEE Trans Inf Technol Biomed*, 7, 16-25.

Rowell, H.F. (1976) The Cells of the Insect Neurosecretory System: Constancy, Variability, and the Concept of the Unique Identifiable Neuron. *Adv Insect Physiol*, 12, 63–123.

Ruben, M., Drapeau, M.D., Mizrak, D., Blau, J. (2012) A Mechanism for Circadian Control of Pacemaker Neuron Excitability. *J Biol Rhythms*, 27, 353-364.

Rulifson, E.J., Kim, S.K., Nusse, R. (2002) Ablation of Insulin-producing Neurons in Flies: Growth and Diabetic Phenotypes. *Science*, 296, 1118-1120.

Rutila, J.E., Suri, V., Le, M., So, W.V., Rosbash, M., Hall, J.C. (1998) CYCLE is a Second bHLH-PAS Clock Protein Essential for Circadian Rhythmicity and Transcription of *Drosophila* period and timeless. *Cell*, 93, 805-814.

Sabado, V., Vienne, L., Nunes, J.M., Rosbash, M., Nagoshi, E. (2017) Fluorescence Circadian Imaging Reveals a PDF-dependent Transcriptional Regulation of the *Drosophila* Molecular Clock. *Sci Rep*, 7, 41560.

Sakai, T., Ishida, N. (2001) Circadian Rhythms of Female Mating Activity Governed by Clock Genes in *Drosophila*. *Proc Natl Acad Sci USA*, 98, 9221-9225.

Schindelin, J., Arganda-Carreras, I., Frise, E., Kaynig, V., Longair, M., Pietzsch, S., Rueden, C., *et al.* (2012) Fiji: An Open-source Platform for Biological-image Analysis. *Nat Methods*, 9, 676-682.

Schlichting, M., Menegazzi, P., Lelito, K.R., Yao, Z., Buhl, E., Dalla Benetta, E., Bahle, A., *et al.* (2016) A Neural Network Underlying Circadian Entrainment and Photoperiodic Adjustment of Sleep and Activity in *Drosophila*. *J Neurosci*, 36, 9084-9096.

Schmid, B., Schindelin, J., Cardona, A., Longair, M., Heisenberg M. (2010) A High-level 3D Visualization API for Java and ImageJ. *BMC Bioinformatics*, 11, 274.

Sehadova, H., Glaser, F.T., Gentile, C., Simoni, A., Giesecke, A., Albert, J.T., Stanewsky, R. (2009) Temperature Entrainment of *Drosophila's* Circadian Clock Involves the Gene nocte and Signaling from Peripheral Sensory Tissues to the Brain. *Neuron*, 64, 251-266.

Sehgal, A., Price, J.L., Man, B., Young, M.W. (1994) Loss of Circadian Behavioral Rhythms and per RNA Oscillations in the *Drosophila* Mutant Timeless. *Science,* 263, 1603-1605.

Selcho, M., Mill'an, C., Palacios-Munoz, A., Ruf, F., Ubillo, L., Chen, J., Bergmann, G., *et al.* (2017) Central and Peripheral Clocks are Coupled by a Neuropeptide Pathway in *Drosophila*. *Nat Communicat*, 8, 15563.

Sellix, M.T., Currie, J., Menaker, M., Wijnen, H. (2010) Fluorescence/luminescence Circadian Imaging of Complex Tissues at Single-cell Resolution. *J Biol Rhythms*, 25, 228-232.

Sepp, K.J., Schulte, J., Auld, V.J. (2001) Peripheral Glia Direct Axon Guidance Across the CNS/PNS Transition Zone. *Dev Biol*, 238, 47-63.

Shafer, O.T., Rosbash, M., Truman, J.W. (2002) Sequential Nuclear Accumulation of the Clock Proteins period and timeless in the Pacemaker Neurons of *Drosophila melanogaster*. *J Neurosci*, 22, 5946-5954.

Shafer, O.T., Helfrich-Förster, C., Renn, S.C.P., Taghert, P.H. (2006) Reevaluation of *Drosophila melanogaster´s* Neuronal Circadian Pacemakers Reveals New Neuronal Classes. *J Comp Neurol*, 498, 180-193.

Shafer, O.T., Kim, D.J., Dunbar-Yaffe, R., Nikolaev, V.O., Lohse, M.J., Taghert, P.H. (2008) Widespread Receptivity to Neuropeptide PDF Throughout the Neuronal Circadian Clock Network of *Drosophila* Revealed by Real-time Cyclic AMP Imaging. *Neuron*, 58, 223-237.

Shaw, P.J., Cirelli, C., Greenspan, R.J., Tononi, G. (2000) Correlates of Sleep and Waking in *Drosophila melanogaster*. *Science*, 287, 1834-1837.

Sheeba, V., Gu, H., Sharma, V.K., O'Dowd, D.K., Holmes, T.C. (2008) Circadian-and Light-dependent Regulation of Resting Membrane Potential and Spontaneous Action Potential Firing of *Drosophila* Circadian Pacemaker Neurons. *J Neurophysiol*, 99, 976-988.

Sheeba, V., Fogle, K.J., Holmes, T.C. (2010) Persistence of Morning Anticipation Behavior and High Amplitude Morning Startle Response Following Functional Loss of Small Ventral Lateral Neurons in *Drosophila*. *PLOS One*, 5, e11628.

Shimosako, N., Hadjieconomou, D., Salecker, I. (2014) Flybow to Dissect Circuit Assembly in the *Drosophila* Brain. *Methods Mol Biol*, 1082, 57-69.

Sidote, D., Majercak, J., Parikh, V., Edery, I. (1998) Differential Effects of Light and Heat on the *Drosophila* Circadian Clock Proteins PER and TIM. *Mol Cell Biol*, 18, 2004–2013.

Siegmund, T., Korge, G. (2001) Innervation of the Ring Gland of *Drosophila melanogaster*. *J Comp Neurol*, 431, 481–491.

Sivachenko, A., Li, Y., Abruzzi, K.C., Rosbash, M. (2013) The Transcription Factor Mef2 Links the *Drosophila* Core Clock to Fas2, Neuronal Morphology, and Circadian Behavior. *Neuron*, 79, 281-292.

Stanewsky, R., Jamison, C.F., Plautz, J.D., Kay, S.A., Hall, J.C. (1997) Multiple Circadian-regulated Elements Contribute to Cycling period Gene Expression in *Drosophila*. *EMBO J*, 16, 5006-5018.

Stanewsky, R., Kaneko, M., Emery, P., Beretta, B., Wager-Smith, K., Kay, S.A., Rosbash, M. (1998) The cryb Mutation Identifies Cryptochrome as a Circadian Photoreceptor in *Drosophila*. *Cell*, 95, 681-692.

Stanewsky, R., Lynch, K.S., Brandes, C., Hall, J.C. (2002) Mapping of Elements Involved in Regulating Normal Temporal period and timeless RNA Expression Patterns in *Drosophila melanogaster*. *J Biol Rhythms*, 17, 293-306.

Stephan, F.K., Zucker, I. (1972) Circadian Rhythms in Drinking Behavior and Locomotor Activity of Rats are Eliminated by Hypothalamic Lesions. *Proc Natl Acad Sci USA*, 69, 1583-1586.

Stephan, F.K., Nunez, A.A. (1977) Elimination of Circadian Rhythms in Drinking, Activity, Sleep, and Temperature by Isolation of the Suprachiasmatic Nuclei. *Behav Biol*, 20, 1-16.

Stevenson, R.D. (1985) Body Size and Limits to the Daily Range of Body Temperature in Terrestrial Ectotherms. *Am Nat*, 125, 102-117.

Stoleru, D., Peng, Y., Agosto, J., Rosbash, M. (2004) Coupled Oscillators Control Morning and Evening Locomotor Behaviour of *Drosophila*. *Nature*, 431, 862-868.

Sutcliffe, B., Ng, J., Auer, T.O., Pasche, M., Benton, R., Jefferis, G.S., Cachero, S. (2017) Second-Generation *Drosophila* Chemical Tags: Sensitivity, Versatility, and Speed. *Genetics*, 205, 1399-1408.

Tang, X., Roessingh, S., Hayley, S.E., Chu, M.L., Tanaka, N.K., Wolfgang, W., Song, S. *et al*. (2017) The Role of PDF Neurons in Setting the Preferred Temperature Before Dawn in *Drosophila*. *eLife*, 6.

Tataroglu, O., Emery, P. (2014) Studying Circadian Rhythms in *Drosophila melanogaster*. *Methods*, 68, 140-150.

Tauber, E., Roe, H., Costa, R., Hennessy, J.M., Kyriacou, C.P. (2003) Temporal Mating Isolation Driven by a Behavioral Gene in *Drosophila*. *Curr Biol*, 13, 140-145.

Ulrych, T.J., Bishop, T.N. (1975) Maximum Entropy Spectral Analysis and Autoregressive Decomposition. *Rev Geophys*, 13, 183-200.

Veelaert, D., Schoofs, L., De Loof, A., (1998) Peptidergic Control of the Corpus Cardiacum-Corpora Allata Complex of Locusts. *Int Rev Cyt*, 182, 249–302.

Veleri, S., Rieger, D., Helfrich-Förster, C., Stanewsky, R. (2007) Hofbauer-Buchner Eyelet Affects Circadian Photosensitivity and Coordinates TIM and PER Expression in *Drosophila* Clock Neurons. *J Biol Rhythms*, 22, 29–42.

Veleri S., Brandes C., Helfrich-Förster C., Hall J.C., Stanewsky R. (2003) A Self-sustaining, Light-entrainable Circadian Oscillator in the *Drosophila* Brain. *Curr Biol,* 13, 1758-1767.

Volkenhoff, A., Weiler, A., Letzel, M., Stehling, M., Klämbt, C., Schirmeier, S. (2015) Glial Glycolysis is Essential for Neuronal Survival in *Drosophila*. *Cell Metab*, 22, 437-447.

Wang, G.K., Ousley, A., Darlington, T.K., Chen, D., Chen, Y., Fu, W., Hickman, L.J., *et al*. (2001) Regulation of the Cycling of timeless (tim) RNA. *J Neurobiol*, 47, 161–175.

Worley, M.I., Setiawan, L., Hariharan, I.K. (2013) TIE-DYE: A Combinatorial Marking System to Visualize and Genetically Manipulate Clones During Development in *Drosophila melanogaster*. *Development*, 140, 3275-3284.

Xiao, H., Peng, H. (2013) APP2: Automatic Tracing of 3D Neuron Morphology Based on Hierarchical Pruning of a Gray-weighted Image Distance-tree. *Bioinformatics*, 29, 1448-1454.

Xiong, W.C., Montell, C. (1995) Defective Glia Induce Neuronal Apoptosis in the Repo Visual System of *Drosophila*. *Neuron*, 14, 581-590.

Xu, T., Rubin, G.M. (1993) Analysis of Genetic Mosaics in Developing and Adult *Drosophila* Tissues. *Development*, 117, 1223-1237.

Xu, K., Zheng, X., Sehgal, A. (2008) Regulation of Feeding and Metabolism by Neuronal and Peripheral Clocks in *Drosophila*. *Cell Metab*, 8, 289-300.

Xu, K., DiAngelo, J.R., Hughes, M.E., Hogenesch, J.B., Sehgal, A. (2011) The Circadian Clock Interacts with Metabolic Physiology to Influence Reproductive Fitness. *Cell Metab*, 13, 639-654.

Yang, Z., Sehgal, A. (2001) Role of Molecular Oscillations in Generating Behavioral Rhythms in *Drosophila*. *Neuron*, 29, 453-467.

Yao, Z., Shafer, O.T. (2014) The *Drosophila* Circadian Clock is a Variably Coupled Network of Multiple Peptidergic Units. *Science*, 343, 1516-1520.

Yoshii, T., Sakamoto, M., Tomioka, K. (2002) A Temperature-dependent Timing Mechanism is Involved in the Circadian System that Drives Locomotor Rhythms in the Fruit Fly *Drosophila melanogaster*. *Zoolog Sci*, 19, 841-850.

Yoshii, T., Heshiki, Y., Ibuki-Ishibashi, T., Matsumoto, A., Tanimura, T., Tomioka, K. (2005) Temperature Cycles Drive *Drosophila* Circadian Oscillation in Constant Light that Otherwise Induces Behavioural Arrhythmicity. *Eur J Neurosci*, 22, 1176-1184.

Yoshii, T., Todo T., Wülbeck C., Stanewsky R., Helfrich-Förster C. (2008) Cryptochrome is Present in the Compound Eyes and a Subset of *Drosophila*'s Clock Neurons. *J Comp Neurol*, 508, 952-966.

Yoshii, T., Vanin, S., Costa, R., Helfrich-Förster, C. (2009) Synergic Entrainment of *Drosophila's* Circadian Clock by Light and Temperature. *J Biol Rhythms*, 24, 452-464.

Yoshii, T., Rieger, D., Helfrich-Förster, C. (2012) Two Clocks in the Brain: An Update of the Morning and Evening Oscillator Model in *Drosophila*. *Prog Brain Res*, 199, 59-82.

Yoshii, T., Hermann-Luibl, C., Helfrich-Förster, C. (2016) Circadian Light-input Pathways in *Drosophila*. *Commun Integr Biol*, 9, e1102805.

Yu, W., Zheng, H., Houl, J.H., Dauwalder, B., Hardin, P.E. (2006) PER-dependent Rhythms in CLK Phosphorylation and E-box Binding Regulate Circadian Transcription. *Gen Dev*, 20, 723-733.

Yu, J.Y., Kanai, M.I., Demir, E., Jefferis, G.S.X.E., Dickson, B.J. (2010) Cellular Organization of the Neural Circuit that Drives *Drosophila* Courtship Behavior. *Curr Biol*, 20, 1602–1614.

Zaretsky, M., Loher, W. (1983) Anatomy and Electrophysiology of Individual Neurosecretory Cells of an Insect Brain. *J Comp Neurol*, 216, 253–263.

Zecca, M., Basler, K., Struhl, G. (1996) Direct and Long-range Action of a Wingless Morphogen Gradient. *Cell*, 87, 833-844.

Zehring, W.A., Wheeler, D.A., Reddy, P., Konopka, R.J., Kyriacou, C.P., Rosbash, M., Hall, J.C. (1984) P-element Transformation with Period Locus DNA Restores Rhythmicity to Mutant, Arrhythmic *Drosophila melanogaster*. *Cell*, 39, 369-376.

Zeng, H., Qian, Z., Myers, M.P., Rosbash, M. (1996) A Light-entrainment Mechanism for the *Drosophila* Circadian Clock. *Nature*, 380, 129-135.

Zhang, Y.Q., Rodesch, C.K., Broadie, K. (2002) Living Synaptic Vesicle Marker: Synaptotagmin-GFP. *Genesis*, 34, 142-145.

Zhou, C., Franconville, R., Vaughan, A.G., Robinett, C.C., Jayaraman, V., Baker, B.S. (2015) Central Neural Circuitry Mediating Courtship Song Perception in Male *Drosophila*. *Elife*, 4, e08477.

7 Supplement

7.1 List of Abbreviations

5^{th} s-LN_v	5^{th} small ventrolateral neuron
AME	Accessory medulla
AME_{vel}	Ventral elongation of the accessory medulla
AOT	Anterior optic tract
AOTU	Anterior optic tubercle
AR	Autoregressive
AVLP	Anterior ventrolateral protocerebrum
AVP	Anterior visual pathway
CA	Calyx
CCD	Charged Coupled Device
clk, CLK	Clock (*gene*, PROTEIN)
CFP	Cyan fluorescent protein
cry, CRY	Cryptochrome (*gene*, PROTEIN)
CRY^+/ CRY^-	CRY expressing/ lacking
CK2	Caseine kinase 2

CT	Circadian time
CX	Central complex
cyc, CYC	Cycle (*gene*, PROTEIN)
DBT	Doubletime-kinase
DD	Constant darkness
DenMark	Dendritic marker (TLN::mCherry)
DILP2	*Drosophila* insulin-like peptide 2
DIV	Days *in vitro*
DN	Dorsal clock neurons
DN_1	Dorsal neurons 1
DN_{1a}	Anterior DN_1
DN_{1p}	Posterior DN_1
DN_2	Dorsal neurons 2
DN_3	Dorsal neurons 3
E-box	Enhancer-box
E1, E2, E3	Evening-oscillator subunit 1, 2, 3
E-...	Evening-... (as in the following)
E-cells	Evening-cells
E-oscillator	Evening-oscillator

EGFP	Enhanced green fluorescent protein
EtOH	Ethanol
FB2.0B	*UAS-Flybow2.0B*
Flp, Flp	Flippase (DNA-recombinase) (*gene*, Protein)
FPs	Fluorescence proteins
FRT	Flippase recognition target
Gal4, GAL4	Galaktose-responsive transcription factor 4 (*gene*, PROTEIN)
gal80, GAL80	Repressor of GAL4 (*gene*, PROTEIN)
GFP	Green fluorescent protein
hs-...	Heat-shock promotor
hs-Flp	Wildtype-like Flippase under control of heat-shock promotor
hs-mFlp5	Modified Flippase under control of heat-shock promotor
HyD	Hybrid detectors
ICL	Inferior clamp
IHC	Immunohistochemistry
ITP	Ion transport peptide
ITP^+/ ITP^-	ITP expressing/ lacking
JFRC2	Janelia Farm Research Campus standard brain
KC	Kenyon cell

L1	Larval stage 1
L2	Larval stage 2
L3	Larval stage 3
LCBR	Lateral cell body rind
LD	Light-dark
lexA/ lexOp	Binary expression system for *Drosophila*
LH	Lateral horn
l-LN_v	Large ventrolateral neurons
l-LN_vx	"extra" l-LN_v
LN	Lateral neurons
LN_d	Dorsolateral neurons
LN_v	Ventrolateral neurons
LO	Lobula
LOP	Lobula plate
LPN	Lateral posterior neurons
M-...	Morning-... (as in the following)
M-cells	Morning-cells
M-oscillator	Morning-oscillator
M7	Margin 7 of the medulla (serpentine layer)

MARCM	Mosaic analysis with repessible cell marker
MB	Mushroom body
mCherry	Monomeric fluorescent protein (red)
mCitrine	Monomeric fluorescent protein (yellow)
MDC	Middle dorsal commissure
ME	Medulla
MESA	Maximum entropy spectral analysis
mFRT71	Modified Flippase recognition target
mTqu	Monomeric fluorescent protein (turquoise)
myr	Myristoylated (membrane localization signal)
myrGFP	Myristoylated green fluorescent protein
nc82	Bruchpilot (active zone protein)
NGS	Normal goat serum
NPF	Neuropeptide F
nSyb	Neuronal Synaptobrevin
OL	Optic lobe
PBS	Phosphate buffered saline
PBST	Phosphate buffered saline with Triton-X
PDF	Pigment dispersing factor

PDFR	Pigment dispersing factor receptor
PDF^{+}/ PDF^{-}	PDF expressing/ lacking
PED	Peduncle
per, PER	Period (*gene*, PROTEIN)
per^{0}	*Per*-null mutant
PER-LUC	Period-Luciferase fusion protein
PFA	Paraformaldehyde
PG	Prothoracic gland
PI	Pars intercerebralis
PLP	Posterior lateral protocerebrum
PLP-LOF	Fascicle connecting the posterior lateral protocerebrum with the dorsomedial lobula
PMT	Photon multiplier tube
POC	Posterior optic commissure
POT	Posterior optic tract (previous terminology for POC)
PTTH	Prothoracicotropic hormone
PVLP	Posterior ventral protocerebrum
QF/ *QUAS*	Binary expression system for *Drosophila*
rAVLPl	Cell body rind lateral to the anterior ventrolateral protocerebrum

RFP/ mRFP1	Red fluorescent protein
rH	Relative humidity
RI	Rhythmicity index
rLHd	Lateral cell body rind dorsal to the lateral horn
rLHl	Lateral cell body rind lateral to the lateral horn
rLHla	Lateral cell body rind lateroanterior to the lateral horn
rLHp	Lateral cell body rind posterior to the lateral horn
rSLPp	Posterior cell body rind posterior to the superior lateral protocerebrum
SAC	Superior arch commissure
SCL	Superior clamp
SCN	Suprachiasmatic nuclei
SGG	Shaggy
SIP	Superior intermediate protocerebrum
s-LN_v	Small ventrolateral neurons
SLP	Superior lateral protocerebrum
SMP	Superior medial protocerebrum
sNPF	Short neuropeptide F
$sNPF^+$/ $sNPF^-$	sNPF expressing/ lacking

TC	Thermophase:cryophase
tim, TIM	Timeless (*gene*, PROTEIN)
TIM^+/ TIM^-	TIM expressing/ lacking
TLN	Telencephalin
TPR	Temperature preference rhythms
TTLF	Transcriptional translational feedback loop
UAS	Upstream activating sequence (GAL4 binding site)
vri, VRI	Vrille (*gene*, PROTEIN)
YFP	Yellow fluorescent protein
ZT	*Zeitgebertime*

7.2 Supplemental Figure

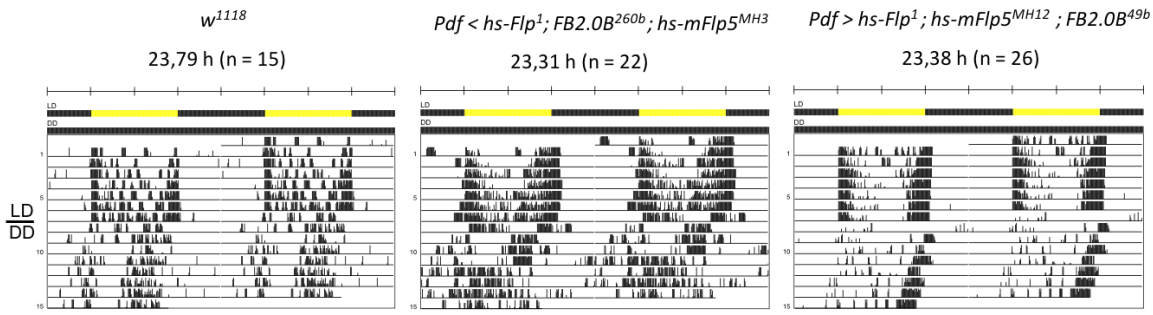

Fig. S1: Behavioral control of Flybow-flies. The test-flies, bearing all required constructs for the Flybow-approach, showed no impaired locomotor rhythmicity in LD or DD, indicating that the clock network was unaltered and intact. From left to right: w^{1118} wildtype strain, *Pdf-Gal4* driven constructs (variant1), *Pdf-Gal4* driven constructs (variant2). Estimated free-running period and sample size (n) are stated beneath the genotype.

7.3 Figures and Tables

Acknowledgements

First and foremost, I want to thank Dr. Dirk Rieger and Prof. Charlotte Helfrich-Förster for giving me the opportunity to work on this project and to be a part of their team within the SFB1047. Thank you for your time, the support, and for giving me the chance and liberties to attend various international conferences, which helped me to develop myself scientifically.

Further, I would like to thank my external supervisors Prof. Dr. Ralf Stanewsky and Prof. Dr. Georg Nagel for the fruitful discussions and technical advice;

Jade Attallah for providing the Matlab script for the analysis of the bioluminescence-data and Nicolas Hagedorn for supporting me in the immunohistochemistry experiments.

Equally, I would like to thank all members of the Chair for Neurobiology and Genetics for the great atmosphere and awesome time. Special thanks to my roommates, Pam, Kathi and Enrico for all the fun hours and for making overtime work enjoyable.

With all my heart, I want to thank my family and Anne, who supported me all the time and without whom this would not have been possible.

Curriculum Vitae

Affidavit

I hereby confirm that my thesis entitled "The circadian clock network of *Drosophila melanogaster"* is the result of my own work. I did not receive any help or support from commercial consultants. All resources and / or materials applied are listed and specified in the thesis.

Furthermore, I confirm that this thesis has not yet been submitted as part of another examination process neither in identical nor in similar form

Place, Date Signature

Eidesstattliche Erklärung

Hiermit erkläre ich an Eides statt, die Dissertation „Das Uhrneuronennetzwerk in *Drosophila melanogaster*" eigenständig, d.h. insbesondere selbständig und ohne Hilfe eines kommerziellen Promotionsberaters, angefertigt und keine anderen als die von mir angegebenen Quellen und Hilfsmittel verwendet zu haben.

Ich erkläre außerdem, dass die Dissertation weder in gleicher noch in ähnlicher Form bereits in einem anderen Prüfungsverfahren vorgelegen hat.

Ort, Datum Unterschrift